The Contribution of Calcium-Activated Potassium Channel Dysfunction to Altered Purkinje Neuron Membrane Excitability in Spinocerebellar Ataxia

by

David D. Bushart

A dissertation submitted in partial fulfillment
of the requirements for the degree of
Doctor of Philosophy
(Molecular and Integrative Physiology)
in The University of Michigan
2018

Doctoral Committee:

Professor Geoffrey G. Murphy, Co-Chair
Associate Professor Vikram G. Shakkottai, Co-Chair
Professor William T. Dauer
Professor W. Michael King
Professor Andrew P. Lieberman
Professor Malcolm J. Low

David D. Bushart

dbushart@umich.edu

ORCiD: 0000-0002-3852-127X

Acknowledgements

I would like to acknowledge three groups which provided me with support and motivation to complete the studies in this dissertation, and for helping me keep my research efforts in perspective.

First, I would like to acknowledge my friends and family. Their emotional support, and the time they have invested in supporting my growth as both a person and a scientist, cannot be overstated. I am eternally grateful to have a network of such caring people around me.

Second, I would like to acknowledge cerebellar ataxia patients for their perseverance and positive outlook in the face of devastating circumstances. My ability to interact with patients at the National Ataxia Foundation meetings, along with the positive messages that my research efforts were met with, was my greatest motivating factor throughout the final years of my dissertation studies. I encourage other researchers to seek out similar interactions, as they will make for a more invested and focused scientist.

Third, I would like to acknowledge the research animals used in the studies of this dissertation. It is without a voice that their sacrifice was made. These studies would have truly been impossible without the use of these animals, and it is essential that we researchers continue to provide research animals with as much compassion and care as possible. While understanding and curing disease is a noble cause, we must keep in mind the sacrifices that must be made in order to find these cures.

Table of Contents

List of Figures

List of Tables

Abstract

Spinocerebellar ataxias are a heterogeneous family of autosomal dominantly-inherited neurodegenerative disorders which affect movement and coordination. Patients experience the shared features of cerebellar ataxia, characterized by uncoordinated limb movements, unsteady gait, and difficulties with balance and posture. Although the underlying genetic causes of cerebellar ataxia are diverse, these diseases are often associated with degeneration of neurons within the cerebellum. Purkinje neurons, which are the sole output of the cerebellar cortex, show enhanced vulnerability to dysfunction and degeneration in ataxia. Therefore, therapies which target aberrant Purkinje neuron function have great potential for the treatment of cerebellar ataxia.

Spinocerebellar ataxia type 1 (SCA1) is a more common and well-studied inherited cerebellar ataxia and results from an expanded CAG repeat sequence in the *ATXN1* gene. This results in cerebellar Purkinje neuron dysfunction and degeneration associated with the expression of polyglutamine-expanded ataxin-1 protein. In mouse models of SCA1, Purkinje neuron dysfunction occurs concurrently with the onset of motor impairment and dendritic degeneration, suggesting that abnormalities in Purkinje neuron spiking correlate with and are potentially causative for motor impairment in SCA1. Previous studies have illustrated that potassium ion channel dysfunction underlies aberrant Purkinje neuron spiking in SCA1 mice. However, the nature of this dysfunction, and how it contributes to motor impairment, is not fully understood. The studies in Chapter 2 explore how potassium channel dysfunction contributes to

alterations in Purkinje neuron membrane excitability, and identifies ion channel-activating compounds which improve these alterations in physiology. Additionally, these studies illustrate how both somatic and dendritic alterations can exist due to the dysfunction of the same ion channels, and that somatic and dendritic pathology separately contribute to motor impairment in ataxia. Finally, these studies provide proof-of-concept evidence of potassium channel-activating compounds as therapeutic targets for the treatment of cerebellar ataxia and argue for future clinical trials of potassium channel activators in human SCA patients.

Similar to SCA1, spinocerebellar ataxia type 7 (SCA7) results from an expanded CAG repeat sequence in the *ATXN7* gene. This results in degeneration of neurons within the brainstem, retina, and cerebellum, including Purkinje neurons. Like SCA1, mouse models of SCA7 display Purkinje neuron dendritic degeneration which accompanies the onset of motor impairment. However, the contribution of Purkinje neuron dysfunction to disease is currently unknown. In order to identify relevant changes in ion-channel gene expression and function in SCA7, we performed RNA sequencing on whole cerebellar lysates from SCA7 mice. We identified decreased expression of genes associated with calcium signaling and a key calcium-activated potassium channel, which contribute to irregular Purkinje neuron spiking in SCA7 mice. However, these changes in RNA transcript expression are relatively modest. In Chapter 3, we further explored how partial disruption of several members of this key calcium homeostasis module can result in irregular Purkinje neuron spiking, and illustrate that a disruption of both calcium sources and calcium-activated potassium channels are required in order to produce irregular spiking. We further demonstrate that activation or

re-expression of the effector calcium-activated potassium channel can compensate for reduced calcium availability and thereby restore repetitive spiking to SCA7 Purkinje neurons. Finally, in Chapter 4, we illustrate that a genetic strategy which improves RNA transcript expression of members of this calcium module also improves Purkinje neuron membrane excitability and spike regularity in SCA7 Purkinje neurons. These studies argue that this calcium homeostasis module is central to Purkinje neuron function, and that members of this module may be important targets not only in SCA7 but also in other cerebellar ataxias.

Together, these studies address the hypothesis that calcium-activated potassium channel dysfunction is central to Purkinje neuron electrophysiologic dysfunction and motor impairment in spinocerebellar ataxia, and that potassium channel-activating compounds are outstanding candidates for the improvement of motor function in spinocerebellar ataxia. The overall impact of these studies is to establish a link between potassium channel dysfunction and motor impairment as a general mechanism of spinocerebellar ataxia and to demonstrate that potassium channel activation merits consideration for the treatment of human ataxia.

Chapter 1

Introduction

1.1 Purkinje neuron dysfunction in spinocerebellar ataxia: a common feature of disease

1.1.1 Overview of spinocerebellar ataxia

Spinocerebellar ataxias (SCAs) are a large, heterogeneous group of movement disorders which affect neurons in the cerebellum and its associated pathways. SCAs are characterized by their autosomal-dominant inheritance pattern and shared clinical features of cerebellar ataxia, a set of signs representing loss of motor coordination. SCA patients often experience uncoordinated limb movements, abnormal gait, and difficulties with balance and posture, frequently resulting in wheelchair confinement. Although many SCAs share clinical features, genetic causes are diverse and highlight the potential difficulty to diagnose and appropriately treat these disorders. For instance, there are over 40 known genetic mutations associated with SCA that affect a wide variety of molecular pathways [1]. The recent discovery of several new disease-causing SCA mutations suggests that many undiscovered disease genes still remain [2-6]. There is a crucial need to develop new therapies for SCA, as no approved treatments currently exist.

In addition to their similar clinical features, SCAs are characterized by a similar pattern of neurodegeneration. Although disease-causing mutations in cerebellar ataxia are diverse, and disease protein expression is often widespread or ubiquitous throughout the central nervous system, cerebellar involvement is prominent. A subset of SCAs result from glutamine-encoding CAG repeat expansions (the so-called polyglutamine SCAs: SCA1, 2, 3, 6, 7, 17). Although polyglutamine-expanded protein expression is widespread, and not necessarily restricted to just the nervous system, degeneration is restricted to specific neurons in the cerebellum and related structures [7]. Purkinje neurons, brainstem neurons, and neurons of the cerebellar nuclei are particularly vulnerable to degeneration. Among these, Purkinje neurons are most prominently involved in SCAs [1]. The increased susceptibility of Purkinje neurons to degeneration in SCA suggests that these neurons may possess unique metabolic or physiologic properties that make them more vulnerable to a variety of insults.

1.1.2 Unique physiology promotes enhanced cerebellar Purkinje neuron susceptibility in spinocerebellar ataxia

Purkinje neurons receive and integrate signals from several distinct neuronal pathways. Purkinje neuron intrinsic firing is modulated by synaptic activity to modify downstream motor pathways, namely neurons of the deep cerebellar nuclei and vestibular nuclei. Under normal conditions, Purkinje neurons can sustain firing at a large dynamic range, up to several hundred spikes per second *in vivo* [8]. In order to properly transmit motor information, Purkinje neurons must be capable of fast modulation of this firing to encode information. There is debate as to whether Purkinje neurons use firing-rate coding, coding through synchronized Purkinje cell activity, or hybrid multiplexed

coding to transmit output signals to motor nuclei [9-11]. Nevertheless, it is clear that rapid and precise modulation of Purkinje neuron membrane potential is necessary to encode coordinated motor output.

Purkinje neuron action potentials are dependent on precise, coordinated activity of a large complement of ion-channels in order to maintain autonomous repetitive spiking. Spontaneous action potentials are driven by resurgent sodium current carried by the voltage-gated sodium channel $Na_v1.6$ [12]. Upon reaching threshold, $Na_v1.6$ and $Na_v1.1$ channels become maximally activated, generating the upstroke of the action potential. The falling phase of the action potential is driven by voltage-gated potassium channels, mostly K_v3 family members [13]. Upon membrane depolarization, voltage-gated calcium channels (mainly $Ca_v2.1$ and Ca_v3 family members) also become activated, allowing external calcium entry into Purkinje neurons [14, 15]. These voltage-gated calcium channels are tightly coupled to calcium-activated potassium channels (K_{Ca} channels), so that the net effect of calcium entry is an outward potassium current which hyperpolarizes the membrane potential [16]. The major K_{Ca} channels in Purkinje neurons are the large-conductance calcium-activated potassium (BK, $K_{Ca}1.1$) channel and the small-conductance calcium-activated potassium (SK) channel (SK2, $K_{Ca}2.2$), which generate the after-hyperpolarization (AHP) [17-19]. The AHP is essential for de-activation of voltage-gated sodium and potassium channels, which allows for their activation during the subsequent action potential. The depolarization of the membrane potential during the interspike interval, which is necessary for autonomous spiking, is mediated by unique resurgent kinetics of voltage-gated sodium channels [12]. Finally, an assortment of subthreshold-activated potassium channels are active during the

interspike interval [20-25], while other channels such as TRPC3 and the inositol 1,4,5-trisphosphate receptor play important roles mediating calcium homeostasis and the modulation of cerebellar learning [26-29]. Purkinje neurons spiking is therefore highly sensitive to perturbations in ion-channels, and mutations in many of these channels are known to promote aberrant Purkinje neuron spiking and impaired motor function.

1.1.3 Channelopathies in spinocerebellar ataxia

Consistent with a role for these ion-channels in supporting Purkinje neuron spiking, conventional ion-channel mutations are known to result in SCA. Mutations in the aforementioned ion-channels which support Purkinje neuron spiking are, in many cases, causative for SCA (Figure 1.1; summarized in Table 1.1). Mouse models have provided valuable insight to the functional implications of disrupted ion-channel function in many of these ataxia-causing channelopathies. These models clearly demonstrate that electrophysiologic dysfunction contributes to motor impairment in ataxia, and suggest that ion-channels are important potential targets in ataxia.

Potassium channel mutations cause SCA in humans. Mutations in the *KCNC3* gene result in the production of the voltage-gated potassium channel, K_v3.3, with either no functional current or altered kinetics [30-32]. In mice, knockout of K_v3.3 causes reduced Purkinje neuron firing frequency due to altered inactivation of other ion-channels during the interspike interval [33-35]. Alternatively, mutations in the *KCND3* gene, which encodes the A-type potassium channel K_v4.3, result in SCA19/22 [36, 37]. Although there are conflicting reports about the functional role of K_v4.3 in adult Purkinje neurons [38, 39], Purkinje neuron degeneration is present in SCA19/22 patients [36] which suggests an important role for K_v4.3 in Purkinje neuron function. In heterologous cells, mutations in

KCND3 tend to impair the stability of K_V4.3-containing protein complexes, which thereby reduces K_V4.3 channel expression at the cell surface and impairs current density of these channels [36, 37, 40, 41]. Finally, a recently-discovered mutation in the *KCNMA1* gene, which encodes the BK channel, produces ataxia with cerebellar atrophy. In heterologous cells, mutant BK channels show reduced macroscopic currents and act in a dominant-negative fashion [5, 6]. While these mutations have not been introduced into mice, both global and Purkinje neuron-specific BK channel-null mice exhibit cerebellar ataxia [18, 42], which corresponds to greatly disrupted Purkinje neuron spiking [18]. These studies illustrate the relevance of potassium channel mutations to human SCA, and suggest that altered Purkinje neuron spiking may be a potential basis for motor impairment in ataxia.

In addition to potassium channels, mutations in other ion-channels are known to result in cerebellar ataxia. Mutations in *ITPR1*, which encodes the inositol 1,4,5-trisphosphate (IP3) receptor gene, result in SCA15/16 and the nonprogressive congenital ataxia, SCA29 [28, 43-48]. IP3 and diacylglycerol are produced upon postsynaptic metabotropic glutamate receptor (mGluR) activation, and IP3 subsequently binds to the IP3 receptor and promotes calcium release from internal stores [29]. In mice, *Itpr1* knockout eliminates long-term depression at Purkinje neuron synapses, while *Itpr1* heterozygous mice exhibit motor impairment on the rotarod [49], as do mGluR1 knockout mice [50]. This suggests that synaptic dysregulation which occurs upon altered IP3 receptor function contributes to cerebellar ataxia. In addition to IP3, mGluR signaling in Purkinje neurons relies upon the transient receptor potential channel type C3 (TRPC3), which is necessary for the induction of long-term depression [26, 27]. In *moonwalker* mice,

a point mutation in *Trpc3* results in motor impairment and progressive Purkinje neuron loss [51]. Notably, Purkinje neuron firing is markedly abnormal in *moonwalker* mice, with depolarization block of Purkinje neuron spiking [52]. In humans, TRPC3 mutations result in SCA41 [3]. Overall, it is possible that synaptic dysregulation and altered Purkinje neuron spiking may contribute to SCA.

Recently, a point mutation in the *CACNA1G* gene was identified as the causative mutation in SCA42 [2, 4]. This mutation, p.Arg1715His, is located in the voltage-sensing domain of the T-type calcium channel, $Ca_V3.1$. When cloned into a heterologous system, this mutation shifts $Ca_V3.1$ activation to more positive membrane potentials [2, 4], suggesting that these channels may not activate as efficiently upon depolarization. This could disrupt calcium entry and, consequently, activation of K_{Ca} channels. In mice, T-type calcium channel blockade reduces Purkinje neuron spike frequency *in vitro*, while mice lacking $Ca_V3.1$ in several brain regions, including the cerebellum, show increased Purkinje neuron spike frequency and irregularity *in vivo* [53, 54]. Synaptic dysfunction and the resulting impairment of motor learning is prominent in $Ca_V3.1^{-/-}$ mice, as these mice demonstrate an impaired ability to produce long-term potentiation at the parallel fiber-Purkinje neuron synapse, impaired performance on a rotarod, and impairments in the vestibulo-ocular reflex [53]. It is possible that reduced $Ca_V3.1$ activity may also reduce calcium availability for calcium-activated potassium channels, thereby impairing the generation of a normal spike after-hyperpolarization (AHP) and reducing spike regularity. However, the contribution of $Ca_V3.1$ as a calcium source for calcium-activated potassium channels remains controversial [16].

1.1.4 Ion-channel dysfunction is associated with mouse models of polyglutamine spinocerebellar ataxia

Although conventional channelopathies present a clear role for altered neuronal membrane excitability in ataxia, these forms of ataxia are less common and are estimated to be responsible for around ten percent of all cases of SCA [1]. Much more common are the polyglutamine SCAs, which result from expanded glutamine-encoding CAG repeat sequences in their respective causative genes. Apart from SCA6, which affects the α-subunit of the $Ca_V2.1$ voltage-gated calcium channel encoded by the *CACNA1A* gene [55], the disease causing proteins in polyglutamine SCA are not directly associated with ion-channel function. ATXN1 (the disease-causing protein in SCA1) is associated with transcriptional regulation and RNA splicing [56-58], ATXN2 (SCA2) plays a role in RNA metabolism [59-61], ATXN3 (SCA3) is a de-ubiquitinating enzyme [62, 63], ATXN7 (SCA7) is a member of the SAGA transcriptional complex [64], and *TBP* (SCA17) is an essential component of tata box-based transcriptional initiation [65] (reviewed in [66]). These related functional roles suggest that transcriptional disruption may be an important initiating event in the polyglutamine SCAs.

Indeed, transcriptional disruption has been noted in mouse models of SCA. Gene expression analyses such as RNA sequencing and gene co-expression network analyses have been useful for the identification of molecular pathways which may be disrupted in SCA [67-69]. Interestingly, several genes show common downregulation of their mRNA transcripts in multiple SCA mouse models. These include several members of neuronal excitability pathways, including key ion-channels for Purkinje neuron function [67-72]. Recent work has demonstrated that altered ion-channel expression in

SCA can disrupt Purkinje neuron membrane excitability, and mouse models of polyglutamine SCA suggest that ion-channel modulators may represent a therapeutic strategy for both motor dysfunction and neurodegeneration.

Ion-channel dysfunction is associated with polyQ SCA in rodent models. In mouse models of SCA1, disrupted Purkinje neuron membrane excitability is associated with reduced expression and function of two potassium channels, BK and the G-protein coupled inwardly-rectifying potassium (GIRK1) channel [71]. Functionally, Purkinje neurons from ATXN1[82Q] mice demonstrate a depolarized somatic membrane potential and a reduced fast afterhyperpolarization (AHP) early in disease, leading to a large proportion of non-firing cells [71, 73]. Through a parallel process, loss of these and related channels results in a persistent increase in dendritic membrane excitability even in the presence of dendritic degeneration [73, 74]. Similarly, in a mouse model of SCA2, altered potassium channel function underlies Purkinje neuron firing abnormalities. ATXN2[127Q] Purkinje neurons show progressive reductions in firing frequency with no change in spike regularity [70, 72]. These changes in firing are accompanied by a progressive reduction in the transcripts encoding the BK channel and $K_v3.3$, a voltage-gated potassium channel, both of which are important for repetitive spiking [70, 72]. Like in SCA1, ATXN2[127Q] Purkinje neurons display an absence of repetitive spiking in association with this reduction in potassium channel function [70], whereas the ATXN2[58Q] transgenic model of SCA2 displays aberrant Purkinje neuron bursting both *in vitro* and *in vivo* [75, 76]. In the ATXN3[84Q] transgenic mouse model of SCA3, changes in Purkinje neuron physiology accompany motor impairment. Purkinje neurons from these mice display altered spiking in association with increased inactivation of K_v1

potassium channels [77]. Finally, a mouse model of SCA6 demonstrates that functional alterations in Purkinje neuron spiking accompany the polyQ mutation in *Cacna1a*, encoding the α-subunit of the $Ca_V2.1$, a voltage-gated calcium channel [78]. Overall, these studies demonstrate that changes in ion-channel expression have functional consequence for Purkinje neuron spiking in models of polyQ SCA.

1.2 Calcium-activated potassium channels are important therapeutic targets in spinocerebellar ataxia

1.2.1 Calcium-activated potassium channel expression and function in cerebellar Purkinje neurons

When modeling spinocerebellar ataxia in mice, neuronal dysfunction typically precedes overt neuron loss, and changes in neuronal function often correlate with the onset of motor dysfunction [71, 72, 79]. As outlined in section 1.1.2, Purkinje neurons rely on the precise activity of a multitude of ion channels in order to maintain spontaneous and regular pacemaking. Mouse studies have demonstrated that Purkinje neuron spiking is sensitive to perturbation in calcium buffering [80], intracellular calcium stores [81], and plasma membrane calcium channels [82, 83]. Proper intracellular calcium concentration through these calcium sources regulates the activity of calcium-activated potassium (K_{Ca}) channels, whose functions are critical for the regularity of Purkinje neuron spiking [82, 83]. In fact, K_{Ca} channel-mutant mice display cerebellar ataxia accompanied by disrupted Purkinje neuron spiking [18, 42]. This suggests that K_{Ca} channels may be particularly important targets in cerebellar ataxia.

Several K_{Ca} channels are expressed and have a functional role in mature Purkinje neurons. These include the large conductance, intermediate conductance, and

small conductance calcium-activated potassium channels (BK, IK, and SK, respectively). Studies have indicated that BK channels are scattered throughout the soma and proximal dendrites of Purkinje neurons, and are also associated with clustered microdomains located near endoplasmic reticulum (ER) [84]. This proximity to the ER has been postulated to allow for IP3-mediated release of local calcium stores, which may be sufficient to activate BK channels [84]. Recently, BK channels were also found to be localized at paranodal junctions in Purkinje neuron axons, where they contribute to high-fidelity firing [85]. In a similar fashion, SK2 channels are also scattered throughout the soma and proximal dendrites of Purkinje neurons [86, 87], although the relationship between SK2 channel expression and ER microdomains is not yet known. Both BK and SK2 channels cluster with $Ca_V2.1$, the P/Q-type voltage-gated calcium channel, and have been postulated to be specifically activated by calcium entry through $Ca_V2.1$ channels [16, 86]. Functionally, BK and SK2 channels are important for regulating the AHP, an essential feature of the action potential which allows for high-frequency firing in Purkinje neurons [17, 18, 71, 87]. IK channels, which were once thought to be expressed only in the peripheral nervous system, were found to be expressed in cerebellar Purkinje neurons, where they couple with $Ca_V3.2$ to form functional microdomains [88]. IK channels modulate parallel fiber input onto Purkinje neurons by controlling local EPSP summation, which was postulated to facilitate high-pass filtering in the dendrite [88].

In addition to regulating somatic spiking, K_{Ca} channels, along with voltage gated potassium channels, are known to modulate dendritic signal integration and intrinsic dendritic excitability. Evidence for heavy dendritic K_{Ca} modulation comes from the

response of Purkinje neurons to simple spike backpropagation and synaptic stimulation. Backpropagating acting potentials attenuate significantly in Purkinje neuron dendrites, as evidenced by low levels of dendritic [Ca^{2+}] in association with backpropagating simple spikes [89, 90]. Purkinje neurons rely on a number of potassium channels in order to limit backpropagation of somatic spikes into the dendrites, including BK, SK2, and $K_v3.3$ [91-95]. Purkinje neurons demonstrate significant increases in cytosolic [Ca^{2+}] upon parallel fiber input, and even more widespread dendritic cytosolic [Ca^{2+}] upon climbing fiber stimulation [96]. Much of this calcium release is associated with mGluR1 activation, which results in the release of ER-mediated calcium stores through IP3 signaling [97], along with Trpc3 [26] and voltage-gated calcium channel [98] activation. Therefore, the spatial and temporal modulation of dendritic cytosolic [Ca^{2+}] must be tightly regulated by K_{Ca} channels in order to properly encode synaptic information. These studies indicate that K_{Ca} channels are important not only for somatic spiking, but also for the local modulation of excitability in Purkinje neuron dendrites.

1.2.2 Calcium channel-mutant mice display abnormal Purkinje neuron membrane excitability and motor impairment

Early studies in calcium channel-mutant mice indicated that impaired Purkinje neuron spiking correlates strongly with motor impairment in ataxia. These studies were performed in mice with mutations in $Ca_v2.1$, the P/Q-type calcium channel encoded by the *Cacna1a* gene [99-101]. Normally, autonomous spiking in Purkinje neurons is very precise, with little variation in the duration of the interspike interval. Strikingly, Purkinje neurons in these mouse models show irregular spiking compared to wild-type controls, as evidenced by an increase in the coefficient of variation of the interspike interval

between action potentials [82, 102]. Consistent with a role for calcium entry to regulate K_{Ca} channel activity, SK channel activators improve both Purkinje neuron spike regularity and motor performance in calcium channel-mutant mice [82, 83]. Additionally, the spiking of neurons of the deep cerebellar nuclei, which receive input from Purkinje neurons and act as the output of cerebellar motor processing, is also dependent on K_{Ca} activity [103]. This suggests that there is a direct link between ion-channel function, Purkinje neuron spiking, and motor output from the cerebellum, and that pharmacologic agents which target ion-channel dysfunction may have therapeutic potential.

1.2.3 Calcium-activated potassium channel modulators improve motor performance in mouse models of polyglutamine spinocerebellar ataxia

As outlined in Section 1.1.4, ion-channel dysfunction is associated with rodent models of polyQ SCA. While these models display some differences in their respectively-affected ion-channel complement, some similarities do exist between these distinct models. For instance, K_{Ca} channel dysfunction appears to be a common source of Purkinje neuron dysfunction across polyQ SCA models. In the ATXN1[82Q] model of SCA1, increased Purkinje neuron excitability and a subsequent lack of somatic spiking can be explained, in part, by BK channel dysfunction. In these mice, genetic re-expression of BK channel transcripts improves motor function on a rotarod [71]. Additionally, non-firing Purkinje neurons from ATXN[82Q] mice display improved spiking and motor performance when treated with K_{Ca} activators [73]. A separate study has demonstrated that alterations in Purkinje neuron spiking can be corrected by aminopyridines [104], compounds which non-selectively block voltage-gated potassium channels and which have been previously shown to indirectly activate K_{Ca} channels [105].

Together, these data suggest that K_{Ca} channels are important therapeutic targets in SCA1.

Similar to SCA1, in the ATXN2[58Q] transgenic model of SCA2, irregular Purkinje neuron spiking is observed both *in vitro* and *in vivo* [75, 76]. When treated with K_{Ca}-activating compounds, Purkinje neuron firing properties are restored to ATXN2[58Q] mice, in addition to improved motor performance [76]. Additionally, a direct interaction between ATXN2 and the inositol 1,4,5-trisphosphate (IP3) receptor results in abnormal calcium signaling in ATXN2[58Q] mice which can be improved by treatment with dantrolene, a ryanodine receptor inhibitor [106]. Dantrolene also improves motor impairment in ATXN2[58Q] mice [106], suggesting that normalizing calcium signaling may either directly reduce calcium-mediated excitotoxicity or may improve the function of K_{Ca} channels to improve Purkinje neuron pacemaking. Overall, these studies indicate a clear role for potassium channel dysfunction which impairs Purkinje neuron spiking and thereby contributes to motor impairment in SCA2.

In the ATXN3[84Q] transgenic mouse model of SCA3, Purkinje neurons display altered spiking in association with increased inactivation of K_v1 potassium channels [77]. The SK channel-activating compound SKA-31 improves spiking in ATXN3[84Q] Purkinje neurons and also improves motor performance, indicating that potassium channel dysfunction can be targeted pharmacologically in these mice [77]. Similar to ATXN2[58Q] mice, abnormal calcium signaling has been noted in ATXN3[84Q] mice. ATXN3 directly interacts with the IP3 receptor to increase calcium release events [107]. Inhibition of intracellular calcium release through dantrolene also improves motor performance and reduces Purkinje neuron degeneration [107], suggesting that a common disease

mechanism may contribute to altered calcium homeostasis across mouse models of SCA2 and SCA3.

Finally, in a mouse model of SCA6, potassium channel modulation targets aberrant Purkinje neuron spiking. The compound 4-aminopyridine (4-AP), a potassium channel blocker which also indirectly activates K_{Ca} channels [105], restores spike regularity to SCA6$^{84Q/84Q}$ Purkinje neurons both *in vitro* and *in vivo* [78]. Interestingly, chronic treatment with 4-AP improves motor function in SCA6$^{84Q/84Q}$ mice [78]. These data suggest that Purkinje neuron spiking abnormalities are present in a mouse model of SCA6, and that these alterations in spiking may be targeted by potassium channel modulators.

These studies in SCA1, SCA2, SCA3, and SCA6 highlight a role for potassium channel dysfunction in altered Purkinje neuron physiology in ataxia. It is important to recognize, however, that alterations in different ion-channels can produce similar alterations in Purkinje neuron firing. It is therefore important to understand the specific ion-channel changes that underlie altered spiking in ataxia. Overall, activating calcium-activated potassium channels appears to correct altered spiking resulting from a variety of different etiologies, and represents a therapeutic target that is shared across multiple forms of ataxia.

1.2.4 Human clinical trials with calcium-activated potassium channel modulators indicate potential efficacy

Designing effective therapies for SCA has proven difficult. Although most SCAs share clinical features, the underlying genetic mutations are diverse and in some cases remain unknown. Recent work has demonstrated the therapeutic potential of gene

silencing therapies for ataxia. Among the most promising of these therapies are the antisense oligonucleotide (ASO)-based strategies in the polyglutamine SCAs. In mouse models of SCA2 and SCA3 [108, 109], ASOs have been shown to reduce expression of the respective disease-causing proteins, along with providing lasting improvements in motor performance in SCA2 mice [108, 109]. Additionally, ASO treatment improves firing abnormalities in two mouse models of SCA2, suggesting that transcriptional changes affecting ion-channel expression may be improved upon ASO treatment [109]. Although ASOs offer an exciting avenue of treatment for the polyglutamine SCAs, these therapies will likely offer limited therapeutic benefit SCAs in which disease-causing mutations are not autosomal dominant gain-of-function mutations, or are in cellular pathways where knocking down mutant protein is deleterious. In these cases, a more appropriate approach to therapy may be to identify shared features of disease which are observed across many etiologies of SCA. Emerging evidence presented in this dissertation suggests that electrophysiologic dysfunction may be a shared feature of many SCAs.

Recent clinical trials with riluzole for the treatment of SCA suggest that shared features of neuronal dysfunction also exist in human disease [110, 111]. While riluzole has several ion-channel targets, it is a known activator of K_{Ca} channels [112, 113]. K_{Ca} channel activators demonstrate therapeutic potential in the treatment of SCAs [76, 77, 83, 114]. A larger clinical trial with a pro-drug of riluzole is ongoing (ClinicalTrials.gov Identifier: NCT02960893). In addition, a recent study indicated that a combination of chlorzoxazone and baclofen, two potassium channel-activating compounds which respectively activate K_{Ca} channels and other potassium channel targets, are tolerated in human SCA patients and may also improve symptoms [73]. While yet preliminary, these

trials suggest the promise of ion-channel modulators for the treatment of SCA. Future research should focus on the design of other ion-channel modulators with increased specificity and potency to correct symptoms that result from neuronal dysfunction.

1.3 Summary and aims of dissertation

Cerebellar Purkinje neuron dysfunction is a common feature of mouse models of SCA, even in models where mutations in ion-channel genes are not the primary cause of disease. Work in these animal models has highlighted a role for ion-channel modulation as a potential symptomatic treatment strategy in SCA. However, these studies largely address alterations in Purkinje neuron physiology on a case-by-case basis and do not explore potential common mechanisms of neuronal dysfunction across different etiologies of SCA. In order to address how specific ion-channel dysfunction contributes to neuronal dysfunction in SCA, my dissertation seeks to explore the underlying mechanisms of altered Purkinje neuron membrane excitability in mouse models of two different SCAs, spinocerebellar ataxia type 1 (SCA1) and spinocerebellar ataxia type 7 (SCA7). In addition to characterizing these alterations in excitability, I seek to determine whether calcium-activated potassium channels, identified in these studies as dysfunctional, may be appropriate pharmacologic targets to improve behavioral deficits in SCA.

Three major aims are addressed in this dissertation. The first aim is to determine the contribution of calcium-activated potassium channel dysfunction to both somatic and dendritic membrane excitability in a mouse model of SCA1, and to determine whether these compartment-specific changes in excitability contribute independently to motor impairment in ataxia. Additionally, this aim seeks to determine whether potassium

channel activating-compounds may be tolerated by human ataxia patients. The second aim is designed to determine whether physiologic alterations exist in a mouse model of SCA7, and to identify the underlying sources of Purkinje neuron dysfunction. Findings from the second aim lead to the third aim, which is to determine whether improving transcriptional dysregulation in SCA7 mice can be accomplished by sirtuin-1 overexpression, and whether improving ion-channel transcript expression can improve Purkinje neuron membrane excitability in SCA7 mice.

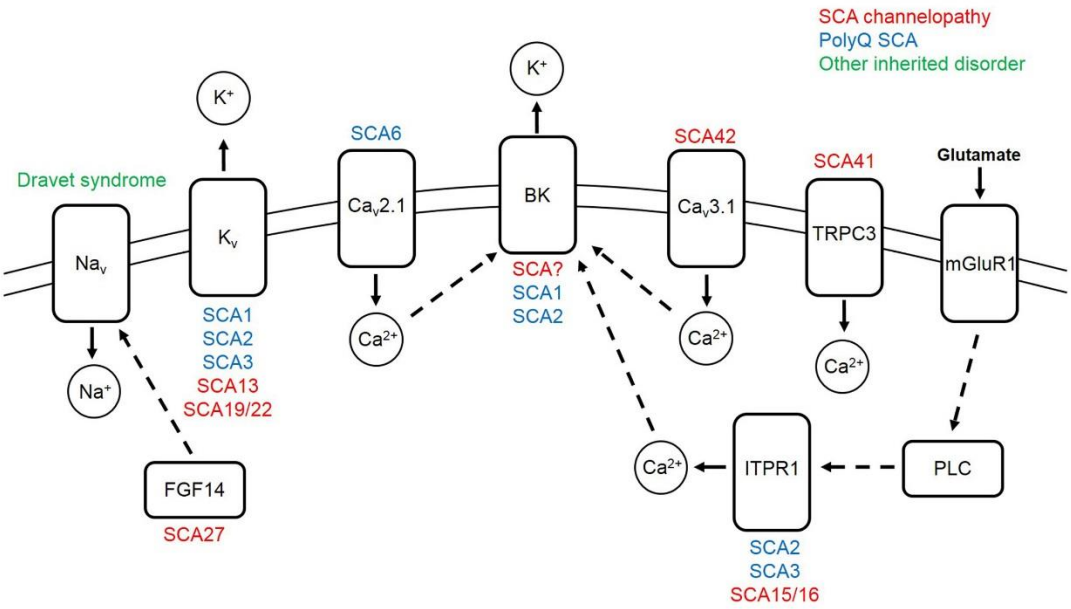

Figure 1.1 Ion-channel dysfunction is associated with spinocerebellar ataxia in humans and rodent models. Ion-channels, which are displayed in the cell membrane, and other ion-channel associated proteins causing spinocerebellar ataxia in humans or rodent models of disease, are shown. SCAs associated with each protein are listed above or under each protein. Mutations which result in an SCA channelopathy are listed in red. Ion-channel dysfunction in mouse models of polyQ SCA are listed in blue. Dravet syndrome, a severe myoclonic epilepsy of infancy which can result in ataxia, is shown in green. Dashed arrows signify a protein-protein interaction. Solid arrows signify the direction of ion movement upon channel activation. Abbreviations: SCA, spinocerebellar ataxia; polyQ, polyglutamine; Na_V, voltage-gated sodium channel; K_V, voltage-gated potassium channel; Ca_V, voltage-gated calcium channel; BK, large conductance calcium-activated potassium channel; TRPC3, transient receptor potential cation channel type 3; mGluR1, metabotropic glutamate receptor type 1; FGF14, fibroblast growth factor 14; ITPR1, inositol 1,4,5 trisphosphate receptor type 1; PLC, phospholipase C; Na^+, sodium ion; K^+, potassium ion; Ca^{2+}, calcium ion.

Gene	Associated ataxia or inherited disorder	Encoded channel or protein	Normal function
CACNA1A	SCA6 [55], Episodic ataxia type 2 [115]	$Ca_v2.1$ Voltage-gated calcium channel, pore-forming subunit	Inward calcium current (P/Q-type) upon depolarization Coupled to K_{Ca} channels to regulate spike frequency and regularity
KCNC3	SCA13 [30-32]	$K_v3.3$ Voltage-gated potassium channel	Potassium entry upon membrane depolarization, causing hyperpolarization
ITPR1	SCA15 [44, 45], SCA16 [43], SCA29 [46-48]	Inositol 1,4,5-trisphosphate (IP3) receptor	Calcium release from internal stores upon IP3 binding
KCND3	SCA19 [36], SCA22 [37]	$K_v4.3$ Voltage-gated potassium channel	Potassium entry upon membrane depolarization, causing hyperpolarization
SCN1A	Dravet syndrome [116]	$Na_v1.1$ Voltage-gated sodium channel, pore-forming subunit	Sodium entry and membrane depolarization during the action potential
FGF14	SCA27 [117]	Fibroblast growth factor 13	Interacts with Na_v to influence excitability
TRPC3	SCA41 [3]	Transient receptor potential cation channel type 3	Essential for mGlur1-mediated synaptic transmission, long-term depression
CACNA1G	SCA42 [2, 4]	$Ca_v3.1$ Voltage-gated calcium channel	Inward calcium current (T-type) upon depolarization
KCNMA1	Unnamed SCA [5, 6]	$K_{Ca}1.1$ Large conductance calcium-activated potassium (BK) channel	Outward K^+ current upon activation Regulates spike frequency and regularity

Table 1.1 Ion-channel mutations resulting in spinocerebellar ataxia. Known SCA channelopathies are listed. The associated gene is listed for each SCA, along with the known functional roles of each ion-channel or protein.

Chapter 2

Potassium channel activation improves Purkinje neuron physiology and motor impairment in a mouse model of spinocerebellar ataxia type 1

2.1 Abstract

Purkinje neuron dysfunction is associated with cerebellar ataxia. However, the link between specific alterations in Purkinje neuron membrane excitability and motor impairment is not fully understood. In a mouse model of spinocerebellar ataxia type 1 (SCA1), reduced potassium channel function contributes to altered membrane excitability resulting in impaired Purkinje neuron spiking. I sought to determine the relationship between altered membrane excitability and motor dysfunction in SCA1 mice. Using patch-clamp recordings in acute cerebellar slices, I found that activating calcium-activated and subthreshold-activated potassium channels improved Purkinje neuron spiking impairment in SCA1 mice. Additionally, dendritic hyperexcitability was improved by activating subthreshold-activated potassium channels but not calcium-activated potassium channels. I found that improving Purkinje neuron spiking and dendritic hyperexcitability through a combination of chlorzoxazone and baclofen produced sustained improvement in motor dysfunction in SCA1 mice. Finally, retrospective review of SCA patient records suggests that co-treatment with chlorzoxazone and baclofen is tolerated and may improve symptoms. Together, these

data suggest that potassium channel activators may improve motor impairment in SCA by improving alterations in Purkinje neuron excitability. Future clinical trials with potassium channel activators are warranted in cerebellar ataxia.

2.2 Introduction

Degenerative cerebellar ataxias are a group of disorders with progressive changes in balance, speech, and gait, often leading to wheelchair confinement. There is a need for agents which improve motor dysfunction in cerebellar ataxia, as there is currently no approved treatment for these debilitating disorders. In mouse models, neuronal dysfunction precedes neuronal loss and occurs with the onset of motor dysfunction[70-72, 77]. In human autopsy material, in addition to cell loss, morphologically abnormal neurons are consistently present[118]. This suggests that neuronal dysfunction may be an important feature of cerebellar ataxia. Defining this neuronal dysfunction represents an outstanding target for treatment of motor dysfunction in cerebellar ataxia.

Spinocerebellar ataxias (SCA) are a group of dominantly inherited disorders affecting the cerebellum and related pathways. The most common SCAs (SCA1, SCA2, SCA3, and SCA6) result from glutamine-encoding repeat expansions in the respective disease-causing genes[1]. Cerebellar Purkinje neuron degeneration is particularly prominent in autopsy tissue from SCA1, SCA2, and SCA6 patients. In addition, recent studies have demonstrated that Purkinje neuron function is altered at the onset of motor impairment in mouse models of SCA1 and SCA2[70-72]. Coordinated activity of an assortment of ion-channels supports repetitive spiking in Purkinje neurons even in the absence of synaptic

input[14, 119, 120]. In mouse models of SCA1-3, a subset of Purkinje neurons exhibit a loss of spontaneous spiking and a depolarized membrane potential early in disease, which is related to reduced function of potassium channels[70, 71, 77]. Similarly, potassium channel dysfunction contributes directly to dendritic hyperexcitability in these neurons, which may disrupt dendritic signal integration and contributes to neurodegeneration [73, 74, 121]. Although these studies demonstrate a clear relationship between altered Purkinje neuron physiology and motor impairment, the exact role for altered spiking and increased dendritic excitability in causing motor dysfunction is unclear.

Ion-channels are becoming increasingly recognized as outstanding targets for the treatment of cerebellar ataxia. Many SCAs are caused by conventional mutations in ion-channel genes (*KCNMA1, KCNC3, KCND3, CACNA1A, CACNA1G, ITPR1, SCA8A, TRPC3*)[1-4, 6, 31, 36, 37, 45], and alterations in ion-channel function are secondary to disease-causing mutations in several mouse models of spinocerebellar ataxia (SCA1, SCA2, SCA3, SCA6)[70-72, 77, 78]. In mouse models of SCA, ion-channel modulators correct irregular Purkinje neuron spiking and improve motor impairment[76, 78]. Recently, clinical trials for the compound riluzole have demonstrated therapeutic promise for the treatment of several forms of SCA[110, 111]. The known targets of riluzole include calcium-activated potassium channels, some subthreshold-activated potassium channels, and voltage-gated sodium channels[112, 113]. It is important to determine which ion-channel targets are relevant for treating symptoms in order to identify effective drugs with reduced potential for off-target effects.

In this study, I identify potassium channel modulators which improve Purkinje neuron spiking and dendritic hyperexcitability in SCA1 mice. These studies suggest that

targeting abnormalities in Purkinje neuron spiking alone may be an effective short-term therapeutic strategy, but that only a strategy which improves both spiking and dendritic hyperexcitability provides long-term benefit of motor dysfunction in SCA1 mice. Potassium channel modulators that are effective in improving motor dysfunction in the mouse model, and are also approved for human use, are tolerated by patients with SCA and may be effective in improving motor dysfunction in forms of ataxia with prominent Purkinje neuron involvement.

2.3 Methods

2.3.1 Mice

All animal procedures were approved by the University of Michigan Committee on the Use and Care of Animals, and were conducted in accordance with the United States Public Health Service's Policy on Human Care and Use of Laboratory Animals. Homozygous ATXN1[82Q] transgenic mice[122], which overexpress human ATXN1 with 82 CAG repeats selectively in cerebellar Purkinje neurons under the *Pcp2* promotor, were maintained on an FVB background. Wild-type FVB mice (Jackson Labs) were used as controls for all experiments. All data presented from these experiments were from mice at either 5 weeks of age or 14 weeks of age. Sexes were balanced for all animal studies. For studies involving animals, an uppercase "N" denotes the number of mice used per group, while a lowercase "n" denotes the number of cells used per group.

2.3.2 Patch-clamp electrophysiology

2.3.2.1 Patch-clamp electrophysiology: solutions

Artificial CSF (aCSF) contained the following (in mM): 125 NaCl, 3.8 KCl, 26 $NaHCO_3$, 1.25 NaH_2PO_4, 2 $CaCl_2$, 1 $MgCl_2$, 10 glucose. For sections made at 4^oC, cutting solution

contained the following (in mM): 87 NaCl, 2.5 KCl, 25 $NaHCO_3$, 1 NaH_2PO_4, 0.5 $CaCl_2$, 7 $MgCl_2$, 75 sucrose, 10 glucose. Unless otherwise specified, pipettes were filled with an internal recording solution containing the following (in mM): 119 K Gluconate, 2 Na gluconate, 6 NaCl, 2 $MgCl_2$, 0.9 EGTA, 10 HEPES, 14 Tris-phosphocreatine, 4 MgATP, 0.3 tris-GTP, pH 7.3, osmolarity 290 mOsm. Proper calcium buffering is important in order to support proper calcium-activated potassium channel function. The EGTA concentration was chosen based on previous studies which indicate that 0.5-1.0 mM EGTA maintains Purkinje neuron calcium-activated potassium channel function similar to endogenous calcium buffering [70, 71, 77, 123-127]. In order to block potassium channels in some dendritic excitability experiments, pipettes were filled with an internal recording solution containing the following (in mM): 140 CsCl, 2 $MgCl_2$, 1 $CaCl_2$, 10 EGTA, 10 HEPES, 4 Na_2ATP, pH 7.3, osmolarity 287 mOsm.

2.3.2.2 Patch-clamp electrophysiology: reagents

Baclofen (Sigma Aldrich, Cat. No. B5399) was used at 10 µM for studies involving somatic spiking, and at 2 µM for experiments assessing dendritic excitability. Chlorzoxazone (Sigma Aldrich, Cat. No. C4397) was used at 50 µM for all *in vitro* experiments. SKA-31 was synthesized in-house and was used at 10 µM for all *in vitro* experiments. 1-EBIO (Tocris, Cat. No 1041) was used at 100 µM for all experiments. Barium chloride (Sigma Aldrich, Cat. No. 217565) was used at 50 µM or 500 µM to block subthreshold-activated potassium channels. Cadmium chloride (Sigma Aldrich, Cat. No. C3141) was used at 100 µM to block voltage-gated calcium channels. Tetrodotoxin (Alomone Labs, Cat. No. T-550) was used at 1µM. During some

assessments of dendritic excitability, U-73122 (Tocris, Cat. No. 1268) was added to the internal pipette solution at a concentration of 10 µM to inhibit phospholipase C.

2.3.2.3 Acute slice preparation for electrophysiological recordings

Mice were anesthetized by isoflurane inhalation, decapitated, and brains removed for slice preparation. For measurements of somatic spiking and whole-cell somatic physiology (Figs 1-3), slices were prepared in cutting solution at 4^{o}C as previously described [70, 71, 77, 103, 128]. For dendritic calcium spike experiments, slices were prepared in pre-warmed (33^{o}C) aCSF. Slice preparation at 33^{o}C for Purkinje neuron recordings has been performed previously [129, 130] and results in better preservation of dendritic morphology in our studies. Slices were prepared using a vibratome (Leica) to 300 µm thickness. Slices were incubated in 33^{o}C aCSF bubbled with 5% CO_2 and 95% O_2 (carbogen) for 45 minutes after sectioning.

2.3.2.4 Patch-clamp recordings

Patch-clamp recordings were performed as described previously [70]. Cell-attached and whole-cell recordings were performed at 33^{o}C in carbogen-bubbled aCSF at a flow rate of 2-3 ml/min 1-5 hours after slice preparation. Recordings were performed using an Axopatch 200B amplifier, Digidata 1440A interface, and pClamp-10 software (MDS analytical technologies, Sunnyvale, CA). Data were acquired at 100 kHz in the fast current clamp mode of the amplifier and filtered at 2 kHz. For some dendritic excitability experiments, data were acquired using an Axon Multiclamp 700B amplifier, with voltage data acquired in current-clamp mode with bridge balance compensation and filtered at 2 kHz. Cells were rejected if the series resistance changed by more than 20% over the duration of the recording, or if it exceeded 15 MΩ. Voltage traces were corrected for a

10 mV liquid junction potential. For all recordings involving pharmacologic agents, baseline data was acquired for 5 minutes before introducing agents into the bath. Effects on spiking persisted for the duration of the experiment, in some cases more than 30 minutes.

2.3.2.5 Analysis of intrinsic dendritic excitability

Analysis of intrinsic dendritic excitability was performed as described previously [91]. Briefly, neurons were held at -80 mV in the whole-cell recording configuration in the presence of tetrodotoxin (1 μM) to block voltage-gated sodium channels. Purkinje neuron somata were then injected with depolarizing current in +50 pA increments until calcium spike events were noted. This amount of injected current was used as a correlate of dendritic excitability for all studies.

2.3.3 Phenotype analysis

Motor phenotype was analyzed by performance on a rotarod. This study was powered to detect a 25% improvement in motor performance, which was estimated to require at least 8 mice in each ATXN1[82Q] group. In order to eliminate sampling bias, entire litters of mice were randomly allocated to treatment groups used for all behavioral experiments. Since litter size is variable, this sometimes resulted in an unequal number of animals used in each experimental group, but all ATXN1[82Q] groups included at least 8 mice. For all experiments, mice were handled for three consecutive days starting at 25 days of age in order to acclimate to the experimenter and test environment. Mice were then trained on an accelerating rotarod (4 to 40 rpm, at a rate of 0.12 rpm/s) for three days followed by one training day at constant speed (24 rpm). Baseline rotarod performance is variable between individual cohorts of mice, so all experimental groups

were represented in each behavioral cohort. Despite baseline differences in performance between cohorts, we always observed impaired motor performance in ATXN1[82Q] mice compared to wild-type controls. In spite of controlling for testing time-of-day and experimenter, inherent biological variability in motor performance exists within both ATXN1[82Q] and wild-type mice. For this reason, all conditions for each experiment were included during each run of an experiment. It is therefore misleading to directly compare performance of either ATXN1[82Q] or wild-type mice across different experimental groups. Because of this inherent variability, mice were randomized into groups based on their baseline performance on the final day of training, and all groups were balanced by sex and mean group performance in order to establish a standard baseline within each behavior cohort. Drug or vehicle was then administered via water bottles for the duration of the experiment after the final day of training. Mice were tested for four or five days at a constant speed (24 rpm) starting at 35 days of age for the early time point, and most groups were re-tested at 98 days (14 weeks) of age for the long-term time point. Latency score was recorded as either the time taken before the animal fell off the bar, or if an animal made three full rotations on the rotating bar, to a maximum time of 300 seconds. Mice were maintained with water bottle delivery of drug for the duration of the behavioral experiment. After testing at the late time point, mice were sacrificed and brains preserved for analysis of drug concentrations. The tester remained blind to genotype and treatment condition during experimentation. Performance on the rotarod was analyzed with a two-way repeated-measures ANOVA by trial with Holm-Sidak multiple comparison test.

2.3.4 Water bottle delivery of pharmacologic agents

Baclofen was dissolved in drinking water at 350 μM for all studies. SKA-31 was dissolved in drinking water at 600 μM for all studies. Since SKA-31 is not easily water-soluble, drinking water also contained 0.05% β-(hydroxypropyl)-cyclodextrin and 40μL/L of 1N NaOH, and supplemented with up to 8% sucrose. Chlorzoxazone was dissolved in drinking water at 15 mM as described previously [131]. Similar to SKA-31, drinking water containing chlorzoxazone also contained 0.05% β-(hydroxypropyl)-cyclodextrin and 40 μL/L of 1N NaOH, and supplemented with up to 8% sucrose. For vehicle treatment, drinking water containing 0.05% β-(hydroxypropyl)-cyclodextrin, NaOH, and sucrose was used. Water bottles were changed twice weekly. Mice were treated with water bottles beginning at 28 days of age and maintained on water bottles for the duration of the experiment.

2.3.5 Mass spectrometry of brain tissue and blood plasma

LC/MS analysis for SKA-31, chlorzoxazone and baclofen was performed with a Waters Acquity UPLC (Waters, NY, USA) interfaced to a TSQ Quantum Access Max mass spectrometer (MS) (Thermo Scientific, Waltham, MA, USA).

2.3.5.1 SKA-31 mass spectrometry

Commercial SPE cartridges (Hypersep C18, 100 mg, 1 mL, Thermo Scientific) were conditioned with acetonitrile, 2×1 mL, followed by water 2×1 mL. After loading the SPE cartridges with plasma samples, they were washed with 2 mL of 20% acetonitrile in water and eluted with 2 mL of acetonitrile. Elute fractions were evaporated to dryness, reconstituted with 200 μL acetonitrile and used for LC-MS analysis. For brain samples 200 mg of tissue were homogenized thoroughly in 4.0 mL of acetonitrile using a T25

digital ULTRA-TURRAX® homogenizer (IKA® Works Inc., NC), centrifuged for 10 min at 4000 rpm, and the supernatant separated and evaporated. The residues were reconstituted in 200 µL acetonitrile and loaded onto the preconditioned SPE cartridges and then eluted as described above. Load and elute fractions were collected and evaporated to dryness. The residues were reconstituted with 200 µL acetonitrile and used for LC-MS analysis on an Acquity UPLC BEH C-18 column 1.7 µM, 2.1 X 50 mM (Waters) using an isocratic mobile phase (45% acetonitrile and 55% water containing 0.1% formic acid) with a flow rate of 0.25 ml/min. Under these conditions SKA-31 had a retention time of 1.17 min. Mass conditions: heated electrospray ionization (HESI II) in positive ion mode, capillary temperature 350°C, vaporizer temperature: 325°C, spray voltage 4000 V, sheath gas pressure (N_2) 30 units, SKA-31 was analyzed by the selective reaction monitoring (SRM) transition of its molecular ion peak 201.04 (M+1) into 115.16 *m/z*.

2.3.5.2 Baclofen mass spectrometry

Baclofen was extracted by plasma precipitation; 1.0 mL ethanol was added to 200 µL plasma and the resulting precipitate vortexed for 30 sec. Samples were the centrifuged for 5 min at 4000 rpm, the supernatant separated and evaporated to dryness under a constant air flow. The residues were reconstituted with 200 µL water:acetonitrile (1:1) and used for LC-MS analysis. For brain samples 200 mg of tissue were homogenized thoroughly in 4.0 mL of acetonitrile using a T25 digital ULTRA-TURRAX® homogenizer, centrifuged for 10 min at 4000 rpm, and the supernatant separated and evaporated. The residues were reconstituted with 200 µL acetonitrile and used for LC-MS analysis on an Acquity UPLC BEH C-8 column 1.7 µM, 2.1 X 150 mM (Waters) using an isocratic

mobile phase (10% acetonitrile and 90% water containing 0.1% formic acid) with a flow rate of 0.20 ml/min. Under these conditions baclofen had a retention time of 2.1 min. Mass conditions: Heated electrospray ionization (HESI II) in positive ion mode, capillary temperature 300°C, vaporizer temperature: 250°C, spray voltage 3000 V, sheath gas pressure (N_2) 35 units, baclofen was analyzed by the SRM transition of its molecular ion peak 214.04 (M+1) into 151.03 *m/z*.

2.3.5.3 Chlorzoxazone mass spectrometry

Chlorzoxazone was extracted by plasma precipitation; 3.0 mL acetonitrile was added to 200 µL plasma, diluted with 200 µL of water and the resulting precipitate vortexed for 30 sec. Samples were then centrifuged for 5 min at 4000 rpm, the supernatant separated and evaporated to dryness. The residues were reconstituted with 200 µL water:acetonitrile (1:1) and used for LC-MS analysis. For brain samples 200 mg of tissue were homogenized thoroughly in 4.0 mL of acetonitrile using a T25 digital ULTRA-TURRAX® homogenizer, centrifuged for 10 min at 4000 rpm, and the supernatant separated and evaporated. The residues were reconstituted with 200 µL acetonitrile and used for LC-MS analysis on a Acquity UPLC BEH C-18 column 1.7 µM, 2.1 X 50 mM (Waters) using mobile phase gradient varying from of 5% acetonitrile and 95% water both containing 0.1% formic acid (0-1.5 min.) to 30% acetonitrile and 70% water (1.51-5.0 min.) and back to 5% acetonitrile and 95% water (5.01-6.0 min.) with a flow rate of 0.20 ml/min. Under these conditions chlorzoxazone had a retention time of 2.7 min. Mass conditions: Heated electrospray ionization (HESI II) in negative ion mode, capillary temperature 300°C, vaporizer temperature: 250°C, spray voltage 3000 V,

sheath gas pressure (N_2) 25 units, chlorzoxazone was analyzed by the SRM transition of its molecular ion peak 167.99 (M-1) into 132.07 *m/z*.

2.3.6 Molecular layer thickness measurements

Mice were anesthetized under isoflurane inhalation and brains were removed, fixed in 1% paraformaldehyde for 1 hour, and then placed in 30% sucrose in PBS for 48 hours. Parasagittal sections of 14 μm were made on a CM1850 cryostat (Leica). To label Purkinje neurons, rabbit anti-calbindin (1:200, Cat. no. 13176, Cell Signaling) and goat anti-rabbit Alexa488-conjugated secondary (1:200, Ref. no. A11008, Life Technologies Invitrogen) or goat anti-rabbit Alexa594-conjugated secondary (1:200, Ref. no. A21125, Life Technologies Invitrogen) were used. Sections were imaged using an Axioskop 2 plus microscope (Zeiss) using CellSens software (Olympus) at 10x magnification. To measure thickness of the molecular layer, the major fissure was identified and captured. Using CellSens, a 100 μm line was drawn down the opening of the fissure. Next, a perpendicular line was drawn from the end of the first line on the fissure and along the molecular layer of the closest Purkinje neuron, to the center of the soma of this neuron. Molecular layer thickness was defined as the distance of this perpendicular line and was recorded for both lobule 5 and lobule 6. For each animal, two measurements were averaged in order to limit variability from slicing or mounting artifacts. Sample preparation, imaging, and analysis were performed with the experimenter blind to genotype.

2.3.7 Review of patient charts

Patients were selected from the University of Michigan Ataxia Clinic. All patients seen between January 2014 and December 2016 with a diagnosis of SCA1, SCA2, SCA6,

SCA7, SCA8, and SCA13, where prominent Purkinje neuron involvement is noted at autopsy, and for whom follow up data were available as of December 2016, were included in this analysis. Patient SARA scores were obtained prior to beginning treatment with chlorzoxazone and baclofen and were measured at all subsequent follow up visits. While patient SARA scores were recorded as part of their clinical care, the primary intent of this retrospective review was to determine the tolerability of combined baclofen and chlorzoxazone treatment. Clinical drug information databases discourage combined treatment with chlorzoxazone and baclofen[132]. In addition, the Beers Criteria of the American Geriatrics Society also discourages treatment with chlorzoxazone[133]. For patients who were maintained on this combination, SARA scores were charted at all follow up visits and are reported until December 2016, through which IRB approval was granted. In order to look for signal for therapeutic benefit, we identified the minimum SARA score relative to the SARA score recorded prior to initiation of medications. Over follow up visits, some patients showed a reduction in SARA score following which they had worsening symptoms, while other patients continued a decline in SARA score across serial visits. The goal of reporting patient SARA scores is to identify whether there is potential benefit in order to justify future randomized controlled clinical trials.

Approval for retrospective review of patient charts seen through the University of Michigan Ataxia Clinic was submitted to the Institutional Review Board (IRB) for human subjects. The IRB reviewed the study application and determined that it is exempt from ongoing IRB review, per the federal exemption category: Exemption #4 of the 45 CFR 46.101.(b): Research involving the collection or study of existing data, documents, records, pathological specimens, or diagnostic specimens, if these sources are publicly

available or if the information is recorded by the investigator in such a manner that subjects cannot be identified, directly or through identifiers linked to the subjects. Approval was granted for review of records through December 2016.

2.3.8 Statistical analysis

Statistical significance for electrophysiology data was assessed by either unpaired Student's t-test, paired Student's t-test, or Fisher's exact test with Bonferroni post-correction for multiple comparisons. For behavioral studies, a two-way ANOVA with Holm-Sidak post-correction for multiple comparisons was used. Data were considered significant if the adjusted $p<0.05$. Data are expressed as mean ± standard error of the mean, unless otherwise specified. Data were analyzed using SigmaPlot (Systat Software, Inc.), GraphPad Prism (GraphPad Software, Inc.) and Excel (Microsoft Corp.).

2.4 Results

2.4.1 ATXN1[82Q] Purkinje neurons display both and absence of repetitive spiking and dendritic hyperexcitability

Alterations in Purkinje neuron spiking have been demonstrated previously in the ATXN1[82Q] mouse model of SCA1 [71]. In order to confirm these findings, I performed cell-attached electrophysiological recordings in acute cerebellar slices from Purkinje neurons from ATXN1[82Q] and wild-type mice at 5 weeks of age (Fig 2.1A-B). As demonstrated previously, I observed that a significant portion of ATXN1[82Q] Purkinje neurons displayed an absence of repetitive spiking when compared to wild-type neurons, which uniformly displayed repetitive spiking (Fig 2.1C; firing frequency 52.2 ± 5.6 Hz, coefficient of variation of spiking 0.112 ± 0.008). In the whole-cell recording configuration, these non-firing cells showed a

depolarized membrane potential of -41 mV (Fig 2.1D), similar to what has been previously described [71]. These alterations in membrane excitability are associated with a reduction in the amplitude of the after-hyperpolarization (AHP) of the action potential (Fig 2.1E-F), which is generated by calcium-activated potassium channels [17, 18, 71]. Since loss of potassium channels is associated with increased dendritic excitability[91], I also determined whether Purkinje neuron dendrites from ATXN1[82Q] mice were hyperexcitable. Purkinje neurons were held in the whole-cell recording configuration at -80 mV in the presence of tetrodotoxin (TTX, 1 µM) in order to block voltage-gated sodium channels, and were injected with incremental steps of depolarizing current until dendritic calcium spikes were detected. In response to depolarizing current injection, ATXN1[82Q] Purkinje neurons displayed a lower threshold to evoke dendritic calcium spikes, a correlate of increased dendritic excitability (Fig 2.1G-I) [91]. Input resistance was not different between wild-type and ATXN1[82Q] Purkinje neurons (data not shown). Therefore, Purkinje neurons from ATXN1[82Q] mice exhibit a phenotype of increased membrane excitability resulting in both altered spiking and increased dendritic excitability in association with membrane depolarization and a reduction in the amplitude of the AHP.

2.4.2 Potassium channel-activating compounds restore spiking in non-firing ATXN1[82Q] Purkinje neurons

Alterations in Purkinje neuron spiking in ATXN1[82Q] mice are associated with reductions in expression and function of large-conductance calcium activated potassium (BK) channels and subthreshold-activated potassium channels at the onset of motor impairment [71]. In order to determine whether the alterations in physiology which

accompany these changes in channel function can be improved pharmacologically, I performed a targeted screen of potassium channel-activating compounds with known roles in membrane repolarization or increasing AHP amplitude. A combination of chlorzoxazone and baclofen restored tonic spiking to non-firing ATXN1[82Q] Purkinje neurons in acute cerebellar slices (Fig 2.2B). Chlorzoxazone is a known activator of calcium-activated potassium (K_{Ca}) channels, both BK and the related small-conductance calcium activated potassium (SK) channel [83, 131, 134, 135]. Baclofen, a $GABA_B$ agonist, potentiates a subthreshold-activated potassium channel current in Purkinje neurons likely mediated by G-protein-coupled inwardly rectifying potassium (GIRK) channels[136]. In order to confirm whether K_{Ca} channels are a target for restored spiking in ATXN1[82Q] Purkinje neurons, I tested other known activators of K_{Ca} channels in the presence of baclofen to determine their ability to restore spiking. Spiking was restored in ATXN1[82Q] Purkinje neurons that displayed no spontaneous spiking when co-perfused with SKA-31 (Fig 2C) or 1-EBIO (Fig 2D), two known K_{Ca} channel activators [137, 138], and baclofen (summarized in Fig 2.2E). The firing frequency that was restored was, however, significantly lower than what is normally seen in wild-type Purkinje neurons (Chlorzoxazone + baclofen, 7.25 ± 3.21 Hz; SKA-31 + baclofen, 10.13 ± 1.86 Hz; 1-EBIO + baclofen, 2.86 ±0.54 Hz). Effects on spiking persisted for the duration of the experiment, in some cases more than 30 minutes (data not shown). Chlorzoxazone, SKA-31, or baclofen alone were unable to consistently restore spiking in non-firing ATXN1[82Q] Purkinje neurons (Fig 2.2E). This suggests that K_{Ca} and

subthreshold activated potassium channels must be targeted simultaneously in order to restore spiking in non-firing ATXN1[82Q] Purkinje neurons.

2.4.3 K_{Ca} activators and baclofen enhance the AHP and repolarize the membrane potential of ATXN1[82] Purkinje neurons

In order to determine the mechanism by which potassium channel activators restore spiking, I examined changes in membrane potential produced by these pharmacological agents. In the whole-cell configuration of the patch-clamp technique, baclofen (10 μM) repolarized the membrane potential of depolarized ATXN1[82Q] Purkinje neurons from -41 mV to -52 mV (Fig 2.3A). As shown previously [71], a combination of TTX and cadmium, to respectively block voltage-gated sodium and calcium channels, restored the normal resting membrane potential of ATXN1[82Q] Purkinje neurons (Fig 2.3A). These results suggest that subthreshold-activated potassium channels contribute in part to the depolarized potential of ATXN1[82Q] Purkinje neurons. The SK channel-activating compound SKA-31 extended the duration of the AHP in ATXN1[82Q] Purkinje neurons, suggesting that K_{Ca}-activating compounds (shown in Fig 2.2) likely act on the AHP to support repetitive spiking (Fig 2.3C-D). The net effect of baclofen and chlorzoxazone was to greatly enhance repolarization during the interspike interval (Fig 2.3E-H). However, the duration of the AHP is extended in ATXN1[82Q] Purkinje neurons perfused with chlorzoxazone and baclofen, consistent with the reduced firing frequencies in cells whose spiking is restored (see Fig 2.2B-E). This indicates that increasing the amplitude of the AHP through activation of K_{Ca} channels, in addition to membrane repolarization through activation of subthreshold-

activated potassium channels, is required to facilitate repetitive spiking in depolarized ATXN1[82Q] Purkinje neurons.

2.4.4 Chlorzoxazone and baclofen, but not SKA-31 and baclofen, sustains improvement in motor dysfunction in ATXN1[82Q] mice

Prior studies in BK channel mutant mice have demonstrated alteration in Purkinje neuron spiking similar to what we observe in ATXN1[82Q] mice [18]. Both pharmacologic and genetic models of BK channel dysfunction also exhibit profound motor impairment referable to cerebellar dysfunction [18, 42, 139]. I therefore sought to determine whether agents which restore spiking could improve motor impairment in ATXN1[82Q] mice. In order to confirm oral absorption of chlorzoxazone, SKA-31, and baclofen, my collaborators and I performed mass spectrometry analysis of whole brain and plasma samples following administration of these agents through drinking water. All three agents achieved significant brain and plasma levels (SKA-31 brain 1.83 ± 1.30 μM, SKA-31 plasma 39.39 ± 8.05 nM; chlorzoxazone brain 4.80 ± 1.72 μM, chlorzoxazone plasma 4.41 ± 2.05 μM; baclofen brain 377.35 ± 58.50 nM, baclofen plasma 3.06 ± 0.51 μM) that reached concentrations previously shown to be important for engagement of their respective targets (Fig 2.4B-D) [131, 136, 137], although the achieved dose of SKA-31 is lower than the maximal concentration achieved through intraperitoneal injection [137]. These agents were therefore administered through drinking water in order to explore the relationship between their ability to improve Purkinje neuron physiology in cerebellar slices and ameliorate motor dysfunction.

ATXN1[82Q] and age-matched wild-type control mice were administered either chlorzoxazone (15 mM in drinking water) and baclofen (350 μM in drinking water) or SKA-31 (600 μM in drinking water) and baclofen (350 μM in drinking water) at 5 weeks, at the onset of motor dysfunction [71, 104] and tested for both short- and long-term improvement in motor dysfunction. After one week of treatment, SKA-31 and baclofen significantly improved motor performance in ATXN1[82Q] mice when compared to vehicle-treated controls (Fig 2.4E). Similarly, following one week of treatment with a combination of chlorzoxazone and baclofen there was a significant improvement in motor performance in ATXN1[82Q] mice (Fig 2.4F). In control studies, neither SKA-31 alone nor chlorzoxazone alone improved short-term motor performance in ATXN1[82Q] mice (Fig. 2.4G). These results suggest that at a time point corresponding to the loss of spiking in ATXN1[82Q] Purkinje neurons, agents which restore spiking are able to improve motor dysfunction.

In prior studies, our laboratory has observed that spiking in ATXN1[82Q] Purkinje neurons is restored due to homeostatic remodeling associated with Purkinje neuron atrophy [71]. In order to determine whether potassium channel activators continue to provide benefit at a stage of disease when there is significant Purkinje neuron atrophy, mice were administered these compounds through drinking water from 5 weeks of age until 14 weeks of age and motor performance was tested. ATXN1[82Q] mice treated with SKA-31 and baclofen displayed impaired motor function at 14 weeks of age (Fig 2.4H), while ATXN1[82Q] mice treated with chlorzoxazone and baclofen showed a sustained improvement in motor performance (Fig 2.4I). These data suggest that although SKA-31 and chlorzoxazone, in combination with baclofen, have a similar role

in restoring spiking, chlorzoxazone but not SKA-31 engages a different target which allows for maintained improvement in motor dysfunction.

2.4.5 K_{Ca} activator and baclofen co-administration does not affect dendritic degeneration in ATXN1[82Q] mice

Chlorzoxazone and baclofen co-administration results in a sustained improvement in motor function in ATXN1[82Q] mice, while SKA-31 and baclofen co-administration does not result in a similar improvement upon prolonged treatment. One possibility for this discrepancy is that chlorzoxazone may promote neuroprotection in ATXN1[82Q] mice through activation of BK channels or another molecular target, while sole activation of SK2 channels via SKA-31 does not promote the same neuroprotective pathway. In order to determine whether this is the case, I performed measures of molecular layer thickness in ATXN1[82Q] and wild-type mice treated with a combination of SKA-31 and baclofen or chlorzoxazone and baclofen after prolonged water-bottle administration of these compounds. At 14 weeks of age, after 10 weeks of treatment with these compounds and when dendritic atrophy is clearly present in ATXN1[82Q] mice [140], SKA-31 and baclofen co-administration did not reduce dendritic degeneration (Figure 2.5A-B). Similarly, chlorzoxazone and baclofen co-administration did not reduce dendritic degeneration in ATXN1[82Q] mice, although this combination of compounds did significantly increase thickness of the molecular layer in wild-type animals for unknown reasons (Figure 2.5C-D). Overall, these studies indicate that ATXN1[82Q] mice treated with chlorzoxazone and baclofen did not experience sustained improvements in motor function because of a neuroprotective effect of these drugs, but rather that dendritic degeneration is still fully present in ATXN1[82Q] mice treated with

either chlorzoxazone and baclofen or SKA-31 and baclofen after prolonged treatment. This suggests another mechanism for improved motor performance independent of dendritic degeneration upon potassium channel activation.

2.4.6 Chlorzoxazone and baclofen reduce dendritic hyperexcitability in ATXN1[82Q] mice by activating subthreshold-activated potassium channels

In recent work, our laboratory has demonstrated that dendritic hyperexcitability begins at the onset of motor dysfunction in ATXN1[82Q] Purkinje neurons and is persistently elevated in spite of relative normalization of spiking in atrophic ATXN1[82Q] Purkinje neurons [74, 121]. As illustrated previously, ATXN1[82Q] Purkinje neurons required a significantly lower amount of injected current to elicit dendritically-generated calcium spikes than wild-type neurons (Fig 2.6A-B) with no change in input resistance (Wild-type + TTX 35.1 ± 4.4, ATXN1[82Q] + TTX 43.1 ± 1.9, p=0.154) Surprisingly, chlorzoxazone (Fig 2.6E and 2.6G) but not SKA-31 (Fig 2.6D) significantly increased the threshold of injected current necessary to elicit dendritic calcium spikes in ATXN1[82Q] Purkinje neurons. The combination of chlorzoxazone and baclofen restored dendritic excitability to near wild-type levels (Fig 2.6F), suggesting that this combination of compounds improves both spiking and dendritic hyperexcitability in ATXN1[82Q] Purkinje neurons. Chlorzoxazone, SKA-31, and baclofen did not alter input resistance in these recordings (ATXN1[82Q] + TTX 51.4 ± 5.3, ATXN1[82Q] + TTX + Chlorzoxazone 49.0 ± 5.3, p=0.705; ATXN1[82Q] + TTX 47.8 ± 6.8, ATXN1[82Q] + TTX + SKA-31 50.8 ± 9.4, p=0.777; ATXN1[82Q] + TTX 46.4 ± 4.3, ATXN1[82Q] + TTX + Baclofen + Chlorzoxazone 48.2 ± 6.3, p=0.590).

SKA-31 is a highly selective activator of SK2 and IK channels [137]. The targets of chlorzoxazone are, however, largely unknown. I therefore sought to determine the ion-channel targets of chlorzoxazone's effect on dendritic excitability. Chlorzoxazone does not likely act through SK channels in the dendrites, since SKA-31 had no effect on dendritic excitability. When tested in the presence of barium (50 μM), which at this dose selectively blocks subthreshold-activated inwardly-rectifying potassium (K_{ir}) channels [71, 141-145], the effect of chlorzoxazone on reducing dendritic excitability was prevented (Fig 2.6G) (input resistance ATXN1[82Q] + TTX + Barium 47.8 ± 6.8, ATXN1[82Q] + TTX + Barium + Chlorzoxazone 57.1 ± 3.8, p=0.173). This suggests that chlorzoxazone likely activates K_{ir} channels in the dendrites of ATXN1[82Q] Purkinje neurons to reduce dendritic hyperexcitability. One possible candidate channel is K_{ir}6.2, an ATP-sensitive potassium channel, which is expressed in cerebellar Purkinje neurons[146]. Tolbutamide, which blocks K_{ir}6.2, partially occludes the effect of chlorzoxazone on dendritic excitability (input resistance ATXN1[82Q] + Chlorzoxazone 47.5 ± 4.7, ATXN1[82Q] + Chlorzoxazone + Tolbutamide 47 ± 5.6). The partial effect of tolbutamide suggests that K_{ir}6.2 is a likely target for chlorzoxazone in ATXN1[82Q] Purkinje neuron dendrites, but that other targets may still remain.

I also sought to determine the molecular target of baclofen on dendritic excitability. Although baclofen is known to activate G-protein coupled K_{ir} channels (GIRK) in Purkinje neurons, barium (500 μM) did not prevent the effect of baclofen in reducing the threshold to elicit dendritic calcium spikes (Fig 2.6H) (input resistance ATXN1[82Q] + TTX +Barium 45.9 ± 5.5, ATXN1[82Q] + TTX + Barium + Baclofen 48.9 ± 5.7, p=0.588), suggesting that baclofen does not modulate dendritic excitability

through these channels in ATXN[82Q] Purkinje neurons. Since baclofen may act downstream of metabotropic glutamate receptor (mGluR) signaling [147], I sought to determine whether the effect of baclofen is dependent on mGluR activation. U73122, a phospholipase C inhibitor, did not prevent the effect of baclofen on dendritic excitability (Fig 2.6H) (input resistance ATXN1[82Q] + TTX 41.4 ± 9.1, ATXN1[82Q] + TTX + U73122 39.1 ± 8.3, p=0.478), suggesting that the effect of baclofen does not require mGluR activation in this context [148]. Cesium, a non-selective potassium channel inhibitor, prevents the effect of baclofen when included in the recording pipette, confirming that baclofen activates a potassium channel conductance in ATXN1[82Q] Purkinje neurons (Fig 2.6H) (input resistance ATXN1[82Q] + TTX + CsCl 78.3 ± 8.0, ATXN1[82Q] + TTX + CsCl + Baclofen 77.8 ± 8.1, p=0.931). Tetraethlyammonium (TEA) does not block the effect of baclofen (Fig 2.6H), excluding K_v3 and BK channels as a target (input resistance ATXN1[82Q] + TTX + TEA 30.9 ± 4.2, ATXN1[82Q] + TTX + TEA + Baclofen 31 ± 2.9, p=0.971). Overall, these data suggest that baclofen activates a relatively barium-insensitive subthreshold-activated potassium channel in ATXN1[82Q] Purkinje neuron dendrites to reduce dendritic hyperexcitability.

2.4.7 Chlorzoxazone and baclofen co-administration is tolerated in SCA patients and improves symptoms

Chlorzoxazone and baclofen are both FDA-approved compounds to reduce muscle spasticity, and chlorzoxazone has previously been demonstrated to reduce downbeat nystagmus in patients with cerebellar ataxia [149]. In mouse models of SCA1, SCA2, and SCA6, ataxias which all display prominent Purkinje neuron involvement, potassium channel dysfunction is present [70, 71, 78]. Since pyramidal signs are a feature of

many SCAs, and some patients with SCA6 can exhibit downbeat nystagmus, patients seen through the University of Michigan Ataxia Clinic with either pyramidal signs or downbeat nystagmus were offered a combination of baclofen and chlorzoxazone. All patients were interested in a trial of the medications. Since the American Geriatrics Society discourages combining muscle relaxants through the updated Beers criteria, it is important to know whether the combination of baclofen and chlorzoxazone is tolerated by patients with ataxia. In order to determine whether the combination of chlorzoxazone and baclofen is tolerated by SCA patients, we reviewed medical records of patients with SCA1 and other SCAs with prominent Purkinje neuron involvement who were seen through the Ataxia Clinic. Patients were started on one agent at a time and the dose was gradually increased to a target dose of 10 mg TID for baclofen and 500 mg TID of chlorzoxazone. If patients could not tolerate 500 mg TID of chlorzoxazone, a lower dose of 250 mg TID was attempted. Patients for whom follow up information was present as of December 2016 are listed in Table 1. Of 17 patients, 4 could not tolerate one of either baclofen or chlorzoxazone due to side effects (Table 1). The Scale for the Assessment and Rating of Ataxia (SARA) is a validated clinical measure of ataxia, with higher scores indicating more prominent ataxia [150]. SARA scores were recorded for all patients prior to beginning treatment and were assessed during subsequent visits. The average interval between visits for patients in the Ataxia Clinic is 6 months. Patients reported subjective improvement in symptoms over time which was corroborated by the reduction in SARA score for individual patients (Fig 2.7A). Patients reported improvement in symptoms that was delayed by weeks, after achieving maximum tolerated doses of medication. In order to assess the maximum benefit, initial SARA

scores were compared to minimum SARA scores subsequent to initiation of chlorzoxazone and baclofen. The SARA score subsequent to initiation of chlorzoxazone and baclofen was significantly lower than the score prior to initiating medication (Fig 2.7B; SARA prior 10.31 ± 4.22 [mean ± standard deviation], SARA minimum 7.85 ± 4.85). Overall, these results indicate that chlorzoxazone and baclofen co-administration is tolerated and may improve symptoms in forms of SCA with prominent cerebellar Purkinje neuron involvement.

2.5 Discussion

In the current study, I demonstrate that Purkinje neuron membrane excitability is altered in ATXN1[82Q] mice, and that the resulting changes in physiology can be targeted by potassium channel activators. My studies also illustrate that targeting somatic spiking is only effective for short-term improvements in motor function. Targeting both spiking and dendritic hyperexcitability is associated with sustained improvement in motor dysfunction. Finally, these studies illustrate that patients with ataxia can tolerate co-administration of baclofen and chlorzoxazone, and that this combination may improve motor dysfunction.

Growing evidence suggests that potassium channel dysfunction may be a feature of many cerebellar ataxias. In mouse models of SCA1, SCA2, and SCA3, alterations in Purkinje neuron spiking are associated with changes in potassium channel function due to either transcriptional downregulation (SCA1 and SCA2) [70, 71] or altered potassium channel kinetics (SCA3) [77]. In the present study, I demonstrate that these changes in potassium channel function in ATXN1[82Q] mice may be targeted by potassium channel-activating compounds. The present study is the first to illustrate that not only do

potassium channel-activating compounds improve motor dysfunction in a mouse model of SCA1, but also show therapeutic promise in human SCA. These studies also illustrate that more than one potassium channel target must be engaged in order to sustain improvements in motor dysfunction.

Previous studies have focused on restoring somatic spiking as an approach to improve motor function in mouse models of ataxia [71, 76, 78, 104]. In the present study, I show that improving Purkinje neuron spiking indeed improves motor performance in the short-term, an effect which has been previously illustrated using K_{Ca} activators in a mouse model of SCA2 [76]. The magnitude of the improvement in motor dysfunction is not to wild-type levels likely due to the inability of these compounds to restore normal firing frequency. However, restoring Purkinje neuron spiking alone is not sufficient to improve motor dysfunction in the long-term. My studies illustrate that in association with the additional reduction in dendritic hyperexcitability, longer term benefit can be sustained in a mouse model of SCA1. Since the targets of chlorzoxazone are unknown, it is possible that other mechanisms in addition to reducing dendritic excitability may play a role in mediating the behavioral improvement demonstrated by chlorzoxazone. While K_{Ca} activating-compounds effectively modulate Purkinje neuron spike frequency and regularity, my data suggest that additional engagement of subthreshold-activated potassium channels may be necessary for the sustained improvement of motor impairment in ataxia. The present studies demonstrate that both baclofen and chlorzoxazone reduce dendritic hyperexcitability in ATXN1[82Q] mice, while SKA-31 does not. Significantly, in this study, improvement in motor dysfunction was sustained by chlorzoxazone and baclofen even at a time point in ATXN1[82Q] mice when there is

significant Purkinje neuron dendritic degeneration. Baclofen and chlorzoxazone both appear to activate different subthreshold-activated potassium channels to reduce Purkinje neuron dendritic hyperexcitability. Addressing intrinsic dendritic hyperexcitability is likely an important aspect of altered physiology which must be addressed in order to sustain benefit in the treatment of SCA, consistent with the critical role that intrinsic dendritic excitability plays in regulating synaptic integration [94]. It is important to note that we and others have demonstrated that in association with dendritic degeneration, ATXN1[82Q] Purkinje neurons display increased subthreshold-activated potassium channel currents [71, 151] that affect spiking. Nevertheless, agents that reduce dendritic excitability through targeting these or other subthreshold-activated potassium channels are beneficial in maintaining improvements in motor dysfunction at a stage of disease associated with dendritic degeneration. It is therefore important to consider whether sustained improvements in behavioral dysfunction are achieved in a neurodegenerative disorder where, depending on disease stage, therapeutic targets may vary. These findings also highlight the importance of considering not only the acute effects of pharmacological agents on motor function, but also the durable effects of these compounds. Long-term administration of these compounds enabled the identification of a role for dendritic hyperexcitability in motor impairment in ATXN1[82Q] mice.

My studies assess alterations in intrinsic Purkinje neuron excitability which are associated with disrupted spiking and dendritic hyperexcitability. Synaptic alterations, specifically in metabotropic glutamate receptor (mGluR) signaling, are associated with motor impairment in mouse models of SCA1[147, 152]. In a lentivirus model of SCA1, direct

cerebellar application of baclofen produces short-term improvements in motor performance [147]. This was attributed to the ability of baclofen to potentiate mGluR1 signaling. In contrast, in association with dendritic degeneration, prolonged and increased mGluR1 responses are now described in models of both SCA1 and SCA2 [152, 153]. At a stage of disease associated with significant dendritic degeneration, inhibiting mGluR1 improves motor function in ATXN1[82Q] mice [152]. In our studies, although baclofen's ability to reduce dendritic hyperexcitability appears to be independent of mGluR signaling, the impairment of motor function upon long-term treatment with baclofen and SKA-31 may represent baclofen mediated activation of mGluR1 that is detrimental to Purkinje neuron physiology. It may therefore be important to target dendritic subthreshold-activated potassium channels without engaging mGluR signaling. Also, the combination of baclofen and chlorzoxazone in patients is dose limited due to sedation. Not all patients were able to tolerate the target dose of the combination. It is therefore important to consider developing subthreshold-activated potassium channel activators, which can ideally also engage K_{Ca} channels, possibly using chlorzoxazone as a template.

Centrally-acting muscle relaxants, such as baclofen and chlorzoxazone, have tolerability concerns in patients with neurological disorders and older adults [132, 133]. It is therefore important to consider whether these compounds are appropriate for the treatment of SCA patients. In this patient population, where motor impairment is prominent, we found that baclofen and chlorzoxazone were tolerated in the majority of patients, and these patients persisted in using these drugs. This is an important finding, and is encouraging for design of a future clinical trial with these agents. Furthermore,

treatment with a combination of chlorzoxazone and baclofen is not only tolerated by SCA patients but may also improve symptoms. Retrospective review of patient records and unblinded assessments in patients are, however, susceptible to bias. Given the duration of follow up, and the sustained improvements in patients where the natural history of disease is progressive [154, 155], our findings in patients are encouraging for the utility of potassium channel activators in the treatment of symptoms in patients with SCA. It is possible that changes in Purkinje neuron membrane excitability are present in many etiologies of SCA, and that the ion-channel targets of chlorzoxazone and baclofen are relevant targets in these SCAs as well. This possibility is supported by recent clinical trials with the compound riluzole, whose targets include K_{Ca} channels [110, 111]. Although riluzole shares common ion-channel targets with chlorzoxazone and baclofen, its effect on improving motor dysfunction is likely to be modest, as it has a relatively low potency for both K_{Ca} channels and subthreshold-activated potassium channels [112, 113]. Compounds with increased target specificity and potency are likely to be more effective than riluzole. A clinical trial with a combination of chlorzoxazone and baclofen should be considered for SCAs with prominent Purkinje neuron involvement, as this combination of compounds targets K_{Ca} channels with moderate potency and effectively targets subthreshold-activated potassium channels. While chlorzoxazone and baclofen appear promising, agents with added target specificity and potency could be designed with these targets in mind.

2.6 Acknowledgements

The work in this chapter was supported by the NIH R01NS085054 (V.G.S.). I would like to thank Ravi Chopra for his assistance in performing dendritic excitability experiments in the ATXN1[82Q] mice. Vikrant Singh and Heike Wulff performed the mass spectrometry analysis of chlorzoxazone, SKA-31, and baclofen from brain tissue and plasma. Vikram Shakkottai and Geoffrey Murphy provided thoughtful comments and suggestions in the design and analysis of these studies. I would finally like to thank Aaron Wasserman, James Dell'Orco, Annie Zalon, Brandon Lee, Alexi Vasbinder, and Allison Sylvia for technical support in these studies.

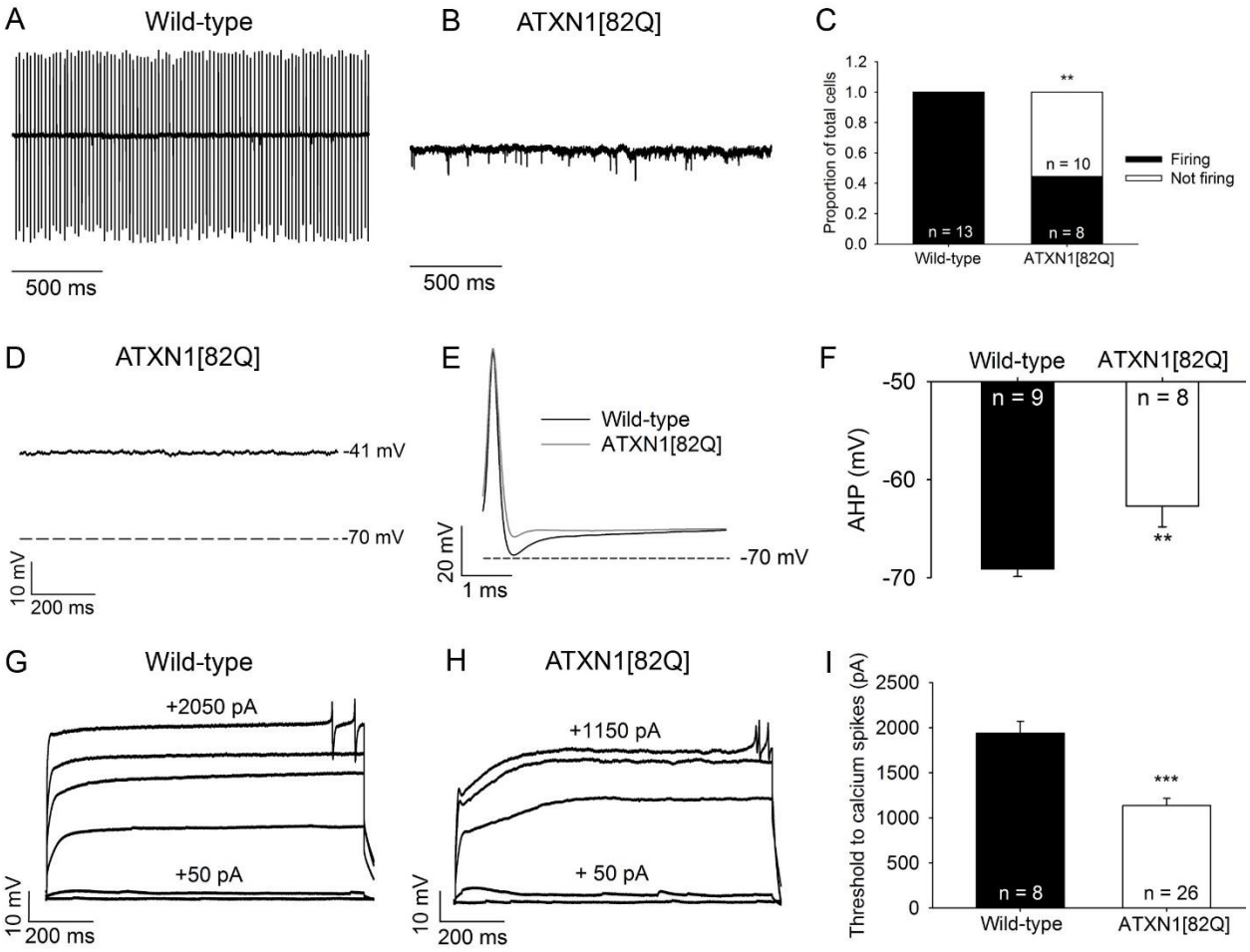

Figure 2.1 ATXN1[82Q] Purkinje neurons display both and absence of repetitive spiking and dendritic hyperexcitability. (A) Representative spiking of a wild-type Purkinje neuron in the cell-attached recording configuration. **(B)** Representative trace of a non-spiking ATXN1[82Q] Purkinje neuron in the cell-attached recording configuration. **(C)** Summary of spiking and non-spiking Purkinje neurons from wild-type and ATXN1[82Q] mice. **(D)** Representative trace of a non-firing ATXN1[82Q] Purkinje neuron in the whole-cell recording configuration. These neurons display a depolarized resting membrane potential. **(E)** After-hyperpolarization (AHP) amplitude in wild-type and ATXN1[82Q] Purkinje neurons. **(F)** Summary of AHP amplitudes in wild-type and ATXN1[82Q] Purkinje neurons. **(G)** Representative trace of a wild-type Purkinje neuron held at -80 mV in the presence of tetrodotoxin. Upon injection of positive current in +50 pA increments, dendritic calcium spikes are noted. **(H)** Representative trace of dendritic calcium spike analysis from an ATXN1[82Q] Purkinje neuron. **(I)** Summary of the threshold of injected current required to elicit dendritic calcium spikes in wild-type and ATXN1[82Q] Purkinje neurons in the presence of tetrodotoxin. *p<0.05, **p<0.01, ***p<0.001, Fisher's exact test **(C)** or two-sample Student's t-test **(I)**.

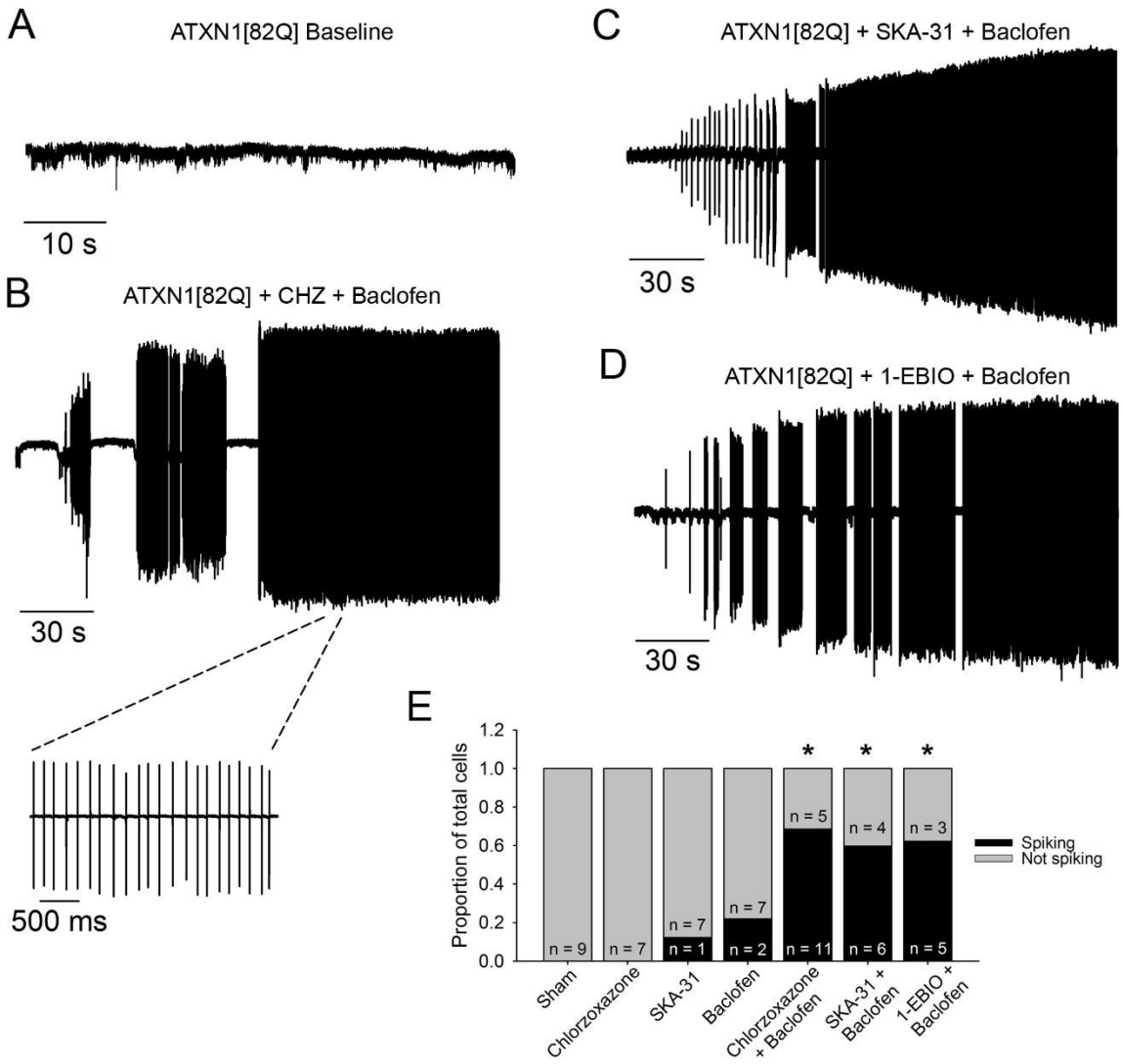

Figure 2.2 Potassium channel-activating compounds restore spiking in non-firing ATXN1[82Q] Purkinje neurons. (A) In a cell-attached recording configuration, the majority of ATXN1[82Q] Purkinje neurons are non-firing at 5 weeks of age. **(B)** Co-application of chlorzoxazone (CHZ, 50 µM) and baclofen (10 µM) restores repetitive spiking to non-firing ATXN1[82Q] Purkinje neurons (p=0.001). Inset of restored spiking with chlorzoxazone and baclofen is shown on an expanded time scale. **(C)** SKA-31 (10 µM) and baclofen (10 µM) co-application also restores spiking to non-firing ATXN1[82Q] Purkinje neurons (p=0.01), as does **(D)** 1-EBIO (100 µM) and baclofen (10 µM) (p=0.009). **(E)** Summary of data from figures B-D. *adjusted p<0.01 when compared to sham, Fisher's exact test with Bonferroni post-correction.

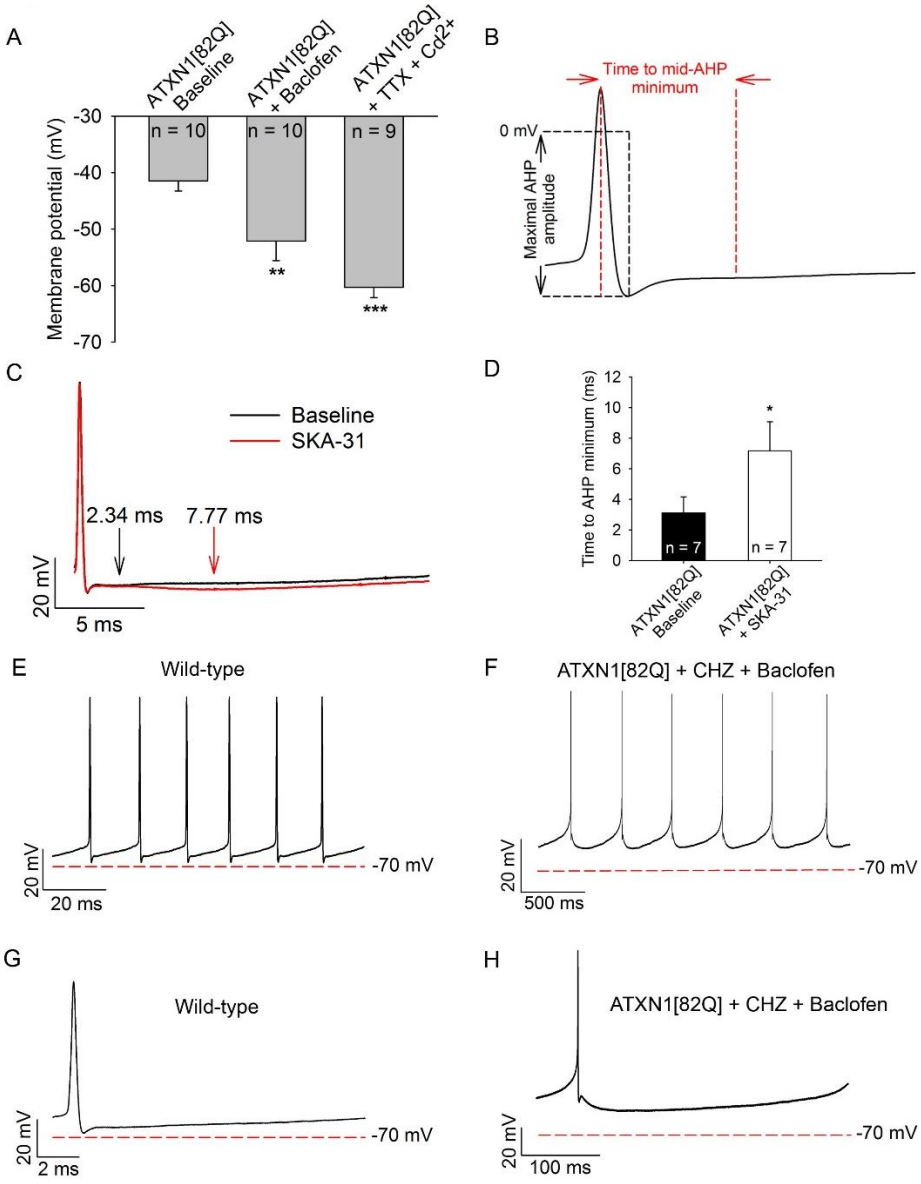

Figure 2.3 K_{Ca} activators and baclofen enhance the AHP and repolarize the membrane potential of ATXN1[82Q] Purkinje neurons. (A) Baclofen (10 µM) hyperpolarizes the membrane potential of depolarized ATXN1[82Q] Purkinje neurons to from -41 mV to -52 mV. Tetrodotoxin (1 µM) and cadmium (100 µM) repolarizes the membrane potential to -60 mV. **(B)** Protocol for analysis of the time to minimal mid-AHP and maximal AHP amplitude. **(C)** Representative trace of the AHP of an ATXN1[82Q] Purkinje neuron before (black trace) and after (red trace) SKA-31 perfusion (10 µM). The time to slow AHP minimum is denoted by arrows. **(D)** Summary of data from panel C. SKA-31 extends the duration of the AHP in ATXN1[82Q] Purkinje neurons (p=0.042). **(E)** Representative trace which displays the interspike interval during spontaneous firing of a baseline wild-type Purkinje neuron and **(F)** ATXN1[8Q] Purkinje neuron in the presence of chlorzoxazone (50 µM) and baclofen (10 µM). **(G)** Single interspike intervals of baseline wild-type and **(H)** ATXN1[82Q] Purkinje neurons in the presence of

chlorzoxazone and baclofen. *p<0.05, **p<0.01, ***p<0.001, paired Student's t-test. CHZ, chlorzoxazone.

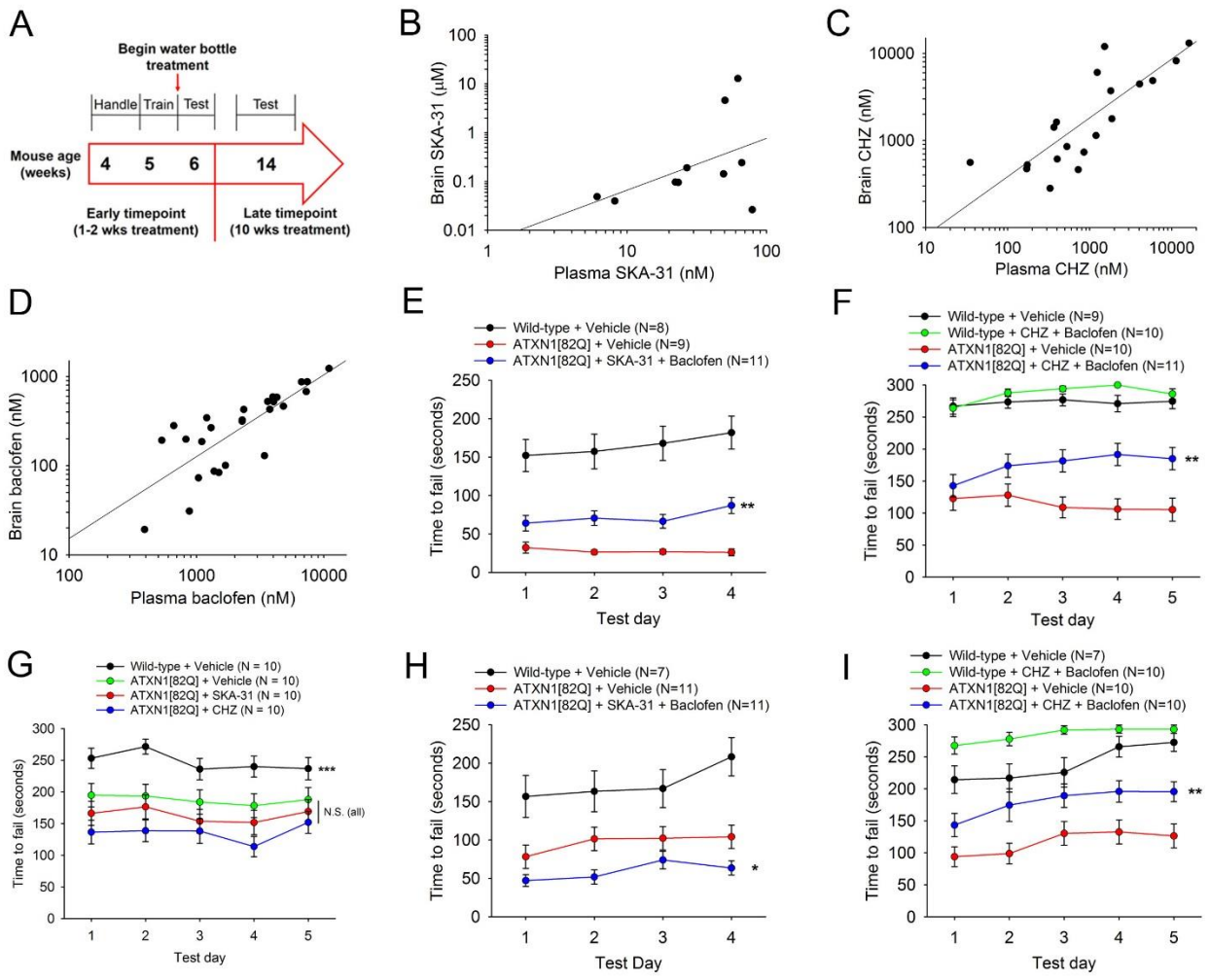

Figure 2.4 Chlorzoxazone and baclofen, but not SKA-31 and baclofen, sustains improvement in motor dysfunction in ATXN1[82Q] mice. (A) Drug administration and behavioral testing paradigm. **(B)** Correlated brain and plasma levels of SKA-31 are seen after administration through drinking water (R^2 = 0.1337). **(C)** Correlated brain and plasma levels of chlorzoxazone are seen after administration through drinking water (R^2 = 0.8904). **(D)** Correlated brain and plasma levels of baclofen are present after administration through drinking water (R^2 = 0.8591). **(E)** After one week of treatment, SKA-31 + baclofen improves motor performance in ATXN1[82Q] mice ($F(2, 113)=15.76$, $p<0.0001$) (Wild-type + Vehicle vs ATXN1[82Q] + Vehicle $p<0.0001$; Wild-type + Vehicle vs ATXN1[82Q] + SKA-31 + Baclofen $p<0.0001$; ATXN1[82Q] + Vehicle vs ATXN1[82Q] + SKA-31 + Baclofen $p=0.004$). **(F)** After one week of treatment, chlorzoxazone + baclofen improves motor performance in ATXN1[82Q] mice ($F(3, 156)=42.23$, $p<0.0001$) (Wild-type + Vehicle vs Wild-type + Chlorzoxazone + Baclofen $p=0.9726$; Wild-type + Vehicle vs ATXN1[82Q] + Vehicle $p<0.0001$; Wild-type + Vehicle vs ATXN1[82Q] + Chlorzoxazone + Baclofen $p<0.0001$; Wild-type + Chlorzoxazone + Baclofen vs ATXN1[82Q] + Vehicle $p<0.0001$; Wild-type + Chlorzoxazone + Baclofen vs ATXN1[82Q] + Chlorzoxazone + Baclofen $p<0.0001$; ATXN1[82Q] + Vehicle vs ATXN1[82Q] + Chlorzoxazone + Baclofen $p=0.0036$). **(G)** After one week of treatment, neither SKA-31 alone nor chlorzoxazone alone improve motor performance in

ATXN1[82Q] mice ($F(3,156)=9.142$,$p<0.0001$)(Wild-type + Vehicle vs ATXN1[82Q] + Vehicle $p=0.0315$; Wild-type + Vehicle vs ATXN1[82Q] + SKA-31 $p=0.011$; Wild-type + Vehicle vs ATXN1[82Q] + Chlorzoxazone $p<0.0001$; ATXN1[82Q] + Vehicle vs ATXN1[82Q] + SKA-31 $p=0.3856$; ATXN1[82Q] + Vehicle vs ATXN1[82Q] + Chlorzoxazone $p=0.0617$; ATXN1[82Q] + SKA-31 + ATXN1[82Q] + Chlorzoxazone $p=0.3856$). **(H)** After 10 weeks of treatment, mice treated with SKA-31 + baclofen show worsened motor performance compared to vehicle-treated controls ($F(2, 109)=36.73$, $p<0.0001$) (Wild-type vs ATXN1[82Q] + Vehicle $p=0.0005$; Wild-type vs ATXN1[82Q] + SKA-31 + Baclofen $p<0.0001$; ATXN1[82Q] + Vehicle vs ATXN1[82Q] + SKA-31 + Baclofen $p=0.0408$). **(I)** After 10 weeks of treatment, ATXN1[82Q] mice treated with chlorzoxazone + baclofen display sustained improvement in motor performance compared to vehicle-treated controls ($F(3, 144)=29.43$, $p<0.0001$) (Wild-type + Vehicle vs Wild-type + Chlorzoxazone + Baclofen $p=0.0292$; Wild-type + Vehicle vs ATXN1[82Q] + Vehicle $p<0.0001$; Wild-type + Vehicle vs ATXN1[82Q] + Chlorzoxazone + Baclofen $p=0.0097$; Wild-type + Chlorzoxazone + Baclofen vs ATXN1[82Q] + Vehicle $p<0.0001$; Wild-type + Chlorzoxazone + Baclofen vs ATXN1[82Q] + Chlorzoxazone + Baclofen $p<0.0001$; ATXN1[82Q] + Vehicle vs ATXN1[82Q] + Chlorzoxazone + Baclofen $p=0.0029$). *$p<0.05$, **$p<0.01$, two-way ANOVA with Holm-Sidak post-test. CHZ, chlorzoxazone.

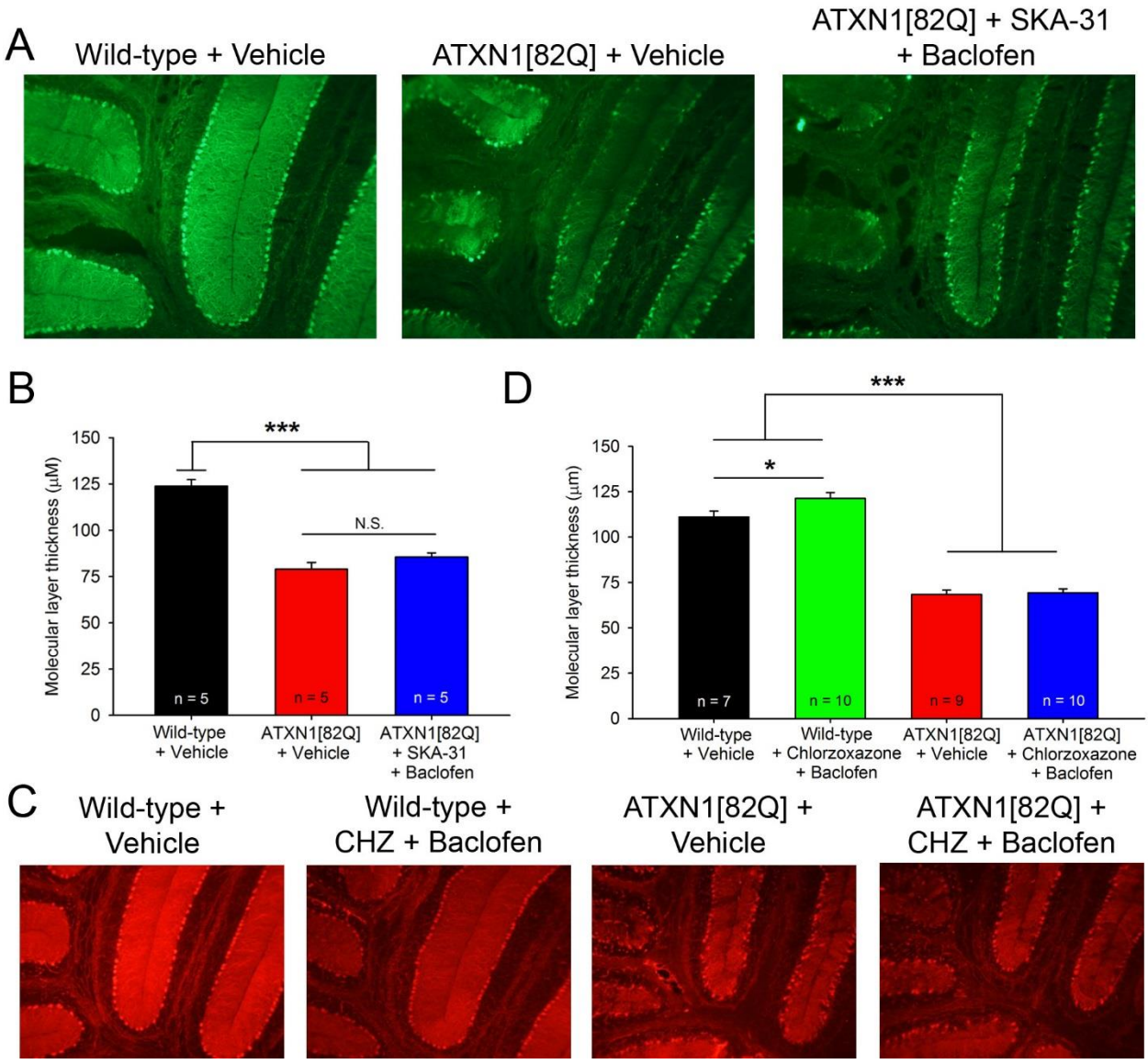

Figure 2.5 K_{Ca} activator and baclofen co-administration does not reduce Purkinje neuron degeneration in ATXN1[82Q] mice. (A) Representative images taken from wild-type mice treated with vehicle, ATXN1[82Q] mice treated with vehicle, and ATXN1[82Q] mice treated with SKA-31 and baclofen via chronic water-bottle administration. Mice received treatment from 5 weeks of age until 14 weeks of age, at which point the thickness of the molecular layer was determined for lobule 5. **(B)** Quantification of data shown in (A), which indicates a significant reduction in molecular layer thickness of both vehicle-treated and SKA-31 + baclofen-treated ATXN1[82Q] mice, but not difference between ATXN1[82Q] treatment groups. **(C)** Representative images taken from wild-type mice treated with vehicle or chlorzoxazone + baclofen, and ATXN1[82Q] mice treated with vehicle or chlorzoxazone + baclofen. **(D)** Quantification of data shown in (C), which indicates no difference between treated and untreated ATXN1[82Q] mice. *p<0.05, ***p<0.001, one-way ANOVA with Holm-Sidak test for multiple comparisons.

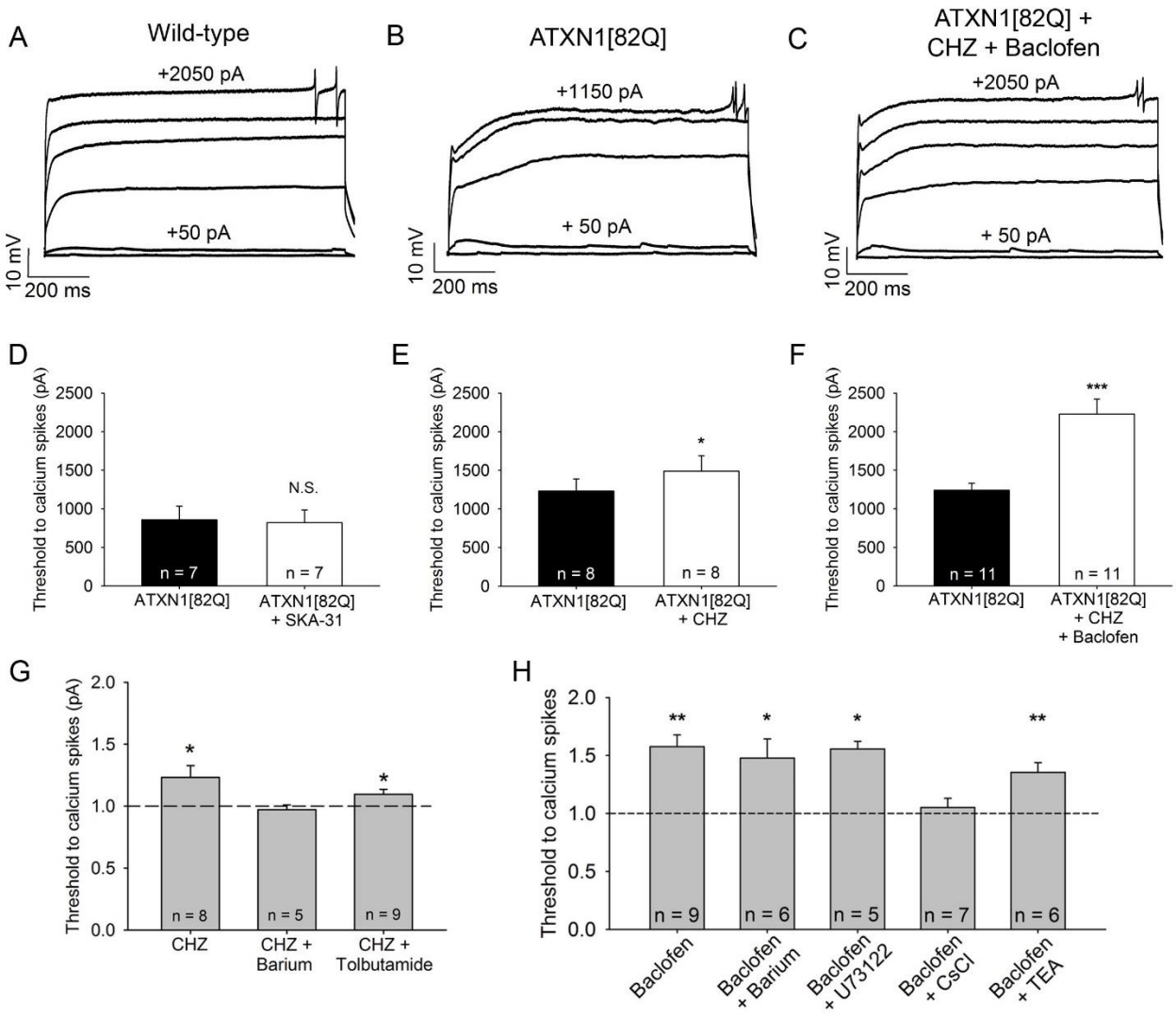

Figure 2.6 Chlorzoxazone and baclofen reduce dendritic hyperexcitability in ATXN1[82Q] mice by activating subthreshold-activated potassium channels. (A) Representative trace of dendritic calcium spikes from a wild-type Purkinje neuron, **(B)** ATXN1[82Q] Purkinje neuron at baseline, and **(C)** the same ATXN1[82Q] Purkinje neuron treated with chlorzoxazone (50 µM) and baclofen (2 µM). **(D)** SKA-31 (10 µM) does not reduce dendritic hyperexcitability in ATXN1[82Q] Purkinje neurons (p=0.376). **(E)** Chlorzoxazone (50 µM) reduces dendritic hyperexcitability in ATXN1[82Q] Purkinje neurons (p=0.025). **(F)** Chlorzoxazone (50 µM) and baclofen (2 µM) co-administration further reduces dendritic excitability in ATXN1[82Q] Purkinje neurons (p<0.001). **(G)** Barium (50 µM) occludes the effect of chlorzoxazone on dendritic excitability (p=0.778), while tolbutamide (500 µM) partially occludes the effect of chlorzoxazone on dendritic excitability (p=0.040). **(H)** Barium (500 µM, p=0.012), U73122 (10 µM in recording pipette, p=0.014), and TEA (1 mM, p=0.009) do not occlude the effect of baclofen on dendritic excitability, but cesium chloride (140 mM in the recording pipette) does occlude the effect of baclofen on dendritic excitability (p=0.356), in ATXN1[82Q]

Purkinje neurons. *p<0.05, **p<0.01, ***p<0.001, paired Student's t-test. CHZ, chlorzoxazone.

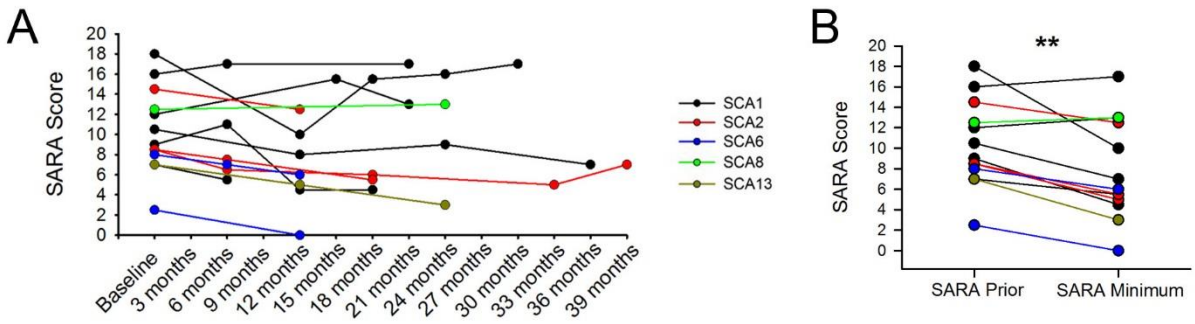

Figure 2.7 Chlorzoxazone and baclofen co-administration is tolerated in SCA patients and improves symptoms. (A) SARA scores were obtained for each patient prior to beginning treatment with chlorzoxazone and baclofen, and subsequent SARA scores were obtained at follow-up visits. SARA scores are only displayed for patients who could tolerate treatment and had at least one follow-up visit. **(B)** SARA scores are displayed prior to treatment and at the time point which showed a minimum SARA score after beginning treatment (p=0.004). ** p<0.01, paired Student's t-test.

Genotype	Repeat size	Sex	Age	Dosage	Other comments
SCA1	52	M	29	Baclofen 40 mg BID, Chlorzoxazone 750 mg BID	
SCA1	54	M	39	Baclofen 10 mg TID, Chlorzoxazone 500 mg TID	
SCA1	Not documented	F	67	Chlorzoxazone 250 mg once daily	Could not tolerate; Chlorzoxazone made swallowing worse
SCA1	52	F	36	Baclofen 10 mg TID, Chlorzoxazone 500 mg TID	Could not tolerate due to nausea
SCA1	52	F	29	Baclofen 20 mg BID, Chlorzoxazone 750 mg BID	
SCA1	53	M	35	Baclofen 30 mg TID, Chlorzoxazone 500 mg TID	
SCA1	43	F	62	Baclofen 10 mg TID, Chlorzoxazone 250 mg TID	
SCA1	46	F	58	Baclofen 10 mg TID, Chlorzoxazone 250/500 mg	
SCA2	38	M	50	Baclofen 20 mg TID, Chlorzoxazone 500 mg TID	
SCA2	38	M	67	Baclofen 10 mg TID, Chlorzoxazone 500 mg TID	
SCA2	43	M	24	Baclofen 20 mg TID, Chlorzoxazone 500 mg TID	
SCA6	21	M	57	Baclofen 10 mg TID, Chlorzoxazone 500 mg TID	
SCA6	22	M	65	Baclofen 10 mg BID, Chlorzoxazone 500 mg BID	Substantial improvement in downbeat nystagmus
SCA8	1268	F	79	Chlorzoxazone 500 mg BID	Could not tolerate due to worsened speech
SCA8	108	F	62	Baclofen 10 mg TID	Could not tolerate; Baclofen caused weakness
SCA8	Not documented	M	51	Baclofen 10 mg TID, Chlorzoxazone 500 mg TID	Improvement in swallowing and speech due to improvement in dystonia
SCA13	n/a	F	56	Baclofen 20 mg TID, Chlorzoxazone 500 mg TID	

Table 2.1 Summary of SCA patients treated with baclofen and chlorzoxazone. Patient demographics and dosage information are indicated. Patient genotype, CAG repeat size, age, sex, treatment dosage, and comments are also listed.

Chapter 3

Potassium channel dysfunction and disrupted calcium homeostasis contributes to Purkinje neuron dysfunction in a mouse model of spinocerebellar ataxia type 7

3.1 Abstract

Spinocerebellar ataxias are a large, heterogeneous group of neurodegenerative disorders that affect neurons in the cerebellum and related pathways. Although these diseases are similar in that overlapping cell types are frequently affected, the underlying basis for motor impairment related to involvement of these areas is not well understood. Mouse models of SCA have indicated that altered neuronal function precedes neurodegeneration in ataxia, and that underlying changes in ion-channel function are therefore important features of disease. In order to determine whether cerebellar Purkinje neuron dysfunction is a common feature of degenerative ataxia, I analyzed Purkinje neuron spiking in a mouse model of SCA7 and found that irregular spiking is present. With the help of collaborators, we found that these changes in spiking as closely associated with disrupted function of a “calcium homeostasis” module, consisting of several ion-channels important for Purkinje neuron function which show decreased transcript expression in SCA7 mouse cerebellum. In wild-type neurons, partial blockade of multiple members of this calcium homeostasis module is required in order to cause irregular spiking; conversely, irregular spiking in SCA7 Purkinje neurons

can be corrected by ion-channel activation or re-expression. Similar transcriptional changes are observed in mouse models of other SCAs. Together, these data suggest a functional role for this calcium homeostasis module in SCA7, and that shared features of disease may be present across multiple SCAs, making this calcium homeostasis module a promising therapeutic target.

3.2 Introduction

As mentioned in previous chapters, the polyglutamine (polyQ) spinocerebellar ataxias (SCA) are a family of six autosomal-dominantly inherited neurodegenerative disorders which cause progressive deterioration of movement and balance. Although the underlying mutations which cause polyQ SCA are well-characterized, the specific mechanisms which govern neurodegeneration and motor dysfunction are not fully understood. One such disorder, spinocerebellar ataxia type 7 (SCA7), results from a pathogenic expansion of a glutamine-encoding CAG repeat sequence in the *ATXN7* gene [156]. In SCA7, expression of polyglutamine-expanded ataxin-7 protein results in selective degeneration of neurons in the retina, brainstem, and cerebellum, including cerebellar Purkinje neurons [7]. Like other polyQ repeat diseases, SCA7 displays genetic instability of the expanded *ATXN7* CAG-repeat, which results in genetic anticipation and earlier symptomatic presentation upon germline transmission [157]. Also similar to other polyQ SCAs, SCA7 is untreatable at the present time.

Although the polyQ SCAs result from mutations in distinct genes, similar functional characteristics of these genes suggests that shared features of dysfunction may underlie neuronal dysfunction and degeneration across seemingly unrelated ataxias. As mentioned in Section 1.1.4, several of the proteins which are causative for

polyQ SCAs share related function roles [66]. ATXN1, the disease-causing protein in SCA1, is associated with transcriptional regulation and RNA splicing [56-58]. This is similar to ATXN2 (SCA2), which is also known to play a role in RNA metabolism [59-61]. ATXN7 (SCA7) is a member of the SAGA transcriptional complex [64, 158], and *TBP* (SCA17) is a central component of tata box-based transcriptional initiation [65]. In these disorders, transcriptional dysregulation can be reasonably considered a potential common source of neuronal dysfunction. Other disease-causing proteins of polyQ SCA include ATXN3 (SCA3), which is a de-ubiquitinating enzyme [62, 63], and *CACNA1A* (SCA6), a subunit of the $Ca_v2.1$ voltage-gated calcium channel [55]. Although the only polyQ SCA which directly affects an ion-channel is SCA6, there is an indication that neuronal excitability pathways may be commonly affected across multiple SCAs. This evidence stems from work in multiple mouse models of polyQ SCA, which indicates that several genes show common downregulation of their mRNA transcripts across models, including key ion-channels for Purkinje neuron function [67-72]. However, the functional relevance of these changes is not yet determined.

Early studies in calcium channel-mutant mice indicate that irregular Purkinje neuron spiking correlates with motor impairment [99-101], and correcting this abnormal spiking with K_{Ca} channel activators improves motor function [82, 83]. In Purkinje neurons, voltage-gated calcium channels are coupled to K_{Ca} channels [16, 86], which become activated upon calcium influx [17]. Since BK channel knockout also produces irregular Purkinje neuron spiking and motor impairment [18, 42], it is likely that K_{Ca} dysfunction is an important molecular mechanism in ataxia. In fact, K_{Ca} channel dysfunction has been noted in mouse models of SCA1 and SCA2, even though these diseases are not

caused by direct ion-channel mutations [70, 71]. In addition, K_{Ca} activators improve motor function in a mouse model of SCA3 [77], suggesting that common features of disease may exist across SCAs with different underlying genetic causes. However, the extent of electrophysiologic dysfunction, including the contribution of K_{Ca} channels or voltage-gated calcium channels, has not been studied for SCA7.

In order to address whether Purkinje neuron dysfunction is a common feature of polyQ SCA, and which molecular pathways contribute to disease, we performed patch-clamp recordings from SCA7 mice, along with RNA sequencing analysis of cerebellar tissue to identify relevant molecular targets. We hypothesized that changes in ion-channel expression and function underlie irregular spiking in SCA7 Purkinje neurons, and that these ion-channel targets can be targeted to improve motor impairment in SCA7 mice. We found that altered transcription of genes which form a functionally-relevant “calcium homeostasis” module contributes to irregular spiking and vestibular deficits in SCA7 mice, and that improving ion-channel expression or function subsequently improves these features of disease. We also observed that similar transcriptional changes exist in mouse models of other polyQ SCAs. These results suggest a role for this calcium homeostasis module in SCA, and suggest that the ion-channels within this module may be particularly important targets for the design of new therapies in ataxia.

3.3 Methods

3.3.1 Mice

All animal experimentation adhered to NIH guidelines and was approved by, and performed in accordance with, the University of Michigan Committee on the Use and

Care of Animals and the University of California, San Diego Institutional Animal Care and Use Committee. mPrP-floxed SCA7-92Q BAC mice [159] (referred to as fxSCA7 92Q) were maintained on a C57BL/6J background by mating hemizygous males to wild-type females, with F1 offspring containing hemizygous and wild-type littermate control animals, which were used for experimentation. In some electrophysiology experiments, wild-type C57BL/6J mice (Jackson Labs) were used. For all experiments excluding RNA transcriptome analysis, mice were used at 12 weeks of age, 25 weeks of age, and 40 weeks of age. For RNA transcriptome analysis, mice were used at 12 weeks of age and 29 weeks of age. Both male and female mice were used in all experiments to eliminate potential sampling bias.

3.3.2 Phenotype analysis: Rotarod

Rotarod analysis was performed as described in Section 2.3.3. Briefly, fxSCA7 92Q mice and wild-type littermate controls were handled for three consecutive days, then trained for three consecutive days on an accelerating rotarod (4-40 rpm at a rate of 0.12 rpm/second) and then a fourth day at a constant speed of 24 rpm. Next, mice were tested on four consecutive days at a constant speed of 24 rpm. Four trials were run per mouse each testing day, and reported scores reflect the average of all four trials. The time to fail is reported as the time that the mouse either fell off of the rotating rod or made three full rotations, to a maximum time of 300 seconds. Mice were tested at 12 weeks, 25 weeks, and 40 weeks of age, with equal balancing of male and female mice within groups. Data were acquired and analyzed with the experimenter blind to genotype.

3.3.3 Patch-clamp electrophysiology

3.3.3.1 Patch-clamp electrophysiology: solutions

Artificial cerebrospinal fluid (aCSF) contained the following: 125 mM NaCl, 2.5 mM KCl, 26 mM $NaHCO_3$, 1.25 mM NaH_2PO_4, 2 mM $CaCl_2$, 10 mM HEPES, and 10 mM glucose. For all recordings, other than dendritic capacitance measurements, pipettes were filled with internal recording solution containing the following: 119 mM K-Gluconate, 2 mM Na-Gluconate, 6 mM NaCl, 2 mM $MgCl_2$, 0.9 mM EGTA, 10 mM HEPES, 14 mM Tris-phosphocreatine, 4 mM MgATP, 0.2 mM Tris-GTP, at pH 7.3 and osmolarity 290 mOsm. For capacitance measurements, internal recording solution contained: 140 mM CsCl, 2 mM $MgCl_2$, 1 mM $CaCl_2$, 10 mM EGTA, 10 mM HEPES, 4 mM Na_2ATP, at pH 7.3 and osmolarity 287 mOsm.

3.3.3.2 Patch-clamp electrophysiology: reagents

For *in vitro* experiments, chlorzoxazone (Sigma Aldrich, Cat. No. C4397) was used at 50 µM, 2-APB (Tocris, Cat. No. 1224) was used at 50 µM to block the IP3 receptor and TRPC3 [160, 161], mibefradil (Sigma Aldrich, Cat. No. M5441) was used at 4 µM to block T-type calcium channels [162], and iberiotoxin (Tocris, Cat. No. 1086) was used at 100 nM to partially block BK channels or 200 nM to fully block BK channels. Tetrodotoxin (Alomone Labs, Cat. No. T-550) was used at 1µM to block voltage-gated sodium channels during dendritic excitability measurements.

3.3.3.3 Acute slice preparation for electrophysiological recordings

Mice were anesthetized by isoflurane inhalation and decapitated. The brain was removed and submerged in pre-warmed (33^{o}C) aCSF. Acute parasagittal slices were prepared in aCSF held at 32.5-34^{o}C on a VT1200 vibratome (Leica) to a thickness of 300 µm. Once slices were obtained, they were incubated in carbogen-bubbled (95% O_2,

5% CO_2) aCSF at 33ºC for 45 min. Slices were then stored in carbogen-bubbled aCSF at room temperature until use. During recording, slices were placed in a recording chamber and continuously perfused with carbogen-bubbled aCSF at 33ºC at a flow rate of 2.5 mL/min.

3.3.3.4 Patch-clamp recordings

Purkinje neurons were visually identified for patch-clamp recordings using a 40x water immersion objective and a Nikon Eclipse FN1 upright microscope with infrared differential interference contrast (IR-DIC) optics. Identified cells were visualized using NIS Elements image analysis software. Borosilicate glass patch pipettes were pulled to resistances of 3-4 MΩ for all recordings. Recordings were performed 1-5 hours after slice preparation. Data were acquired using an Axopatch 200B amplifier, Digidata 1440A interface (MDS Analytical Technologies), and pClamp-10 software (Molecular Devices). All data were digitized at 100 kHz. Whole-cell recordings were rejected if the series resistances changed by >20% during the course of recording, or if the whole-cell series resistance rose above 15 MΩ. All voltages are corrected for the liquid gap junction potential, which was calculated to be 10 mV [71].

3.3.3.5 Capacitance measurements

Acute cerebellar slices were obtained as described above. Capacitance measurements were performed in the presence of 50 µM picrotoxin to block spontaneous $GABA_A$ synaptic currents, and recording pipettes were filled with a cesium chloride-based internal pipette solution as described above. Recordings were performed at RT. Capacitative transients were obtained in voltage-clamp mode using 1 second steps to -70 mV from a holding potential of -80 mV. Recordings were excluded if the measured

input resistance was under 100 MΩ. Dendritic capacitance was determined using a method for the analysis of an equivalent circuit which represents Purkinje neurons[91, 163]. Input resistance was corrected offline and the decay of the capacitative transient was fit using a two-exponential decay function:

$$I(t) = A_1 e^{-\frac{t}{\tau_1}} + A_2 e^{-\frac{t}{\tau_2}}$$

The constants obtained from fitting the decay function of each cell was then used to obtain four parameters: C_1 (capacitance of the soma and main proximal dendrites), C_2 (capacitance of the distal dendritic arbor), R_1 (pipette access resistance), and R_2 (composite resistance of dendritic segments separating the main proximal dendritic segments from the distal dendritic arbor). The equations for this analysis are as follows:

$$C_1 = \frac{\tau_1 (A_1 + A_2)^2}{A_1 \Delta V}$$

$$C_2 = \frac{A_2 \tau_2}{\Delta V}$$

$$R_1 = \frac{\Delta V}{A_1 + A_2}$$

$$R_2 = \frac{\Delta V}{A_2} - \frac{\Delta V}{A_1 + A_2}$$

In our measurements, total capacitance was indicated by $C_1 + C_2$.

3.3.3.6 Analysis of firing properties

Electrophysiology data were analyzed offline using Clampfit 10.2 software (Molecular Devices). Firing frequency and coefficient of variation (CV) calculations were performed in the cell-attached configuration on spikes in a 150 second time interval obtained ~5 minutes after formation of a stable seal. The CV was calculated as follows:

$$CV = \frac{Standard\ Deviation\ of\ Interspike\ Interval}{Mean\ Interspike\ Interval}$$

The firing frequency distribution was obtained by identifying the percentage of cells in each incrementing 10 spike/second bin. The CV distribution was similarly obtained by sorting CV values into incrementing 0.02 bins.

3.3.3.7 Analysis of intrinsic dendritic excitability

Threshold to elicit dendritic calcium spikes was performed at 25 weeks of age as described previously [164]. Briefly, cells were held at -80 mV in whole-cell current clamp mode and injected with current in +50 pA increments in the presence of tetrodotoxin to block somatic sodium spikes. The amount of injected current to elicit calcium spikes was recorded, and these thresholds were considered representative of intrinsic dendritic excitability. Input resistance for each cell was calculated by generating an input-output curve for injected current vs. membrane potential, with only membrane potential values of under -75 mV in an effort to minimize active conductances during measurements [164].

3.3.3.8 AHP decay

Analysis of the after-hyperpolarization (AHP) was performed by analyzing spikes in a 10 second interval ~1 minute after break-in. The AHP value was calculated as the maximum anti-peak voltage, and the mean value over the 10 second interval is reported as the AHP for each neuron. To measure decay of the AHP during the inter-spike interval (ISI), the mean ISI duration was determined in the same 10 sec interval for each cell. AHP amplitude was then measured at different fractional intervals of the ISI (maximal anti-peak amplitude, 0.5*ISI, 0.65*ISI, 0.85*ISI) in order to characterize AHP decay.

3.3.4 Transcriptome analysis

Total RNA from the cerebellum of fxSCA7 92Q mice and wild-type littermates aged 12 and 29 weeks (n=3 per group) was isolated using TRIzol (Life Technologies) and purified using an RNeasy kit (Qiagen). Samples were then sent to BGI Americas for deep sequencing on the Illumina HiSeqTM 2000 system (50SE). Analysis of genome-wide expression data was performed by aligning raw reads of biologically independent samples to the reference mouse genome (mm10) using TopHat [165]. Cufflinks software package [166] was used to assemble individual transcripts from the mapped reads. Cuffdiff, a part of the Cufflinks package, was used to calculate gene expression levels and test for the statistical significance of differences in gene expression. Reads per kilobase per million mapped reads (RPKM) were calculated for each gene and used as an estimate of expression levels. Heatmaps and hierarchical clustering were generated using Genesis software [167].

3.3.5 Real-time quantitative RT-PCR

Real-time quantitative RT-PCR was performed as described previously [71]. Briefly, mice were euthanized under deep isoflurane anesthesia, and cerebella were promptly removed and flash-frozen in liquid nitrogen. Brains were stored at -80 C until processing, at which point TRIzol reagent (Invitrogen) was used to extract total RNA from cerebellar tissue. Extracted RNA was then purified using the RNeasy mini kit (Qiagen) per the manufacturer's instructions. The iScript cDNA synthesis kit (Bio-Rad) was then used to synthesize cDNA from 1.5 µg of purified RNA. Quantitative real-time PCR assays were performed using iQ SYBR Green Supermix (Bio-Rad) in a MyiQ Single Color Real-Time PCR Detection System (Bio-Rad). Reactions were performed with a 20 µL sample volume on an iCycler iQ PCR 96-well Plate (Bio-Rad) which was

sealed with Microseal optical sealing tape (Bio-Rad). Relative mRNA transcript levels were determined using the comparative C_t method for quantitation, with *Actb* mRNA serving as the reference gene. C_t values were obtained in triplicate for each sample and averaged for statistical comparison. The primers used for qRT-PCR studies are as follows:

Gene	Forward primer	Reverse primer
Kcnma1	5'-GGGCCAAGAAAAGAAATGGT-3'	5'-GATCAGGCTGCTTGTGGATT-3'
Cacna1g	5'-GTCGCTGGTATCTTTGG-3'	5'-TACTCCAGCATCCCAGCAAT-3'
Itpr1	5'-GGCAGAGATGATCAGGGAAA-3'	5'-AGCTCGTTCTGTTCCCCTTC-3'
Trpc3	5'-GAGGTGAATGAAGGTGAACTGA-3'	5'-CGTCGCTTGGCTCTTATCTT-3'
Actb	5'-CGGTTCCGATGCCCTGAGGCTCTT-3'	5'-CGTCACACTTCATGATGGAATTGA-3'

3.3.6 Immunohistochemistry

3.3.6.1 Sample preparation

Mice were anesthetized under isoflurane inhalation and brains were removed, fixed in 1% paraformaldehyde for 1 hour, and then placed in 30% sucrose in PBS for 48 hours. Parasagittal sections of 14 µm were made on a CM1850 cryostat (Leica). For double-labeling experiments, $Ca_v3.1$ was labeled with mouse anti-$Ca_v3.1$ (1:150, clone N178A/9, Cat. No. 75-206, Neuromab) and goat anti-mouse Alexa594-conjugated secondary antibody (1:200, Ref. no. A11005, Life Technologies Invitrogen). To label Purkinje neurons, rabbit anti-calbindin (1:200, Cat. No. 13176, Cell Signaling) and goat anti-rabbit Alexa488-conjegated secondary (1:200, Ref. no. A11008, Life Technologies Invitrogen) were used. Sections were imaged using an Axioskop 2 plus microscope

(Zeiss) at 4x and 10x magnification. Sample preparation and imaging was performed with the experimenter blind to genotype.

3.3.6.2 Fluorescence intensity measurements

To measure relative intensity of calbindin and $Ca_V3.1$ staining, images acquired at 10x magnification were used. Fluorescence intensity analysis was performed using ImageJ. A rectangular box was placed in the molecular layer, spanning the dendritic arbors of Purkinje neurons. Mean pixel intensity was measured for each rectangle, and this mean value was used as the relative fluorescence value for each section. The box was an identical size in all cases, and was placed in the same location for calbindin and $Ca_V3.1$ analysis in a single section. Two sections were imaged per animal, and the mean of those two fluorescence values were used as the fluorescence intensity value for that animal. All tissue processing and imaging was performed at the same session, and microscope settings were identical for all acquired images. During imaging and analysis, the experimenter was blind to genotype.

3.3.6.3 Confocal microscopy

Imaging was performed on a Nikon C2+ confocal microscope. Images were acquired at 60x magnification with an oil-immersion lens. Single-plane images were acquired, with microscope settings kept constant between all samples under a specific set of antibodies. Samples were prepared and imaged with the experimenter blind to genotype.

3.3.7 Stereotaxic cerebellar delivery of adeno-associated virus

Previously, mSlo1 MBr5/3 (BK channel) was cloned into a pAAVmcsCMV plasmid under a cytomegalovirus promoter. Recombinant serotype AAV2/5 vectors encoding

either a BK channel or GFP transcript were generated by the University of Iowa Vector Core (http://www.medicine.uiowa.edu/vectorcore/). Under isoflurane anesthesia, fxSCA7 92Q and littermate control mice were injected bilaterally with either BK-AAV or GFP-AAV into both medial and lateral deep cerebellar nucleus, which results in efficient Purkinje neuron expression [71]. Injection coordinates were as follows, as measured from bregma:

	Anterior-posterior	Medial-lateral	Dorsal-ventral
Medial DCN	-6.4 mm	±1.3 mm	-1.9 mm
Lateral DCN	-6.0 mm	±2.0 mm	-2.2 mm

At each injection coordinate, ~2.5 x 10^{12} vg/mL of virus (3.0 µL total volume) was delivered at a rate of 0.5 µL/minute using a 10 µL Hamilton syringe (BD Biosciences). Mice were injected at 24.5 weeks of age and given 14 days for the virus to fully express before being sacrificed for patch-clamp electrophysiology studies.

3.3.8 Vestibular phenotype testing

In order to assess potential alterations in postural control in fxSCA7 92Q mice, we performed vestibular phenotype testing as described below.

3.3.8.1 Surgical implant of IMU

Four fxSCA7 92Q mice and four wild-type littermate control mice were surgically implanted with a head post at 19.5 weeks of age. Mice were anesthetized with light isoflurane anesthesia and the scalp was opened to expose the skull surface. A custom titanium head post was glued just posterior to bregma at a precise flat angle using C&B

Metabond (Parkell). Once dried in place, the scalp was sutured and mice were allowed to recover for three days before the onset of vestibular testing.

3.3.8.2 Vestibular testing procedure

During testing, mice were placed individually in a clear enclosure located in a sound-proofed booth and allowed to explore for 5 minutes (300 seconds) in darkness, in order to isolate vestibular function from visual input, while experimenters watched their motion using an infrared camera. An inertial measurement unit (IMU) was placed on the surgically-implanted titanium head post prior to the onset of the experiment. The IMU recorded linear and angular acceleration of the head at a 1 kHz sampling rate. Data were acquired and recorded using a CED Power 1401 data acquisition system and Spike2 software (Cambridge Electronic Design) [168, 169]. Mice were tested 2-3 times per week from 20 weeks of age to 30 weeks of age. Data was digitized and filtered offline prior to analysis. During testing, the experimenter was blind to genotype.

3.3.8.3 Vestibular testing: Statistical analysis

IMU data was analyzed using MATLAB software (MathWorks). A custom script was written to retrieve IMU data and plot changes in linear velocity and angular acceleration of the pitch, yaw, and roll axes during head movement. Data was averaged for each genotype on all testing days, and data were plotted and fit to a linear trend line.

3.3.9 Analysis of RNA sequencing and microarray datasets

Published RNA sequencing and microarray datasets from ATXN1[82Q] [68], ATXN1^{154Q} [170], and ATXN2[127Q] mice [171], in addition to unpublished data from fxSCA7 92Q mice, were compared in order to identify commonly-downregulated mRNA transcripts across models. This comparison was performed using a custom script written in Python

(Python Software Foundation). Once complete, transcripts which were downregulated across all four models were examined based on known function, and genes related to neuronal excitability were displayed.

3.3.10 Statistical analysis

Statistical tests are described in the figure legends for all data. Statistical analysis was performed using Excel (Microsoft), Prism 6.0 (GraphPad), SigmaPlot (Systat Software), and Origin (Origin Labs). Statistical significance was defined at $p<0.05$. For one-way and two-way analysis of variance (ANOVA), if statistical significance ($p< 0.05$) was achieved, then we performed post hoc analysis corresponding to the experiment, as specified, to account for multiple comparisons. All *t*-tests were two-tailed Student's *t*-tests, and level of significance (alpha) was always set to 0.05.

3.4 Results

3.4.1 Purkinje neuron dysfunction begins in the posterior cerebellum of fxSCA7 92Q mice and progresses globally

In order to investigate whether Purkinje neuron dysfunction accompanies motor impairment in SCA7, as is the case in other mouse models of polyQ SCA [71, 72, 77, 78] (Chapter 2), we assessed motor impairment, dendritic degeneration, and Purkinje neuron spiking in a mouse model of SCA7. These mice, the mPrP floxed SCA7 92Q BAC model (referred to hereafter as fxSCA7 92Q), has been previously shown to express mutant ataxin-7 protein along with motor dysfunction and neurodegeneration [159]. We wished to explore Purkinje neuron physiology in fxSCA7 92Q mice. We analyzed the motor phenotype of fxSCA7 92Q mice and confirmed findings from previous studies [159], that motor impairment is not initially present but becomes

pronounced by 25 and 40 weeks of age (Figure 3.1A). Changes in Purkinje neuron spiking correspond to initial motor impairment in other mouse models of SCA [71, 72], and altered Purkinje neuron membrane excitability can be associated with structural changes related to Purkinje neuron degeneration [74]. We wished to determine whether these characteristics of disease are also true for fxSCA7 92Q mice. We use capacitance as a measure of early dendritic degeneration in Purkinje neurons, as capacitance is linearly proportional to membrane surface area and is highly sensitive to even modest reductions in cell membrane [163]. We found that at 25 weeks of age, total Purkinje neuron capacitance is reduced in the posterior cerebellar lobules of fxSCA7 92Q mice, but is unchanged in the anterior cerebellar lobules (Figure 3.1B). However, by 40 weeks of age, total Purkinje neuron capacitance is significantly reduced in both anterior and posterior cerebellar lobules (Figure 3.1C). This indicates that Purkinje neuron dysfunction and degeneration may be present initially in the posterior cerebellum of fxSCA7 92Q mice and later progress globally.

3.4.2 Purkinje neuron dysfunction is present in the posterior cerebellar lobules, but not anterior cerebellar lobules, of fxSCA7 92Q mice

Next, we wished to determine whether alterations in Purkinje neuron spiking are present in fxSCA7 92Q cerebellum, and whether regional differences exist in Purkinje neuron physiology as suggested by capacitance measurements of Purkinje neuron surface area. We performed patch-clamp recordings from 25 week-old fxSCA7 mice and wild-type littermate controls to investigate Purkinje neuron firing frequency and regularity of spiking. We found that at 25 weeks, Purkinje neurons in the anterior cerebellar lobules show no differences in firing frequency or the coefficient of variation

(CV) of spiking, indicating that spiking is unchanged between genotypes (Figure 3.2A-C). However, the distribution of CV values was slightly right-shifted in fxSCA7 92Q Purkinje neurons compared to wild-type neurons (Figure 3.2D). In the posterior cerebellar lobules, no changes in Purkinje neuron firing frequency were observed between fxSCA7 92Q mice and wild-type littermate controls at 25 weeks of age (Figure 3.2F). However, fxSCA7 92Q Purkinje neurons show a significantly increased CV when compared to wild-type (Figure 3.2E and G). In addition, the distribution of CV values is right-shifted in fxSCA7 92Q mice (Figure 3.2H). Together, these data indicate that irregularities in Purkinje neuron spiking are present in the posterior cerebellar lobules but not the anterior cerebellar lobules at 25 weeks of age.

Since motor impairment becomes profound in fxSCA7 92Q mice by 40 weeks of age, and since Purkinje neuron capacitance is significantly reduced in both anterior and posterior cerebellar lobules at this time, we wished to determine whether alterations in Purkinje neuron spiking may progress globally by 40 weeks of age. While firing frequency remains unaffected (Figure 3.3 B), Purkinje neuron spiking appears to become more irregular in the anterior cerebellar lobules of fxSCA7 92Q by 40 weeks (Figure 3.3 C-D), although statistical significance was not reached ($p = 0.056$). In addition, irregular Purkinje neuron spiking persists in the posterior cerebellar lobules at 40 weeks of age (Figure 3.3 G-H, $p = 0.073$) and appears similar to Purkinje neurons at 25 weeks of age in both firing frequency and CV. No significant changes in Purkinje neuron firing frequency were noted in the posterior cerebellum at 40 weeks of age (Figure 3.3 F). This indicates that electrophysiologic dysfunction is a feature of disease in fxSCA7 92Q mice, and that early changes in Purkinje neuron spiking are restricted to

the posterior cerebellar lobules before progressing globally later in disease. Importantly, these data suggest that Purkinje neurons in the posterior cerebellum of fxSCA7 92Q mice exhibit no significant progression of electrophysiologic dysfunction between 25 and 40 weeks of age, since firing frequency and CV appear equally disrupted at both of these experimental timepoints. This is in contrast to other mouse models of SCA, where changes in Purkinje neuron spiking are progressive [70-72].

3.4.3 Dendritic hyperexcitability is present in Purkinje neurons from the posterior cerebellar lobules of fxSCA7 92Q mice

While alterations in somatic spiking are clearly present in Purkinje neurons of the posterior cerebellar lobules of fxSCA7 92Q mice, Purkinje neurons also rely upon active dendrites whose functions are not assessed by a gross characterization of spiking. The studies in Chapter 2 of this dissertation have highlighted the importance of dendritic pathology to electrophysiologic dysfunction and motor impairment in a mouse model of SCA1, and have suggested that dendritic hyperexcitability is an important feature of disease that must be considered when designing therapies for the treatment of SCA [73, 74]. It is therefore important to assess whether dendritic hyperexcitability is a common feature of SCA. We assessed the threshold to elicit dendritic calcium spikes fxSCA7 92Q Purkinje neurons and wild-type littermate controls in the presence of tetrodotoxin to block somatic spiking. We found that Purkinje neurons in the posterior cerebellum of fxSCA7 92Q mice show a significantly decreased threshold to elicit dendritic calcium spikes when compared to wild-type littermate controls, with no change in input resistance (Figure 3.4). This indicates that at 25 weeks of age, when fxSCA7 92Q Purkinje neurons exhibit altered somatic spiking, dendritic hyperexcitability is also

present. This is reminiscent of findings in a mouse model of SCA1 [73, 74](Chapter 2) and indicates that dendritic hyperexcitability may be an important feature of disease in multiple models of SCA.

3.4.4 Genes necessary for Purkinje neuron function show reduced expression in fxSCA7 92Q cerebellum

To determine the molecular basis for altered spiking and neurodegeneration in SCA7, we performed unbiased transcriptome analysis on cerebellar RNA isolated from presymptomatic (12 week-old) and visibly symptomatic (29 week-old) fxSCA7 92Q mice and wild-type littermate controls, since changes in motor function and Purkinje neuron spiking become noticeable at 25 weeks of age (see Figure 3.1). RNA sequencing analysis produced a list of 100 genes with significantly altered expression levels between fxSCA7 92Q and wild-type cerebellum in both presymptomatic and symptomatic fxSCA7 92Q mice (Figure 3.5A). In order to identify putative molecular pathways that contribute to fxSCA7 92Q Purkinje neuron dysfunction, we performed pathway analysis using DAVID v6.7 (https://david.ncifcrf.gov/). This analysis identified both phosphatidyl-inositol signaling (*P*=3.2E-4) and calcium signaling (*P*=5.0E-3) pathways as overrepresented in fxSCA7 92Q cerebellum, both of which were down-regulated (Figure 3.5B). Many of the identified genes, which are key members of the aforementioned calcium homeostasis pathways, are causative mutations in several human and mouse ataxias (Figure 3.5B) [2-6, 28, 43-48], suggesting their importance for normal cerebellar function. Among these, several ion-channels known to be important for Purkinje neuron spiking show decreased expression in fxSCA7 92Q cerebellum, indicating that these channels may contribute to altered Purkinje neuron spiking in

SCA7. To validate these findings, we performed qRT-PCR analysis on RNA isolated from the cerebellum of fxSCA7 92Q mice, and confirmed significant reductions in expression of these ion-channel transcripts (Figure 3.5C). This suggests that perturbations in calcium homeostasis may be an important contributing factor to Purkinje neuron dysfunction in fxSCA7 92Q mice.

In order to further examine the physiological relevance of identified reductions in gene expression, we performed immunostaining for calbindin, a calcium-binding protein that regulates intracellular calcium concentrations and specifically labels Purkinje neurons in the cerebellum, along with $Ca_v3.1$, the voltage-dependent T-type calcium channel encoded by *Cacna1g* (Figure 3.6A). While calbindin intensity was not significantly altered between groups (Figure 3.6B), we observed a significant reduction in $Ca_v3.1$ immunoreactivity in the molecular layer of posterior cerebellar lobules of fxSCA7 92Q mice, suggesting reduced protein expression on the dendritic membrane of fxSCA7 92Q Purkinje neurons (Figure 3.6C). Confocal images indicate that some Purkinje neurons in the posterior cerebellar lobules of fxSCA7 92Q mice appear to be more affected than others (Figure 3.6D). This may be due to the expression pattern of the SCA7 transgene in these mice, in which only about 50% of Purkinje neurons show transgene expression [159]. These results indicate that in addition to reductions in transcript expression, reductions in ion-channel protein expression may contribute to the functional alterations in Purkinje neuron spiking observed in fxSCA7 92Q mice.

3.4.5 Impaired BK channel function results from decreased calcium availability and contributes to irregular Purkinje neuron spiking in fxSCA7 92Q mice

The observed alterations in calcium homeostasis gene expression seen in Figure 3.5, along with the alterations in Purkinje neuron spiking observed in Figures 3.2 and 3.3, suggest that disrupted calcium homeostasis may contribute to irregular Purkinje neuron spiking in fxSCA7 92Q mice. Purkinje neurons rely on the precise activity of a multitude of ion-channels in order to maintain spontaneous and regular pacemaking. Purkinje neuron spiking is sensitive to perturbations in calcium buffering [17, 80], intracellular calcium stores [81], and plasma membrane calcium channels [82, 83], many of which show reduced transcript levels in fxSCA7 92Q cerebellum (Figure 3.5). Importantly, calcium-activated potassium (K_{Ca}) channels, such as BK, regulate the after-hyperpolarization (AHP), an important component of the spike which allows voltage-gated ion-channels to fully deactivate before the subsequent spike [17]. Both calcium-channel mutant mice and K_{Ca}-channel mutant mice display aberrant Purkinje neuron spiking [18, 42, 82, 83], suggesting that K_{Ca} channel dysfunction may also underlie altered spiking in fxSCA7 92Q Purkinje neurons.

In order to determine whether alterations in calcium homeostasis gene expression may alter the AHP in fxSCA7 92Q Purkinje neurons, we performed whole-cell recordings in acute cerebellar slices to investigate action potential waveform during spontaneous firing. Consistent with calcium-activated potassium channel dysfunction, the AHP decayed more rapidly in fxSCA7 92Q Purkinje neurons (Figure 3.7A-B). The loss of the AHP in SCA7 mice is consistent with calcium-activated potassium channel dysfunction, which, in turn, reflects aberrant calcium homeostasis secondary to variable intracellular calcium concentration [71, 82, 83]. These data provide functional validation of

the calcium regulatory gene expression alterations revealed by the unbiased transcriptome analysis (Figure 3.5).

Purkinje neurons from fxSCA7 92Q mice exhibit profound firing irregularity (Figures 3.2 and 3.3) despite rather modest reductions in ion-channel gene expression (Figure 3.5). We hypothesized that a synergistic reduction in the function of both putative calcium sources (e.g. $Ca_v3.1$, TRPC3, IP3 receptor) and the effector K_{Ca} channel (e.g. BK) results in irregular Purkinje neuron spiking. In order to address this hypothesis, we performed cell-attached patch clamp recordings in wild-type Purkinje neurons in the presence of pharmacologic inhibitors of these ion-channels. Current understanding of Purkinje neuron physiology suggests that P/Q-type calcium channels are the main calcium source for K_{Ca} channels [16], but other calcium sources may contribute to proper calcium homeostasis as well. In the presence of 100 nM iberiotoxin, which partially occludes BK channels (Figure 3.7C), wild-type Purkinje neuron spike regularity is not disrupted (Figure 3.7D). Similarly, $Ca_v3.1$ blockade (via 4 µM mibefradil [162]) or IP3 receptor/TRPC3 blockade (via 2-APB [160, 161]) alone does not affect Purkinje neuron spike regularity (Figures 3.7D and 3.7F). However, simultaneous application of 100 nM iberiotoxin and either mibefradil or 2-APB significantly increases spike irregularity in wild-type Purkinje neurons (Figures 3.7D and 3.7F) without affecting firing frequency (Figures 3.7E and 3.7G). This suggests that a simultaneous partial reduction in the function of both calcium channels and K_{Ca} channels is sufficient to cause irregular Purkinje neuron spiking.

If BK channel dysfunction is responsible for irregular spiking in fxSCA7 92Q Purkinje neurons, these neurons may respond to pharmacologic or genetic modifiers of

BK channel activity. We assessed the regularity of fxSCA7 92Q Purkinje neuron spiking in the presence of chlorzoxazone, a pharmacologic activator of K_{Ca} channels including BK [135]. In irregularly-spiking fxSCA7 92Q Purkinje neurons, chlorzoxazone significantly improved the regularity of spiking without affecting firing frequency (Figure 3.8A-C). In addition, we used an adeno-associated virus (AAV) to genetically overexpress BK channel transcripts in fxSCA7 92Q cerebellum [71]. BK-AAV restored fxSCA7 92Q Purkinje neuron spike regularity to wild-type levels, while a control GFP-AAV did not (Figure 3.8D-G). AAV expression did not affect firing frequency across experimental groups (Figure 3.8H). Similar to data observed previously (Figure 3.7), Purkinje neurons from fxSCA7 92Q mice treated with GFP-AAV show a significantly depolarized AHP throughout the interspike interval when compared to wild-type Purkinje neurons treated with GFP-AAV (Figure 3.8I). Upon genetic re-expression of BK, fxSCA7 92Q Purkinje neurons did not display a restoration of the decay of the AHP (Figure 3.8I). However, the coefficient of variation of the AHP, which was significantly increased in Purkinje neurons from fxSCA7 92Q mice treated with GFP-AAV, was restored to the level of wild-type Purkinje neurons treated with GFP-AAV in fxSCA7 92Q Purkinje neurons treated with BK-AAV (Figure 3.8J). This suggests that consistent calcium availability, rather than fully saturating concentrations of calcium to completely activate K_{Ca} channels, may be sufficient to normalize Purkinje neuron spike regularity in fxSCA7 92Q mice. Overall, the results of this series of experiments suggest that synergistic effects of reduced calcium homeostasis and BK channel dysfunction contribute to irregular spiking in fxSCA7 92Q Purkinje neurons, and that reduced calcium availability for BK channel function can be overcome by activation or overexpression of BK.

3.4.6 Purkinje neuron dysfunction in the posterior cerebellum contributes to specific deficits in vestibular control of posture

Potassium channel dysfunction contributes to irregular spiking in the posterior cerebellar lobules of fxSCA7 92Q mice (Figure 3.2). We sought to determine whether these alterations in Purkinje neuron spiking correspond to specific behavioral changes. Although fxSCA7 92Q mice exhibit profound motor impairment, Purkinje neuron dysfunction is initially present in only the posterior cerebellar lobules (Figure 3.2). Since the polyQ expanded SCA7 transgene is driven by the murine prion protein promoter, this protein is expressed throughout the central nervous system and may drive pathology in other brain regions in addition to cerebellar Purkinje neurons [159]. It is likely that pronounced impairment on rotarod performance of fxSCA7 92Q mice is driven by both cerebellar and extracerebellar pathology. In order to more directly gauge the contribution of region-specific alterations in Purkinje neuron physiology in fxSCA7 92Q mice, we considered the functional connectivity of cerebellar output projections. Purkinje neurons in the posterior cerebellum project specifically to neurons in the vestibular nuclei, rather than the deep cerebellar nuclei which are the target of neurons in the anterior cerebellar lobules [172]. Therefore, altered functional connectivity to the vestibular nucleus in fxSCA7 92Q mice may generate a specific vestibular deficit which could be attributed to irregular Purkinje neuron spiking.

In order to determine whether such a vestibular deficit exists, we performed a measure of vestibular head posture in fxSCA7 92Q mice and wild-type littermate controls. At a presymptomatic timepoint (20 weeks of age), vertical head tilt is identical in fxSCA7 92Q and wild-type mice, but once motor symptoms are clearly present (30

weeks of age) a negative vertical head tilt is present in fxSCA7 92Q mice (Figure 3.9B). A reduced standard deviation of vertical head posture suggests that negative vertical head tilt is persistent in these mice (Figure 3.9C). This persistent vertical head tilt is consistent with cerebellar dis-inhibition of the vestibular nuclei and could result from irregular Purkinje neuron spiking in the posterior cerebellar lobules. The cerebellum clearly contributes to head postural control in humans, as patients with bilateral cerebellar lesions display an impaired head stabilization reflex [173]. Abnormalities in head postural control, including lateral drift and a persistent vertical head tilt, has been observed in patients with cerebellar dystonia, in which reduced cerebellar output to the vestibular nucleus was proposed [174]. Together, clinical data and findings from these studies suggest that cerebellar dis-inhibition of the vestibular nuclei may result in head postural abnormalities in fxSCA7 92Q mice and may be a relevant feature of disease in human patients with cerebellar pathology, including ataxia.

3.4.7 Calcium homeostasis module genes are similarly disrupted in mouse models of other SCAs, suggesting a common disease pathway

The data within this chapter provide evidence that reduced expression of key ion-channel genes contributes to altered Purkinje neuron excitability and motor impairment, and that targeting these changes in excitability can improve both spiking ad motor performance. This link between neuronal excitability and motor performance has been illustrated previously and is notably disrupted in cerebellar ataxia [71, 73, 76, 78, 82, 83]. Recently, a human study assessing risk factor genes for SCA illustrated that calcium homeostasis and IP3 receptor signaling pathways are likely to be important for the pathogenesis of ataxia [67], and the data presented in this chapter have corroborated

those results. Taking these factors into consideration, we considered an important question: are the sources of electrophysiologic dysfunction unique for each SCA variant, or do convergent mechanisms of disease exist among SCAs?

In order to address this question, we investigated the transcriptional profiles of several mouse models of polyQ SCA and compared changes in mRNA expression across models. In addition to the RNA sequencing analysis presented for fxSCA7 92Q cerebellum in Figure 3.5, we accessed publically-available RNA sequencing data from mouse models of SCA1 (ATXN1[82Q], from Ingram et al. [68], and $ATXN1^{154Q}$, from Gatchel et al. [170]) and SCA2 (ATXN2[127Q], from Dansithong et al. [171]). When cerebellar RNA transcriptomes were compared, we identified 31 genes which showed commonly downregulated expression across all four models (Figure 3.10A). In order to determine whether excitability pathways may be involved in pathogenesis of polyQ SCA, we searched these 31 genes for ion-channel genes or genes related to neuronal excitability and found that only *Kcnma1, Cacna1g, Itpr1, and Trpc3* transcripts showed significantly reduced cerebellar expression across all models (Figure 3.10B). These are the same genes which were identified as part of the functional calcium homeostasis module presented in this chapter. In addition, the potassium channel scaffold protein *Kcnip2* and the potassium channel tetramerization protein *Kctd12* also showed reduced expression across all four models, while *Ryr1* (ryanodine receptor, an important calcium release protein) and several other potassium channel transcripts showed reduced expression in several but not all models (Figure 3.10B). This indicates that calcium homeostasis pathways related to K_{Ca} function and neuronal excitability may be preferentially vulnerable in polyQ SCA and may therefore represent a common

mechanism of disease which could be targeted for therapy. Overall, neuronal excitability appears to contribute significantly to neuronal dysfunction in SCA, in particular the disrupted function of K_{Ca} channels and their calcium sources.

3.5 Discussion

The studies in this chapter present evidence that alterations in the cerebellar transcriptome are present in fxSCA7 92Q mice. As a result, neuronal excitability pathways related to calcium homeostasis and K_{Ca} function are consequently disrupted, leading to increased irregularity of Purkinje neuron spiking. This leads to functional alterations in both overall motor performance and specific alterations in vestibular control of posture. Additionally, these studies illustrate that a partial disruption of multiple components of a calcium homeostasis pathway is necessary in order to elicit irregular spiking in wild-type neurons. Importantly, improving BK channel function without affecting deficiencies in calcium sources, either through AAV-mediated re-expression or activation via chlorzoxazone, normalizes Purkinje neuron spike regularity in fxSCA7 92Q mice. Finally, this calcium homeostasis pathway may be relevant in other SCAs, as multiple mouse models of polyQ SCA exhibit disruption of genes within this network and also exhibit altered Purkinje neuron membrane excitability. Overall, these studies argue for the relevance of K_{Ca} channel dysfunction as a driver of altered spiking and motor impairment in SCA7 and other ataxias, and for the relevance of K_{Ca} channel activation as a potential mechanism to improve motor impairment in SCA.

As noted in other mouse models of polyQ SCA [70-72, 77, 78], disrupted Purkinje neuron spiking is present in fxSCA7 92Q mice at the onset of motor impairment and early dendritic degeneration. However, one striking difference exists in fxSCA7 92Q

mice: Purkinje neuron dysfunction begins in the posterior cerebellar lobules at 25 weeks of age and progresses globally later in disease. This is in stark contrast to what is observed in mouse models of SCA1 and SCA2, in which Purkinje neuron dysfunction is notable in the anterior cerebellar lobules early in disease [70, 71]. This discrepancy is not due to background strain, as both SCA2 and SCA7 mice are maintained on a C57/BL6 background but exhibit separate regional tendencies to neuronal dysfunction. Recent studies have illustrated that Purkinje neurons in the anterior and posterior cerebellar lobules display noticeable differences in their physiology, and that these changes in spiking correspond to the expression pattern of the protein aldolase C, also known as zebrin. The cerebellum is organized into sagittal bands of zebrin positive and negative Purkinje neurons, where cells in the anterior cerebellum are mostly zebrin negative and cells in the posterior cerebellum are almost exclusively zebrin positive [175]. Zebrin positive neurons have a much lower spontaneous firing rate than zebrin negative neurons [176] and also display differences in synaptic plasticity [177]. It is possible that zebrin negative neurons are more strongly affected in SCA1 and SCA2, while zebrin positive neurons are preferentially vulnerable in SCA7. This could be due to a variety of factors, but one possibility is that regional control of transcription is modulated by both ATXN1 and ATXN7, but these proteins regulate neuronal function in a regional fashion that tracks with zebrin expression. This could also be due to region-specific differences in the expression of one or more members of the aforementioned calcium homeostasis module. For instance, the differences in simple spike frequency between zebrin positive and negative Purkinje neurons can be alleviated by blocking Trpc3 channels in zebrin negative neurons [176], suggesting that zebrin negative neurons may either express Trpc3

at a higher level or may be more dependent on its function for a higher baseline firing frequency. It is also known that several other proteins, such as the IP3 receptor, mGluR1b, and EAAT-4 are also expressed in band patterns similar to zebrin [177-180]. This suggests the possibility of lobule-specific dependence on certain ion-channels for function, and therefore lobule-specific changes in the expression of these channels in fxSCA7 92Q mice. This is illustrated to some extent in Figure 3.6, as $Ca_v3.1$ expression is reduced the posterior cerebellar lobules but not anterior cerebellar lobules in fxSCA7 92Q mice. Future studies should be conducted to explore the relative mRNA transcript and protein expression of *Kcnma1*, *Cacna1g*, *Itpr1*, *Trpc3*, and other channels related to Purkinje neuron excitability in both the anterior and posterior cerebellar lobules, in order to determine whether region-specific differences exist in SCA7, SCA1, and other ataxias. These studies would improve current understanding of how ion-channel dysfunction contributes to Purkinje neuron dysfunction in SCA and would argue for the importance of considering zebrin positive and negative neurons independently in the study of cerebellar disease.

Another known feature of zebrin positive and zebrin negative Purkinje neurons is a difference in functional connectivity. In general, zebrin positive Purkinje neurons tend to project to the vestibular nuclei, while zebrin negative Purkinje neurons project to the deep cerebellar nuclei [175]. This is particularly true for the recording site which we chose for our studies, the cerebellar nodulus, which is comprised of lobules 9 and 10 and sends zebrin-positive terminals to the fastigial nucleus, which is a presynaptic projection of the vestibular nucleus [175]. Interestingly, fxSCA7 92Q mice exhibit Purkinje neuron dysfunction in the posterior cerebellar lobules at 25 weeks of age, when motor

impairment is first apparent, while altered Purkinje neuron spiking progresses globally by 40 weeks of age (Figures 3.2 and 3.3) in association with profound impairment of motor performance on a rotarod (Figure 3.1). However, rotarod performance is not specific to cerebellar function and cannot assess the function of neurons in a specific cerebellar region. When we performed a more specific assessment of vestibular function, corresponding to function of Purkinje neurons in the posterior cerebellum, fxSCA7 92Q mice displayed a pronounced postural deficit compared to wild-type littermate controls. However, it is unclear whether this postural abnormality is a consequence of altered Purkinje neuron spiking, primary vestibular neuron dysfunction, or a combination of these possibilities. In order to address these possibilities, future studies will be performed. As illustrated in Figure 3.8, Purkinje neuron spiking can be normalized to wild-type levels in fxSCA7 92Q mice upon AAV-mediated overexpression of BK channel transcripts. Future experiments will involve the same injection procedure, where fxSCA7 92Q mice and wild-type mice will be injected with either BK-AAV or a control GFP-AAV prior to undergoing vestibular testing. If postural impairment in fxSCA7 92Q mice is purely cerebellar in origin, a normalization of head postural control should be observed upon BK-AAV injection while all other injected mice should remain unaffected. If this rescue is not observed, it is possible that primary vestibular dysfunction is present in fxSCA7 92Q mice and may drive this impairment in vertical head tilt. This is certainly a possibility, as brainstem nuclei including neurons in the vestibular nucleus show pronounced degeneration in human SCA7 patients [7, 181].

Another major finding from these studies is the presence of a functional “calcium homeostasis” module important for Purkinje neuron spiking and which is disrupted in

fxSCA7 92Q mice. Transcriptome analysis of whole cerebellar lysate from fxSCA7 92Q and wild-type mice identified a series of downregulated genes, and subsequent pathway analysis determined that many of these genes are related to calcium homeostasis or IP3 signaling. Several of these genes are ion-channels which are enriched in Purkinje neurons and are important for their function (i.e. *Kcnma1, Cacna1g, Itrp1, Trpc3*). Irregular Purkinje neuron spiking can be elicited in wild-type neurons by blocking a combination of calcium sources and BK channels, the effector potassium channel in this module (Figure 3.7). In addition, BK channels appear to be an essential node in this excitability module, as genetic replacement or pharmacologic activation of BK improves Purkinje neuron spiking in fxSCA7 92Q mice (Figure 3.8). This relationship between ion-channel gene expression and spiking is outlined in Figure 3.11. However, it is possible that this calcium homeostasis module consists of a larger network of genes and is not limited to the aforementioned channel genes described. Alternatively, the core components of the module investigated in these studies (Figure 3.11) may be common to several polyQ SCAs, while these individual SCAs may have several unique components which contribute to dysfunction. For instance, comparisons of transcriptome data between mouse models of SCA1, SCA2, and SCA7 identified the ryanodine receptor gene *Ryr1* as disrupted in SCA1 and SCA2, but not SCA7, while other potassium channel genes (*Kcna6, Kcng4, Kcnc3*) and the voltage-gated sodium channel gene *Scn1a* are commonly downregulated in both models of SCA1 (Figure 3.10) but not SCA2 or SCA7. This suggests that while convergent mechanisms of disease appear likely between SCAs of unique etiologies, other important considerations must be made for individual underlying genetic causes when designing a

broad strategy to target neuronal excitability. In addition, further analysis of the transcriptome data may uncover important transcriptional targets which were not considered in the present studies. It is important to note that the convergent transcriptional changes seen were not limited to the 6 excitability-related genes presented in Figure 3.10. In total, 31 mRNA transcripts were identified as significantly downregulated in all four models investigated. This suggests that other pathways independent of neuronal excitability may be involved in neuronal dysfunction and degeneration in SCA7 and other polyQ SCAs. However, an initial pathway analysis of these 31 transcripts with DAVID 6.8 indicates enrichment of IP3 signaling and calcium signaling pathways, with no other pathway receiving more than 4 hits out of the 31 possible genes. This strengthens the argument that the pathways identified in this chapter are likely to have a unique influence on Purkinje neuron physiology in ataxia. Once available, future studies could also include transcriptome data from mouse models of SCA3, SCA6, and SCA17 in order to fully characterize transcriptional alterations across all polyQ SCAs. However, these SCAs show unique pathology in human patients compared to SCA1, SCA2, and SCA7, including variable Purkinje neuron involvement and greater involvement of other nuclei throughout the CNS [7], suggesting that disease mechanisms unrelated to the aforementioned excitability pathway may be involved.

Overall, the studies in this chapter highlight the relevance of ion-channel dysfunction to altered Purkinje neuron excitability and motor impairment in a mouse model of SCA7. Importantly, these studies demonstrate that neuronal dysfunction is present in many models of SCA and convergent mechanisms of disease related to

neuronal excitability may be present in ataxia. These studies set a foundation for future work investigating transcriptional regulation in both SCA7 and other polyQ SCAs and suggest that neuronal excitability is likely an important consequence of transcriptional dysregulation in Purkinje neurons.

3.6 Acknowledgements

I would like to thank collaborators at Duke University, in particular Colleen Stoyas, Pawel Switonski, Terry Gaasterland, and Albert La Spada, for their contribution to this work by performing the RNA sequencing analysis. I would also like to thank Ravi Chopra for his assistance with the analysis of RNA sequencing data from all four polyQ SCA mouse lines, along with thoughtful contributions to the interpretation of these data. Brandon Lee, Courtney Stewart, Megan Wampler, Tarana Joshi, and W. Michael King assisted with the acquisition and analysis of vestibular phenotype data. I would finally like to thank Annie Zalon, Allison Sylvia, Mariam Reda, John Cooper, Aaron Wasserman, James Dell'Orco, Haoran Huang, and Vikram Shakkottai for technical assistance and helpful discussion while performing these studies.

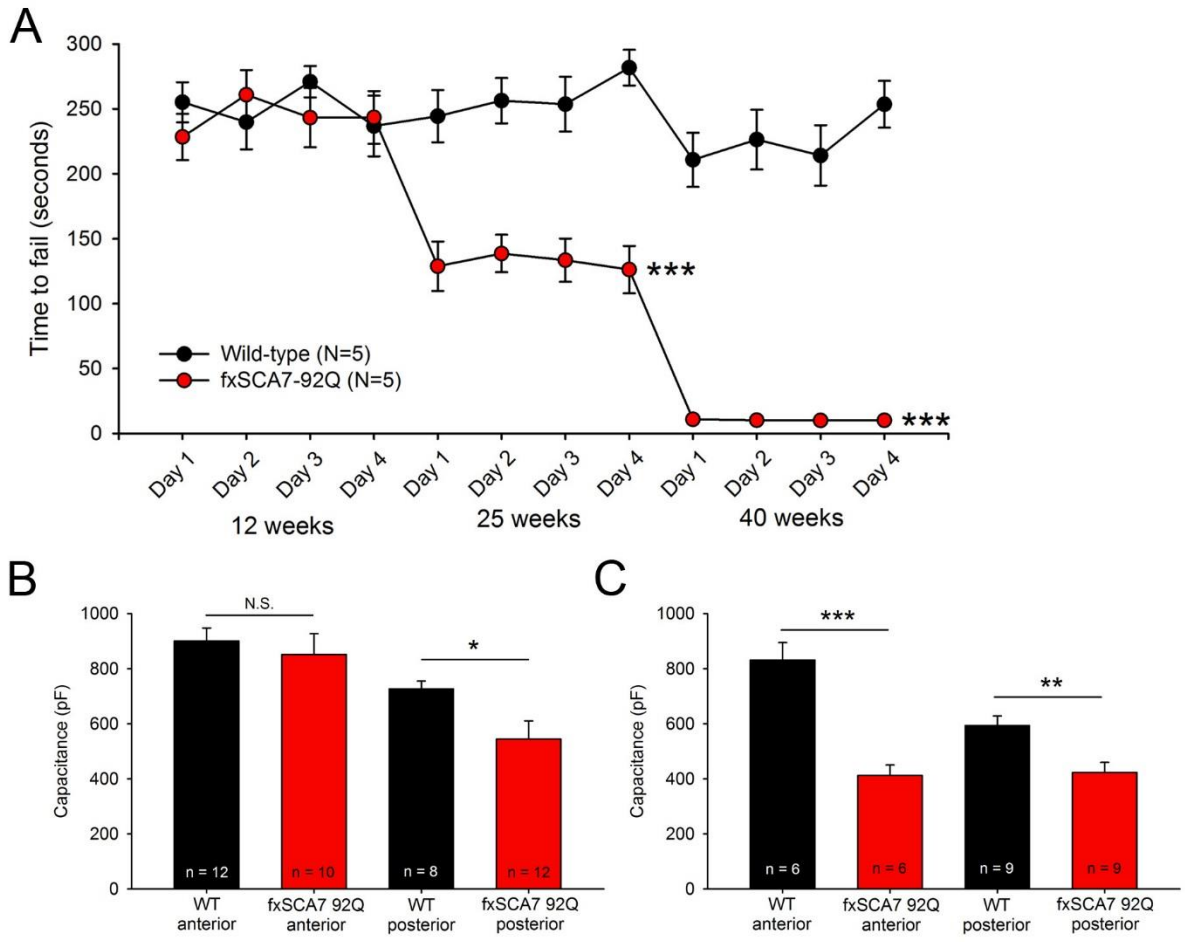

Figure 3.1 Motor impairment and Purkinje neuron degeneration begins at 25 weeks of age in fxSCA7-92Q mice and progresses at 40 weeks of age. (A) As assessed by performance on a constant-speed rotarod, fxSCA7-92Q mice (red) exhibit no motor impairment at 12 weeks of age, but motor impairment becomes significant by 25 weeks of age and 40 weeks of age. **(B)** Total Purkinje neuron capacitance is unchanged in the anterior cerebellar lobules at 25 weeks of age, but is significantly decreased in the posterior lobules of fxSCA7-92Q mice. **(C)** By 40 weeks of age, Purkinje neurons in both the anterior and posterior cerebellar lobules display a significant reduction in total capacitance. Black = wild-type, Red = fxSCA7-92Q. * $p<0.05$, ** $p<0.01$, * $p<0.001$, Two-way repeated-measures ANOVA with Holm-Sidak post-comparison (A) or Student's t-test (B and C).

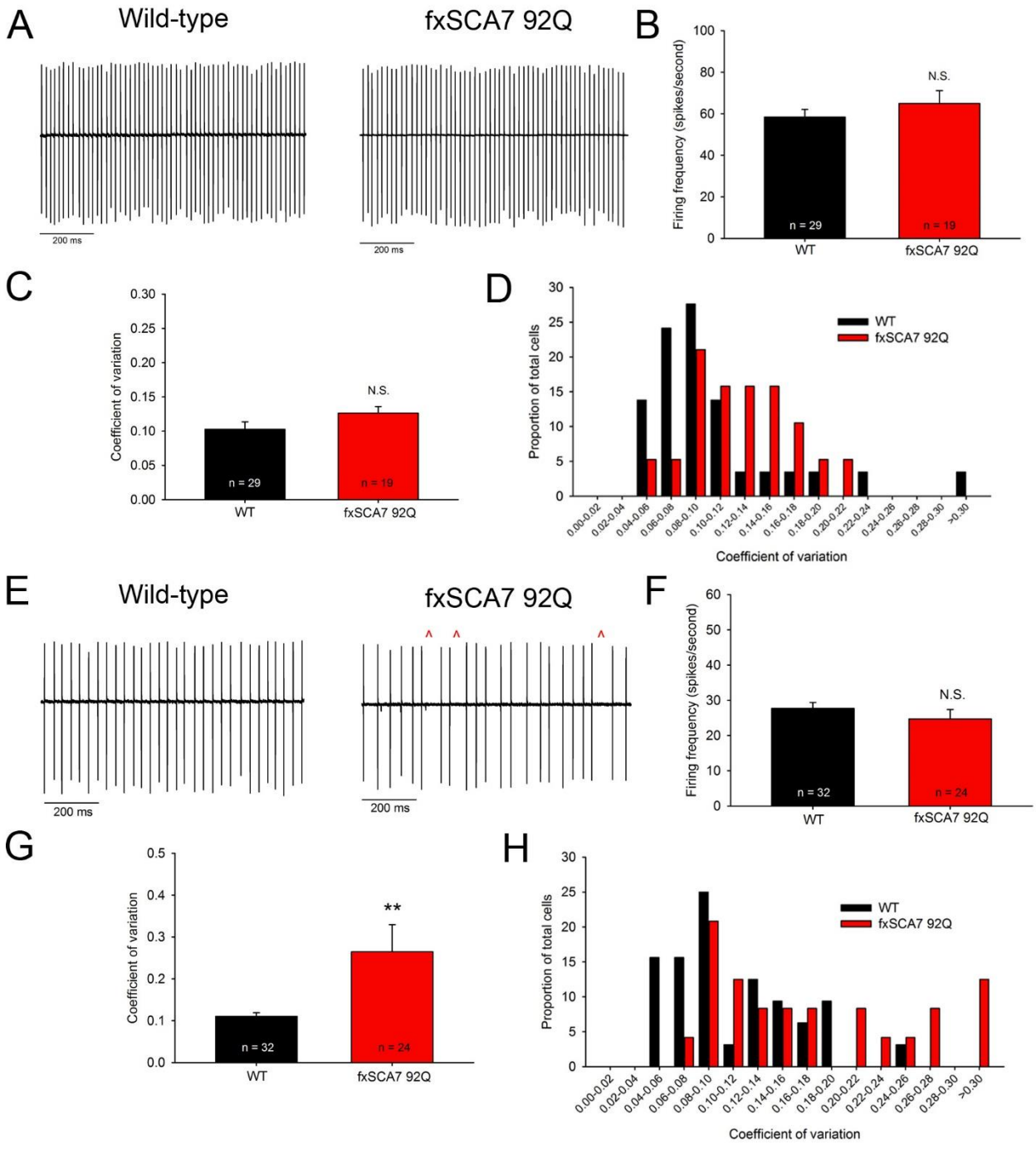

Figure 3.2 Alterations in Purkinje neuron physiology begin in the posterior cerebellar lobules at 25 weeks of age. (A) Representative cell-attached recordings from wild-type and fxSCA7 92Q mice in the anterior cerebellar lobules. **(B)** Purkinje neuron firing frequency is unchanged between genotypes in the anterior cerebellar lobules. **(C)** The regularity of Purkinje neuron spiking, as represented by the coefficient of variation (CV) of the interspike interval, is unchanged between genotypes in the anterior cerebellar lobules. **(D)** Distribution of CV values indicates no major shift in the anterior cerebellar lobules, although a trend of higher CV values is present for fxSCA7

92Q mice. **(E)** Representative cell-attached recordings from wild-type and fxSCA7 92Q mice in the posterior cerebellar lobules. **(F)** Purkinje neuron firing frequency is unchanged between genotypes in the posterior cerebellar lobules. **(G)** The CV of Purkinje neuron spiking is significantly increased in the posterior cerebellar lobules of fxSCA7 92Q mice, indicating more irregular spiking. **(H)** Distribution of CV values indicates a shift to higher CV values in Purkinje neurons of the posterior cerebellar lobules of fxSCA7 92Q mice when compared to wild-type littermate controls. $^{**}p<0.01$, Student's t-test.

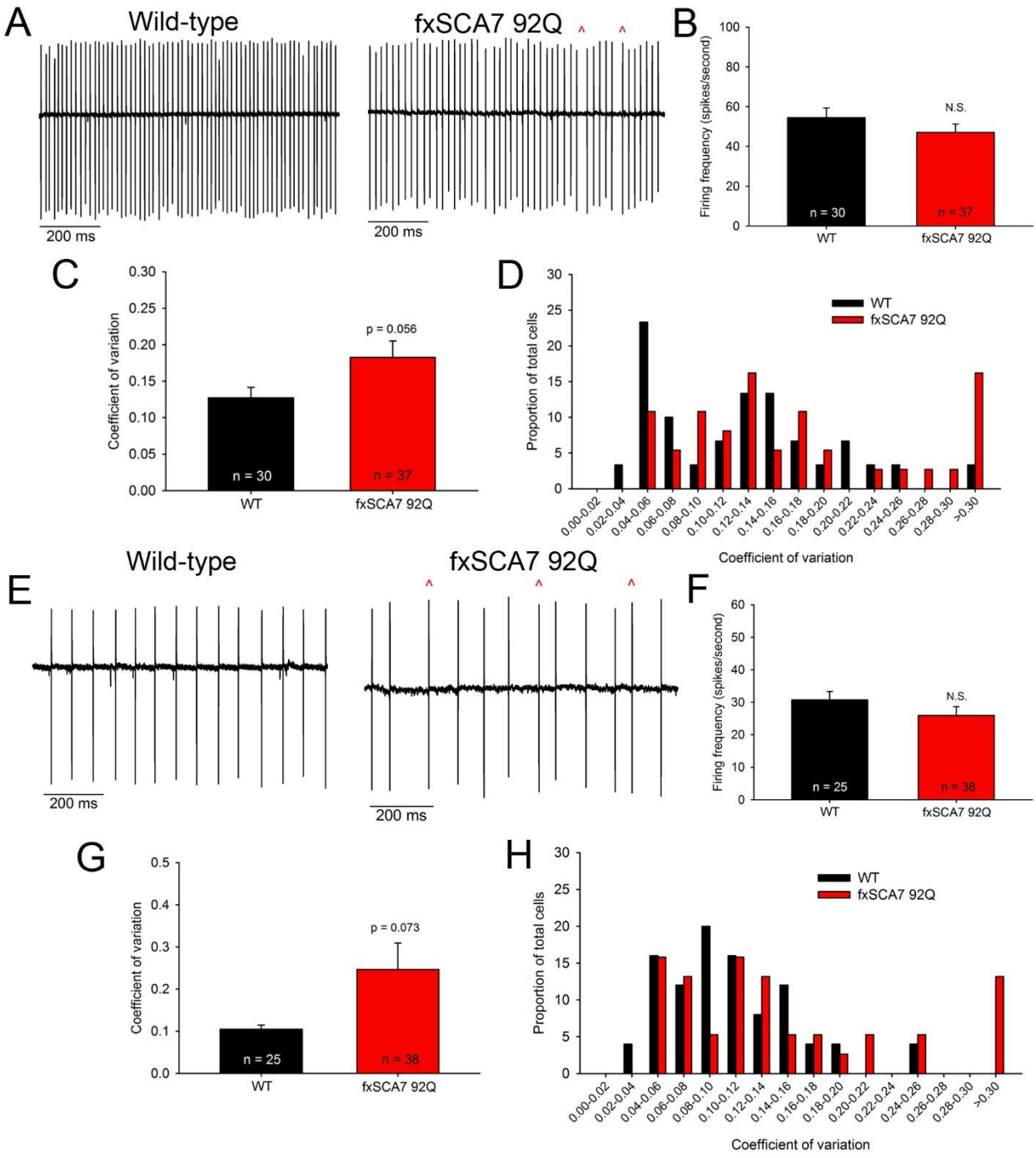

Figure 3.3 Alterations in Purkinje neuron spiking are present in both anterior and posterior cerebellar lobules at 40 weeks of age. (A) Representative cell-attached recordings from wild-type and fxSCA7 92Q mice in the anterior cerebellar lobules. **(B)** Purkinje neuron firing frequency is unchanged between genotypes in the anterior cerebellar lobules. **(C)** The regularity of Purkinje neuron spiking is slightly, but not significantly, increased in the anterior cerebellar lobules of fxSCA7 92Q mice. **(D)** Distribution of CV values indicates fewer low-CV and more high-CV Purkinje neurons in the anterior cerebellar lobules of fxSCA7 92Q mice. **(E)** Representative cell-attached recordings from wild-type and fxSCA7 92Q mice in the posterior cerebellar lobules. **(F)**

Purkinje neuron firing frequency is unchanged between genotypes in the posterior cerebellar lobules. **(G)** The CV of Purkinje neuron spiking is increased in the posterior cerebellar lobules of fxSCA7 92Q mice, indicating more irregular spiking, although statistical significance was not reached. **(H)** Distribution of CV values indicates a shift to higher CV values in Purkinje neurons of the posterior cerebellar lobules of fxSCA7 92Q mice when compared to wild-type littermate controls. Statistical significance determined by Student's t-test.

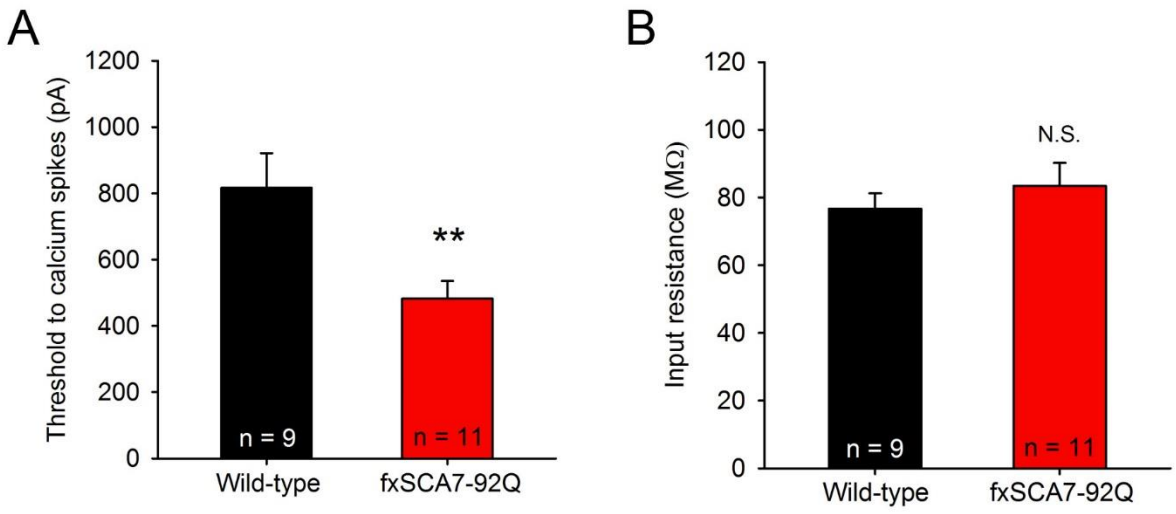

Figure 3.4 Dendritic excitability is increased in Purkinje neurons from the posterior cerebellar lobules of fxSCA7-92Q mice. (A) In the presence of tetrodotoxin, the threshold to elicit dendritic calcium spikes upon somatically-injected current is significantly lower in fxSCA7-92Q mice compared to wild-type littermate controls. **(B)** Input resistance does not differ significantly between experimental groups. ***p*<0.01, Student's t-test.

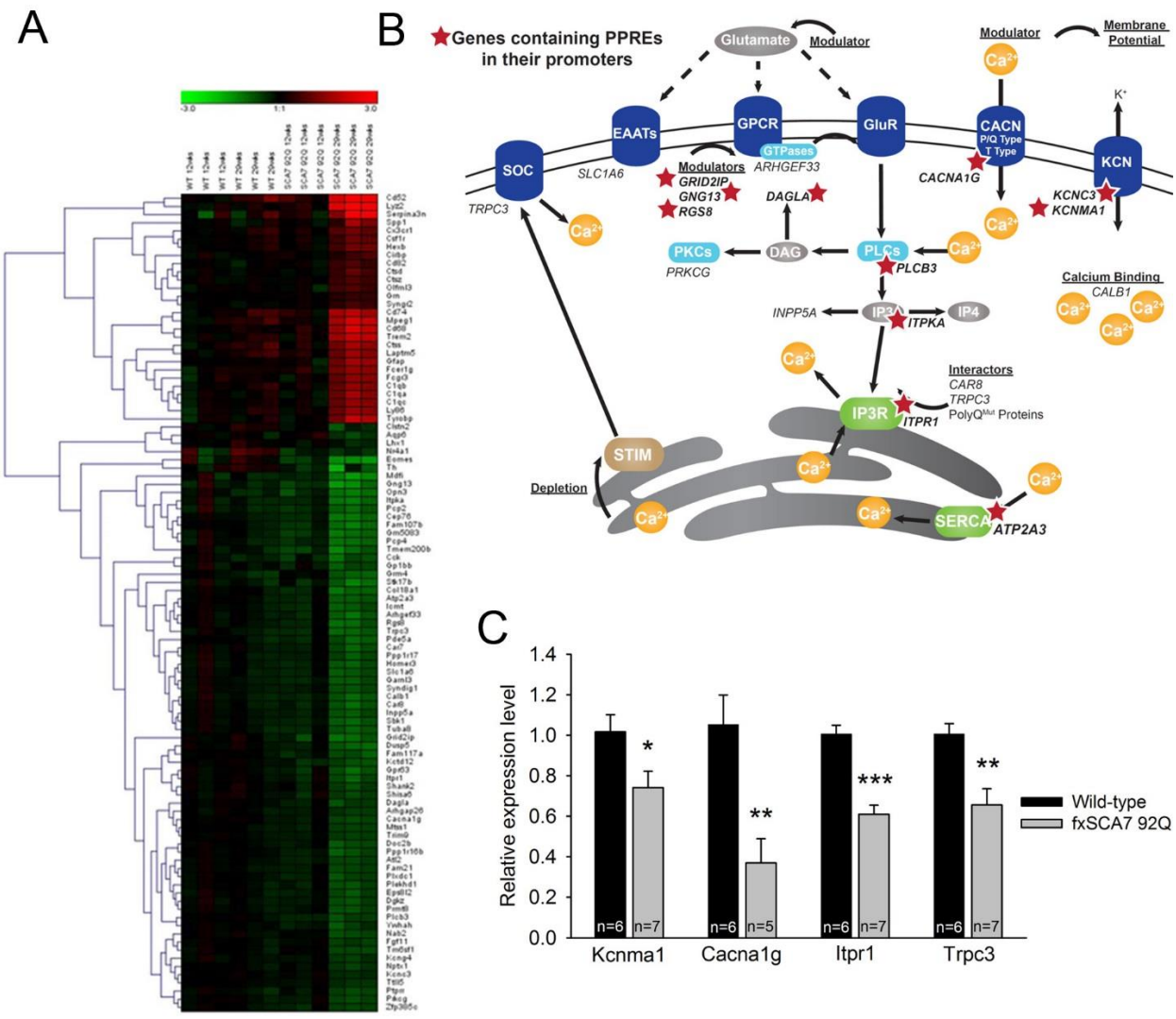

Figure 3.5 Transcriptome analysis indicates reduced expression of genes important for calcium homeostasis and IP3 receptor signaling. (A) RNA sequencing data from whole cerebellar lysate of wild-type and fxSCA7 92Q mice indicates a list of 100 genes with significantly altered expression. Upregulated genes are listed in red, and downregulated genes are listed in green. **(B)** Downregulated genes within the calcium homeostasis and IP3 receptor signaling modules are presented, with relevant pathways highlighted. Several of the genes identified in RNA sequencing analysis are known to cause ataxia either in human SCAs or mice, as indicated. **(C)** Quantitative PCR analysis of whole cerebellar lysate confirms that mRNA transcript expression for several ion-channel genes is reduced in fxSCA7 92Q mice. These genes are essential components of the calcium homeostasis module outlined in (B). **p*<0.05, ***p*<0.01, ****p*<0.001, Student's t-test. *Note: experiments for 3.5 (A-B) performed by Colleen Stoyas and Albert La Spada, University of California, San Diego.*

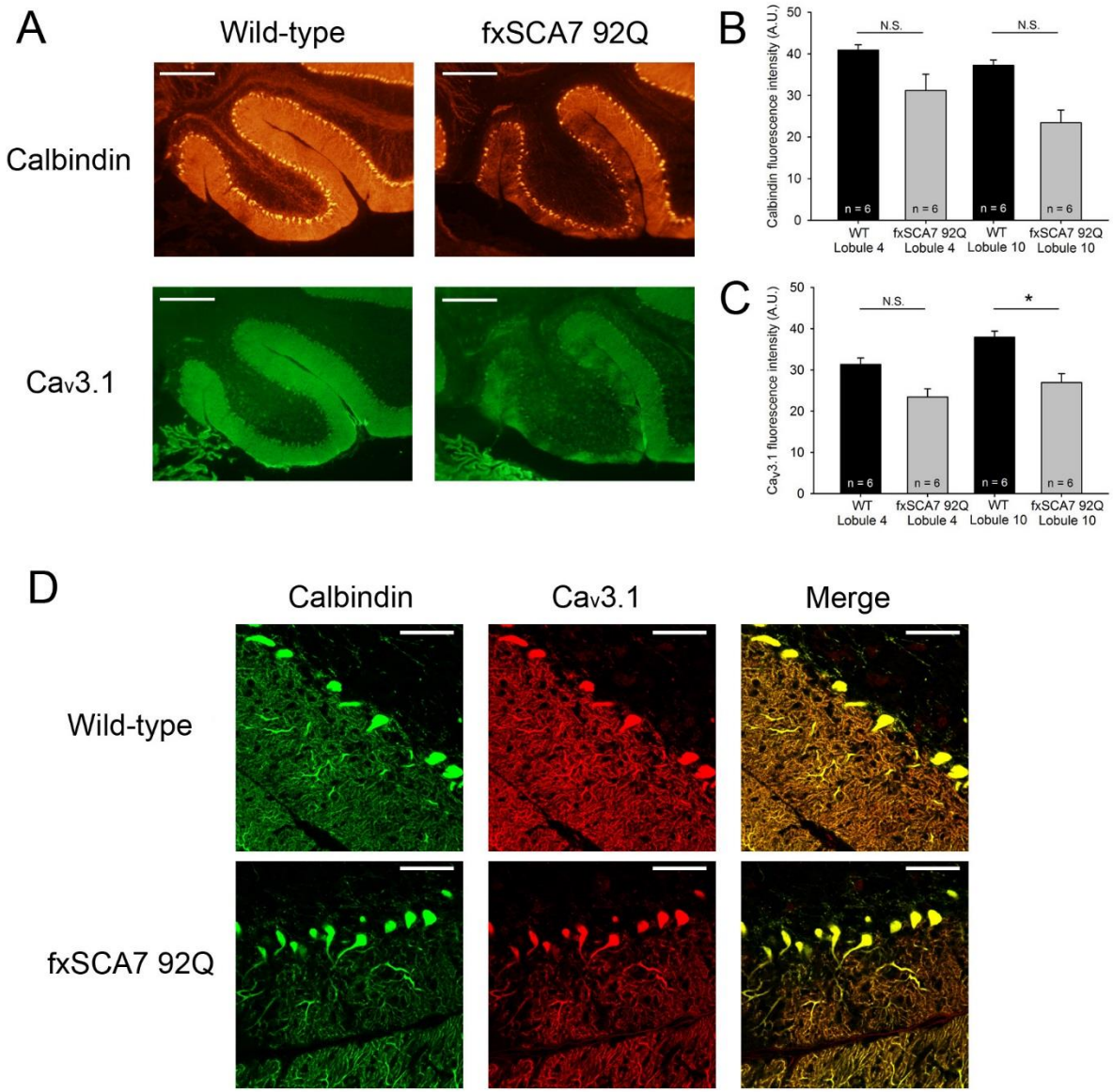

Figure 3.6 T-type calcium channel expression is reduced in the posterior cerebellar lobules of fxSCA7 92Q mice. (A) When stained for calbindin, to label Purkinje neurons (orange), and $Ca_V3.1$ (green), protein expression appears reduced in cerebellar lobule 10 of fxSCA7 92Q mice when compared to wild-type littermate controls. Scale bar: 200 µm **(B)** Upon quantification, calbindin expression was not significantly changed but was trending downward in both lobule 4 and lobule 10 of fxSCA7 92Q mice. **(C)** $Ca_V3.1$ expression was significantly reduced in lobule 10, but not lobule 4, of fxSCA7 92Q mice. **(D)** Confocal images confirm that dendritic expression of calbindin and $Ca_V3.1$ is reduced in some regions of fxSCA7 92Q cerebellum but unchanged in other neurons. Scale bar: 60 µm. *p<0.05, Student's t-test.

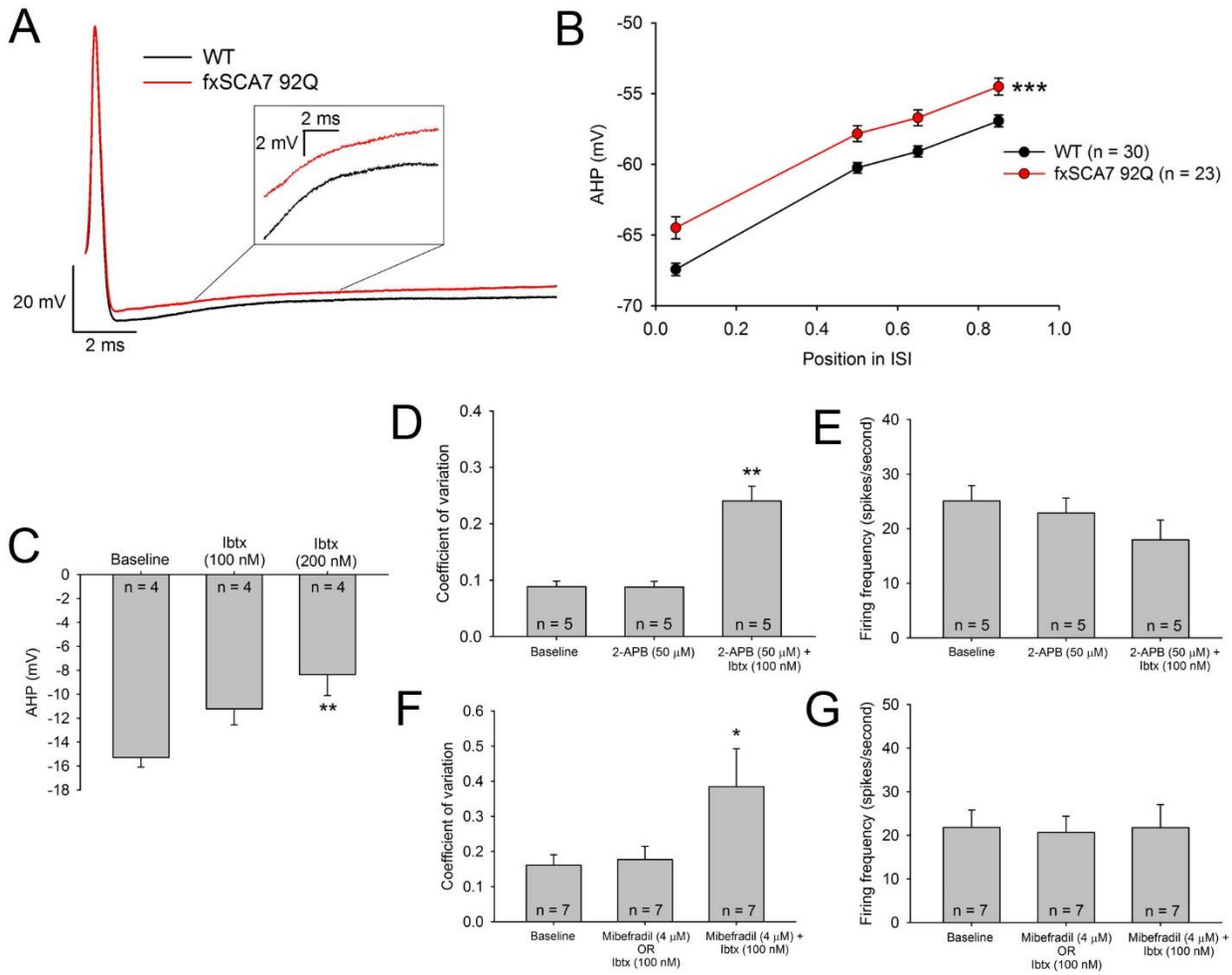

Figure 3.7 An impaired calcium homeostasis module, composed of K_{Ca} channels and calcium sources, contributes to irregular spiking in Purkinje neurons from the posterior cerebellar lobules of fxSCA7 92Q mice. (A) Representative trace of the afterhyperpolarization (AHP) in wild-type and fxSCA7 92Q Purkinje neurons at 25 weeks of age. **(B)** The membrane potential is significantly depolarized throughout the interspike interval in fxSCA7 92Q Purkinje neurons, indicating K_{Ca} channel dysfunction. **(C)** In wild-type Purkinje neurons, 100 nM Iberiotoxin partially inhibits BK channel function, as indicated by a reduction in the amplitude of the fast AHP, compared to 200 nM Iberiotoxin which is known to fully occlude BK channel currents [125]. **(D)** 2-APB (50 μM), which blocks IP3 receptor and TRPC3 currents [160, 161], does not increase the coefficient of variation of wild-type Purkinje neuron spiking. When BK channels are partially blocked with iberiotoxin (100 nM), 2-APB significantly increases the coefficient of variation. **(E)** Neither 2-APB nor 2-APB + iberiotoxin alters firing frequency. **(F)** Neither mibefradil alone (4 μM), which blocks $Ca_V3.1$ [162], nor iberiotoxin alone (100 nM) alters the coefficient of variation of wild-type Purkinje neuron spiking. When combined, iberiotoxin (100 nM) and mibefradil (4 μM) significantly increases the coefficient of variation. **(G)** None of mibefradil alone, iberiotoxin alone, nor mibefradil + iberiotoxin

alters firing frequency. *p<0,05, **p<0.01, ***p<0.001, two-way repeated measures ANOVA with Holm-Sidak post-comparison test (B), or one-way ANOVA with Holm-Sidak post-comparison test (C-G).

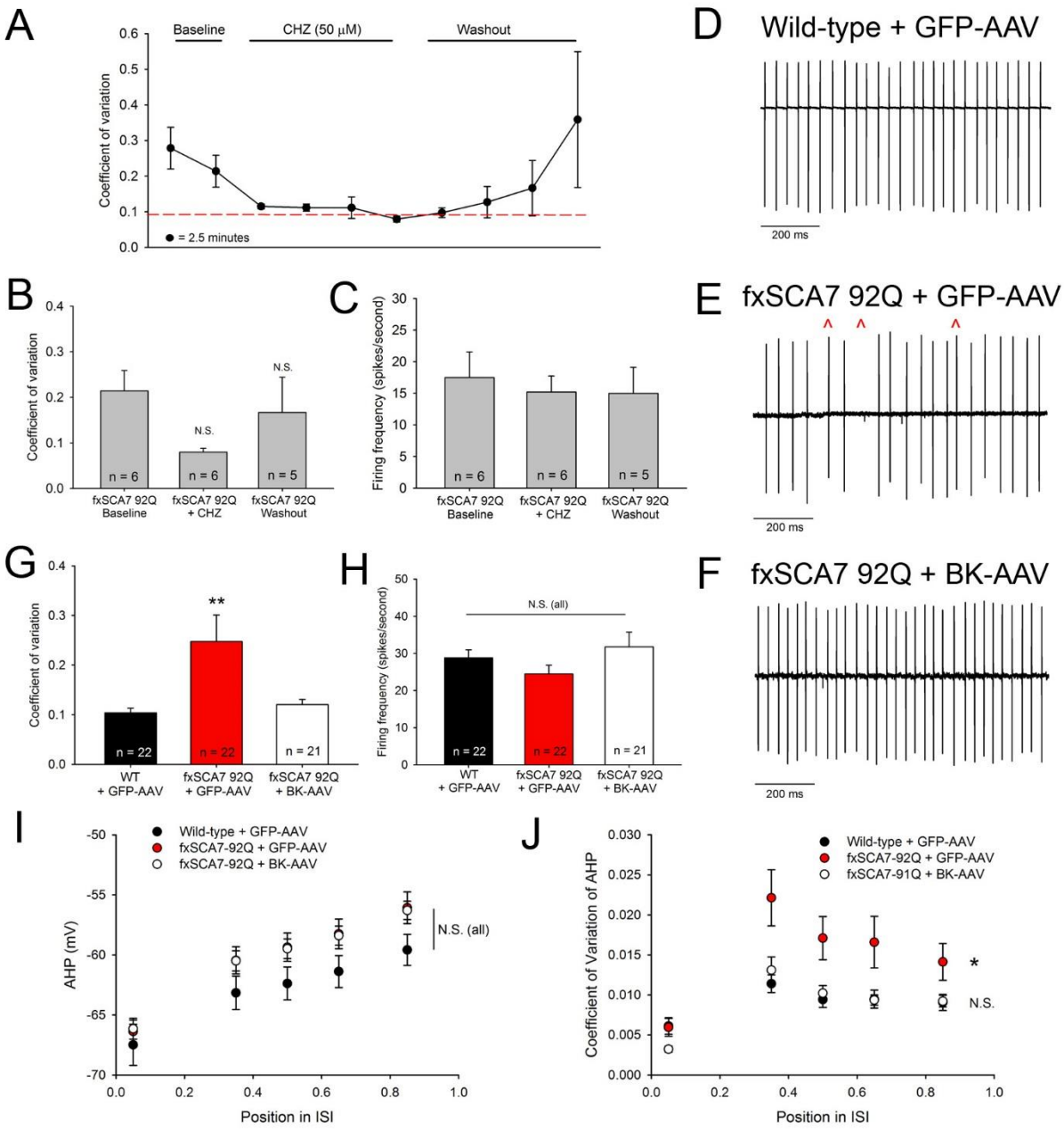

Figure 3.8 K_{Ca} channel activation or re-expression normalizes spike regularity in fxSCA7 92Q Purkinje neurons. (A) Regularity of fxSCA7 92Q Purkinje neuron spiking over time. Spiking becomes more regular in the presence of chlorzoxazone (CHZ, 50 μM) and returns to baseline upon washout **(B)** Summarized data from (A). **(C)** CHZ does not alter fxSCA7 92Q Purkinje neuron spike frequency. **(D-F)** Representative cell-attached recordings from Purkinje neurons of wild-type treated with GFP-AAV, fxSCA7 92Q treated with GFP-AAV, and fxSCA7 92Q treated with BK-AAV, respectively. Red carats denote irregular interspike intervals. **(G)** The coefficient of variation of the interspike interval, which is significantly increased in fxSCA7 92Q Purkinje neurons

treated with GFP-AAV, is restored to wild-type levels in fxSCA7 92Q Purkinje neurons treated with BK-AAV. **(H)** Firing frequency is not significantly altered across groups. **(I)** Absolute AHP decay is not visibly changed upon BK-AAV treatment in fxSCA7 92Q Purkinje neurons, although **(J)** the coefficient of variation of the AHP is restored upon BK-AAV treatment in fxSCA7 92Q Purkinje neurons. *p<0.05, **p<0.01, (B,C,G,H) one-way ANOVA with Holm-Sidak post-comparison test, (I,J) two-way repeated-measures ANOVA with Holm-Sidak post-comparison test.

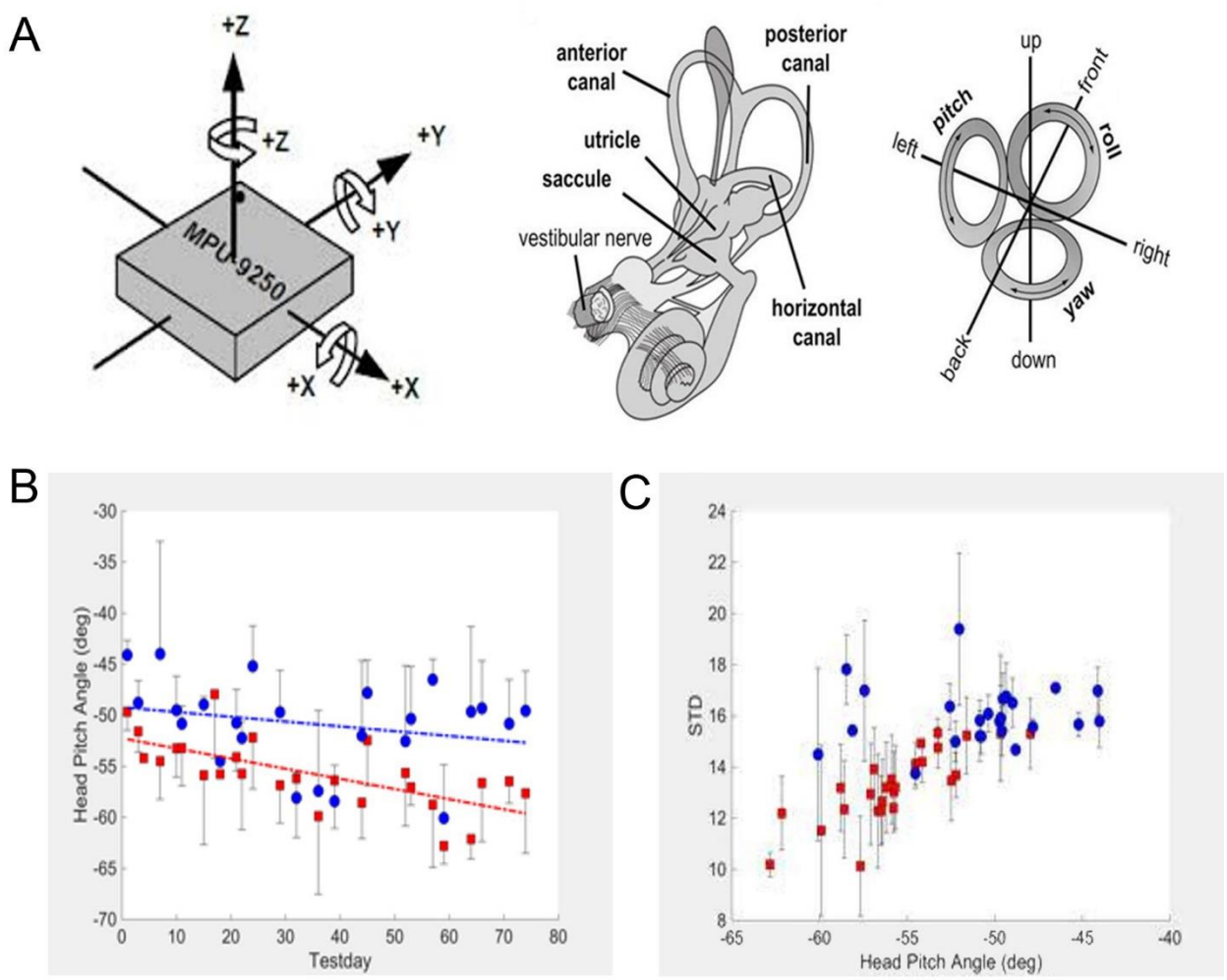

Figure 3.9 fxSCA7 92Q mice possess a specific postural deficit in association with altered cerebellar physiology. (A) Schematic of the inertial measurement unit (IMU), along with how data acquired by the IMU provide information about head orientation, including pitch, yaw, and roll. These movements reflect the function of the vestibular system, which receives input from Purkinje neurons in the posterior cerebellar lobules. **(B)** fxSCA7 92Q mice (red) begin to exhibit a vertical head tilt between 20 and 30 weeks of age, as indicated by a reduction in the head pitch angle over time, when compared to wild-type littermate control animals (blue). **(C)** The standard deviation of the head pitch angle shown in (B) indicates that fxSCA7 92Q mice display less overall variability in head pitch angle than wild-type littermate controls, indicating that the increase in head pitch angle is persistent.

A

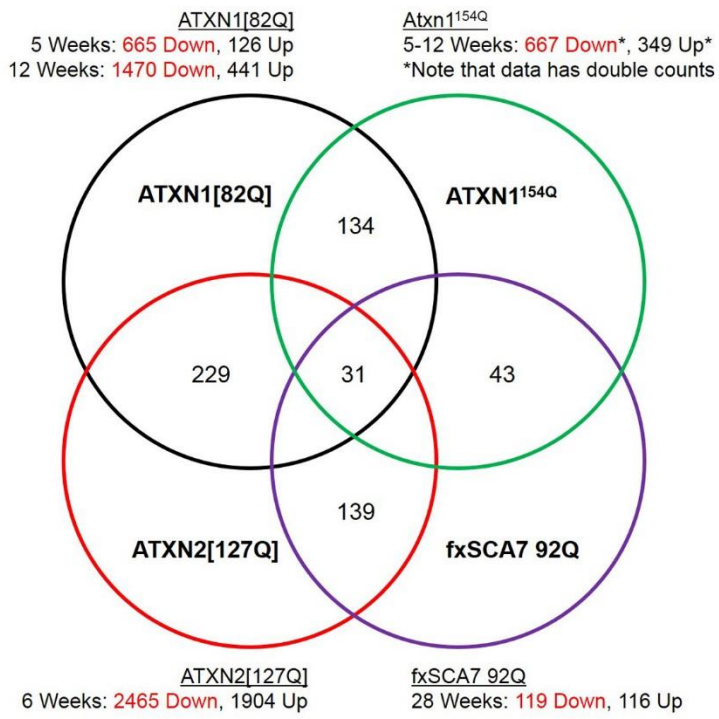

B

All models	Three models	Two models
Kcnma1	*Ryr1*	*Kcna6*
Trpc3		*Kcng4*
Cacna1g		*Kcnc3*
Itpr1		*Scn1a*
Kcnip2		
Kctd12		

Figure 3.10 Transcriptome analysis indicates shared molecular targets between SCAs of different etiologies. (A) Publically-available transcriptome data from mouse models of SCA1 (ATXN1[82Q], [68] and ATXN1^{154Q}, [170]), SCA2 (ATXN2[127Q], [171]), and SCA7 (fxSCA7 92Q, Figure 3.5) were used to identify commonly disrupted RNA transcripts in whole cerebellar lysate. In total, transcripts of 31 unique genes were identified as downregulated across all four models of SCA. **(B)** Of the 31 downregulated genes from (A), we identified only four ion-channel transcripts which are commonly downregulated across all four models of SCA, along with the potassium channel activating protein *Kcnip2* and potassium channel tetramerization protein *Kctd12*. These ion-channel genes (*Kcnma1, Trpc3, Cacna1g, Itpr1,* in bold) form the calcium homeostasis module outlined in this chapter, indicating the potential importance of this module for Purkinje neuron physiology and its disruption as a pathogenic mechanism in SCA. Other ion-channel genes showed reduced transcript expression in three or two models of SCA, indicating that these genes may also be important targets.

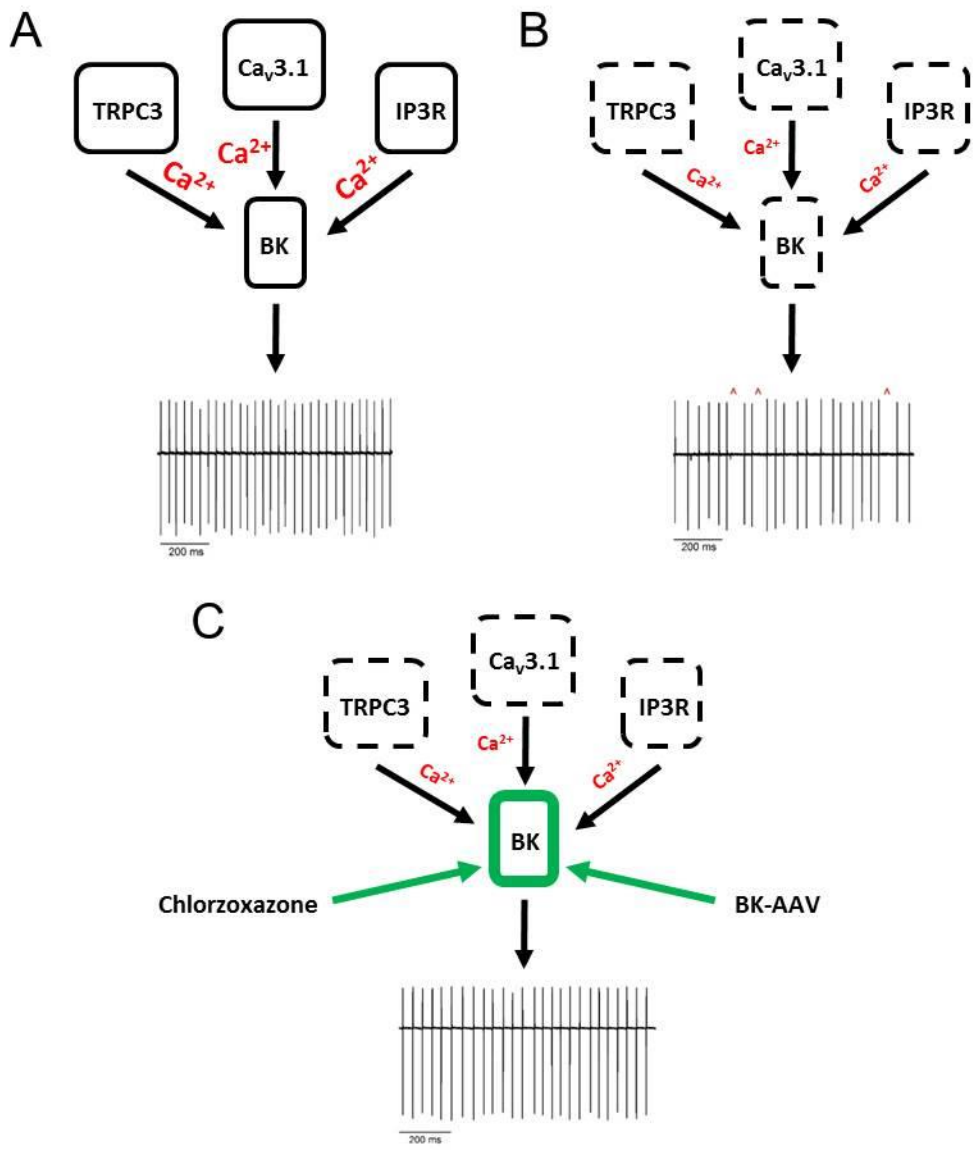

Figure 3.11 Targeting altered function of a calcium homeostasis module improves altered Purkinje neuron spiking in fxSCA7 92Q mice. (A) In wild-type Purkinje neurons, BK channels largely control the regularity of spiking and rely on intracellular calcium and depolarization for activation. Traditionally, $Ca_V2.1$ channels have been thought to preferentially couple to BK channels in Purkinje neurons [16]. Through the studies in this thesis, I postulate that other calcium sources exist for BK, including $Ca_V3.1$, the IP3 receptor, and TRPC3. **(B)** In fxSCA7 92Q mice, or upon pharmacologic blockade, reduced function of both calcium sources and BK channels produces irregular Purkinje neuron spiking. **(C)** In fxSCA7 92Q Purkinje neurons, activation or genetic re-expression of BK channels is sufficient to normalize the regularity of spiking. This suggests that targeting the effector BK channel may be a reasonable pharmacologic approach to improve Purkinje neuron spiking in SCA7. Relative amount of calcium indicated by the size of "Ca^{2+}" labels. Reduced expression or function of ion-channels indicated by dotted lines. Re-expression or activation of BK is indicated with green.

Chapter 4

Sirtuin-1 overexpression improves Purkinje neuron dysfunction in spinocerebellar ataxia type 7

4.1 Abstract

Spinocerebellar ataxia type 7 (SCA7) is a fatal neurodegenerative disorder characterized by a progressive loss of motor function along with blindness due to retinal degeneration. SCA7 results from an expansion of a CAG repeat sequence in the *ATXN7* gene beyond a pathogenic length, making it one of nine known polyglutamine repeat-associated disorders, all of which are associated with neuronal dysfunction and degeneration. In SCA7 mice, widespread transcriptional alterations accompany impairments in motor function, changes in cerebellar Purkinje neuron spiking, and dendritic degeneration. Sirtuins are a class of nutrient-sensing protein deacetylases involved in a number of cellular processes. Evidence from studies in yeast and mammals suggests that sirtuin activation promotes lifespan expansion and may offer neuroprotective benefits in a number of neurodegenerative disorders. In order to determine whether sirtuin activation may have a potential role in the treatment of SCA7, we genetically overexpressed Sirt1 in fxSCA7 92Q mice and assessed transcriptional status of cerebellar target genes, along with Purkinje neuron physiology and dendritic degeneration. In these studies, Sirt1 overexpression improved the cerebellar mRNA transcript levels of several genes important to calcium homeostasis and Purkinje neuron

physiology, which correspond to improvements in Purkinje neuron spiking and dendritic degeneration. These studies indicate a potential role for Sirt1 activation in treating cerebellar ataxia.

4.2 Introduction

Neurodegenerative disorders are largely heterogeneous, demonstrating variability in age-of-onset, neuronal vulnerability, and patient symptoms. Although these diseases are as diverse as their underlying causative genetic mutations, several trends exist across a number of disorders. Many neurodegenerative disorders are age-related, the most striking example being Alzheimer's disease which is thought to affect 15% of individuals aged 65 or older and with an incidence of almost 50% in individuals above the age of 85 [182]. Age-related neurodegenerative disorders, including but not limited to Alzheimer's disease, demonstrate a number of cellular pathologies which may contribute to negative disease outcomes, such as neuronal inclusions, mitochondrial dysfunction, disruptions in protein homeostasis, and electrophysiologic abnormalities [183-186]. Age-related neurodegenerative disorders are a public health concern as the global aging population continues to grow on a yearly basis, with the total number of American citizens aged 65 or older expected to double from 46 million to 98 million by 2060 [187]. As such, the search for neuroprotective therapies which increase the likelihood of healthy aging is of particular importance.

Among the aforementioned neurodegenerative disorders are the polyglutamine (polyQ) repeat-expansion diseases, including Huntington's disease, spinal and bulbar muscular atrophy (SBMA), and six forms of inherited spinocerebellar ataxia (SCA1, 2, 3, 6, 7, & 17). In polyQ disorders, expansion of a CAG repeat sequence, which encodes

the amino acid glutamine, exceeds a pathologic length and results in symptoms of the respective disorder, depending on the affected protein [1]. Although the disease-causing proteins are widely or ubiquitously expressed throughout the central nervous system, specific neuronal structures are affected in these disorders and result in distinct symptoms [7]. The common feature of cell death links these degenerative disorders, and this neurodegeneration was initially thought to correspond with symptom onset and severity. However, mouse models of many neurodegenerative disorders have indicated that a period of neuronal dysfunction precedes over neuronal loss [71, 72], and that this neuronal dysfunction may therefore more closely relate to symptom onset and progression.

Sirtuins are a family of NAD^+-dependent protein deacetylases. In yeast studies, overexpression of the protein Sir2 was found to result in lifespan extension [188]. Sirtuin-1 (Sirt1) is the mammalian orthologue of Sir2 and has been the focus of many recent research efforts, along with other members of this protein family (Sirt2 – Sirt7) [189]. The compound resveratrol, which activates Sirt1, has been reported to promote lifespan extension in yeast [190], flies [191], and mice placed on a high-calorie diet [192], although untreated wild-type mice do not experience lifespan extension upon resveratrol treatment [193]. While the ability of sirtuins to extend lifespan in mammals remains controversial [194], some neurodegenerative disorders respond positively to caloric restriction [195-198], suggesting that NAD^+ availability may slow degenerative processes. In addition, recent studies suggest that Sirt1 may be capable of achieving neuroprotection in degenerative disorders such as Huntington's disease [199, 200] and Alzheimer's disease [201], and that several Sirt1 targets are members of neuroprotective pathways in the CNS

[202]. Despite evidence for longevity and neuroprotection, the mechanisms of sirtuin activation are not fully understood.

One mechanism of action of Sirt1 is to deacetylate and activate specific transcription factors to promote expression of specific target genes [203]. In order to determine whether sirtuin activation may represent a potential strategy to reverse transcriptional alterations and improve outcomes in SCA, we genetically overexpressed Sirt1 in fxSCA7 92Q mice, a model of SCA7. The resulting studies indicate that Sirt1 overexpression partially improves transcriptional alterations, abnormalities in Purkinje neuron spiking, and Purkinje neuron dendritic degeneration. These studies add to evidence that sirtuin activation may be a broad therapeutic strategy for age-related neurodegenerative disorders including SCA.

4.3 Methods

4.3.1 Mice

The Sirt1 overexpression line was derived by mating SIRT1^{STOP} transgenic mice [204] to *Cre*-hemizygous mice to generate Sirt1 uOE mice, which overexpress Sirtuin-1 in all tissues under a CAGGS promoter. These mice were mated with the previously characterized mPrP-fx SCA7-92Q BAC mouse model of SCA7 [159] (chapter 3) to be utilized in rescue studies. Sirt1 uOE and fxSCA7 92Q lines were maintained on the C57BL/6J background. Heterozygous Sirt1 uOE mice were bred to hemizygous fxSCA7 92Q mice, in which the F1 mice of crosses were used for experimentation. The resulting genotypes are as follows:

1. SCA7 (-), Sirt1 (-): denoted wild-type
2. SCA7 (+), Sirt1 (-): denoted fxSCA7 92Q

3. SCA7 (-), Sirt1 (+): denoted Sirt1 uOE
4. SCA7 (+), Sirt1 (+): denoted Sirt1 uOE-fxSCA7 92Q

Efforts were made to balance the sex of animals used for all experiments.

4.3.2 oPOSSUM analysis of transcriptome data

Gene set enrichment analysis was performed on RNA sequencing data comparing whole cerebella lysate from fxSCA7 92Q mice and wild-type littermate controls at 29 weeks of age (Section 3.3.4). In order to identify transcription factor binding sites (TFBSs) which are enriched in the promoter regions on downregulated genes, we used oPOSSUM v3.0 and applied a 'z' score threshold of ≥ 10. Results were analyzed by number of hits and strength of 'z' score in order to identify putative TFBSs.

4.3.3 Western blot analysis

Mouse cerebella were lysed in RIPA buffer (Life Technologies) and homogenized by trituration. We used the following antibodies for immunoblot analysis: PCG-1α (SC-13067, Santa Cruz; 1:1000); acetyl-lysine (9441, Cell Signaling; 1:1000); and β-actin (ab8226, Abcam; 1:10000). Immunoprecipitation was performed with antibody for PCG-1α (SC-13067, Santa Cruz; 1:20), and densitometry was performed in ImageJ.

4.3.4 Real-time quantitative RT-PCR

Mice were euthanized under isoflurane anesthesia, and cerebella were rapidly removed and flash-frozen in liquid nitrogen. Tissue was stored at -80^{o}C until processing. RNA was isolated from the whole cerebellum of animals using TRIzol (Life Technologies or Invitrogen), and treated with DNAse I in the form of TURBO-DNAse (Life Technologies) to remove traces of genomic DNA, or purified with the RNeasy mini-kit (Qiagen). Reverse transcription was performed with SuperScript Reverse Transcriptase (Life

Technologies) or with the iScript cDNA synthesis kit (Bio-Rad). Quantitative PCR was performed using TaqMan probes (Life Technologies) and TaqMan Universal PCR Mix (Life Technologies) on a CFX384 Touch system (Bio-Rad), or with the iQ SYBR Green Supermix (Bio-Rad) in a MyiQ Single Color Real-Time PCR Detection System (Bio-Rad). Gene expression was normalized to GAPDH levels. Delta CT values were calculated as $C_t^{target} – C_t^{GAPDH}$. All experiments were performed with at least three technical replicates. Relative fold changes in gene expression were calculated using the $2^{-\Delta\Delta Ct}$ method [205]. Data are presented as the average of the biological replicates + standard error of the mean (S.E.M.).

4.3.5 Nanostring transcriptome analysis

Cerebellar transcriptome analysis of wild-type, fxSCA7 92Q, Sirt1 uOE, and Sirt1 uOE-fxSCA7 92Q mice was performed by Nanostring Technologies. 100 of the most highly-downregulated transcripts were analyzed for total copy number and normalized to wild-type expression levels. Transcripts were analyzed by one-way ANOVA, with statistical significance indicated for transcripts which show improved expression in Sirt1 uOE-fxSCA7 92Q mice compared to fxSCA7 92Q mice.

4.3.6 Patch-clamp electrophysiology

Patch-clamp recordings were performed as described in section 3.3.3. Since no gross changes in Purkinje neuron physiology were observed between 25 weeks and 40 weeks of age (chapter 3), mice from Sirt1 uOE-fxSCA7 92Q crosses were treated as equivalent in these studies. In general, most mice were 29-31 weeks of age at the time of recording.

4.3.6.1 Patch-clamp electrophysiology: solutions

Artificial cerebrospinal fluid (aCSF) contained the following: 125 mM NaCl, 2.5 mM KCl, 26 mM $NaHCO_3$, 1.25 mM NaH_2PO_4, 2 mM $CaCl_2$, 10 mM HEPES, and 10 mM glucose. For all recordings, other than dendritic capacitance measurements, pipettes were filled with internal recording solution containing the following: 119 mM K-Gluconate, 2 mM Na-Gluconate, 6 mM NaCl, 2 mM $MgCl_2$, 0.9 mM EGTA, 10 mM HEPES, 14 mM Tris-phosphocreatine, 4 mM MgATP, 0.2 mM Tris-GTP, at pH 7.3 and osmolarity 290 mOsm. For capacitance measurements, internal recording solution contained: 140 mM CsCl, 2 mM $MgCl_2$, 1 mM $CaCl_2$, 10 mM EGTA, 10 mM HEPES, 4 mM Na_2ATP, at pH 7.3 and osmolarity 287 mOsm.

4.3.6.2 Acute slice preparation for patch clamp recordings

Mice were anesthetized by isoflurane inhalation and decapitated. The brain was removed and submerged in pre-warmed (33^{o}C) aCSF. Acute parasagittal slices were prepared in aCSF held at 32.5-34^{o}C on a VT1200 vibratome (Leica) to a thickness of 300 µm. Once slices were obtained, they were incubated in carbogen-bubbled (95% O_2, 5% CO_2) aCSF at 33^{o}C for 45 min. Slices were then stored in carbogen-bubbled aCSF at room temperature until use. During recording, slices were placed in a recording chamber and continuously perfused with carbogen-bubbled aCSF at 33^{o}C at a flow rate of 2.5 mL/min.

4.3.6.3 Patch-clamp recordings

Purkinje neurons were visually identified for patch-clamp recordings using a 40x water immersion objective and a Nikon Eclipse FN1 upright microscope with infrared differential interference contrast (IR-DIC) optics. Identified cells were visualized using NIS Elements image analysis software. Borosilicate glass patch pipettes were pulled to

resistances of 3-4 MΩ for all recordings. Recordings were performed 1-5 hours after slice preparation. Data were acquired using an Axopatch 200B amplifier, Digidata 1440A interface (MDS Analytical Technologies), and pClamp-10 software (Molecular Devices). All data were digitized at 100 kHz. Whole-cell recordings were rejected if the series resistances changed by >20% during the course of recording, or if the whole-cell series resistance rose above 15 MΩ. All voltages are corrected for the liquid gap junction potential, which was calculated to be 10 mV [71]. All recordings performed in Sirt1 crosses were performed with the experimenter blind to genotype.

4.3.6.4 Capacitance measurements

Acute cerebellar slices were obtained as described above. Capacitance measurements were performed in the presence of 50 µM picrotoxin to block spontaneous $GABA_A$ synaptic currents, and recording pipettes were filled with a cesium chloride-based internal pipette solution as described above. Recordings were performed at RT. Capacitive transients were obtained in voltage-clamp mode using 1 second steps to -70 mV from a holding potential of -80 mV. Recordings were excluded if the measured input resistance was under 100 MΩ. Dendritic capacitance was determined using a method for the analysis of an equivalent circuit which represents Purkinje neurons [163]. Input resistance was corrected offline and the decay of the capacitive transient was fit using a two-exponential decay function:

$$I(t) = A_1 e^{-\frac{t}{\tau_1}} + A_2 e^{-\frac{t}{\tau_2}}$$

The constants obtained from fitting the decay function of each cell was then used to obtain four parameters: C_1 (capacitance of the soma and main proximal dendrites), C_2 (capacitance of the distal dendritic arbor), R_1 (pipette access resistance), and R_2

(composite resistance of dendritic segments separating the main proximal dendritic segments from the distal dendritic arbor). The equations for this analysis are as follows:

$$C_1 = \frac{\tau_1 (A_1 + A_2)^2}{A_1 \Delta V}$$

$$C_2 = \frac{A_2 \tau_2}{\Delta V}$$

$$R_1 = \frac{\Delta V}{A_1 + A_2}$$

$$R_2 = \frac{\Delta V}{A_2} - \frac{\Delta V}{A_1 + A_2}$$

In our measurements, total capacitance was indicated by $C_1 + C_2$.

4.3.6.5 Analysis of firing properties

Electrophysiology data were analyzed offline using Clampfit 10.2 software (Molecular Devices). Firing frequency and coefficient of variation (CV) calculations were performed in the cell-attached configuration on spikes in a 150 second time interval obtained ~5 minutes after formation of a stable seal. The CV was calculated as follows:

$$CV = \frac{Standard\ Deviation\ of\ Interspike\ Interval}{Mean\ Interspike\ Interval}$$

The firing frequency distribution was obtained by identifying the percentage of cells in each incrementing 10 spike/second bin. The CV distribution was similarly obtained by sorting CV values into incrementing 0.02 bins. A moving average trend-line was added to the CV distribution histogram to outline the shape of the distribution.

4.3.6.6 AHP decay

Analysis of the after-hyperpolarization (AHP) was performed by analyzing spikes in a 10 second interval ~1 minute after break-in. The AHP value was calculated as the

maximum antipeak voltage, and the mean value over the 10 second interval is reported as the AHP for each neuron. To measure decay of the AHP during the Inter Spike Interval (ISI), the mean ISI duration was determined in the same 10 sec interval for each cell. AHP amplitude was then measured at different fractional intervals of the ISI (0.5*ISI, 0.65*ISI, 0.85*ISI) in order to characterize AHP decay.

4.3.7 Data analysis

Statistical tests are described in the figure legends for all data. Statistical analysis was performed using Excel (Microsoft), Prism 6.0 (GraphPad), SigmaPlot (Systat Software), and Origin (Origin Labs). Statistical significance was defined at $p<0.05$. For one-way and two-way analysis of variance (ANOVA), if statistical significance ($p< 0.05$) was achieved, then we performed post hoc analysis corresponding to the experiment, as specified, to account for multiple comparisons. All *t*-tests were two-tailed Student's *t*-tests, and level of significance (alpha) was always set to 0.05.

4.4 Results

4.4.1 Many disrupted RNA transcripts in fxSCA7 92Q are enriched for peroxisome proliferator response elements and hypoxia response elements in their regulatory domains

Previously, we have illustrated that widespread transcriptional disruption is present in fxSCA7 92Q cerebellum (Chapter 3). Additionally, we have shown that altered transcript expression correlates with changes in Purkinje neuron spiking and neurodegeneration in fxSCA7 92Q mice (Chapter 3). In order to better characterize the mechanism for transcriptional dysregulation in fxSCA7 92Q mice, we performed a gene set enrichment analysis to identify transcription factor binding sites (TFBSs) in the

promotor regions of downregulated genes (Chapter 3). Using oPOSSUM v3.0 (http://opossum.cisreg.ca/oPOSSUM3/), we applied a 'z' score threshold of ≥ 10 to investigate potential TFBSs and found that PPARG::RXRA (Peroxisome Proliferator Response Element [PPRE]) and HIF1::ARNT (Hypoxia Response Element[HRE]) are enriched in the promoter regions of downregulated target genes in fxSCA7 92Q cerebellum (Figure 4.1A). PPREs and HREs are positively regulated by PGC-1α and HIF-1α, respectively, which are both Sirt1 substrates and are become stabilized and activated upon Sirt1 deacetylation [206, 207]. Of the calcium homeostasis genes outlined in Chapter 3, 11 contain putative PPREs and may potentially be responsive to Sirt1 activity (Figure 4.1B).

4.4.2 Sirtuin-1 is a candidate protein to modify transcriptional alterations in fxSCA7 92Q cerebellum

In order to determine whether Sirt1 activity is disrupted in fxSCA7 92Q mice, we determined the acetylation status of PGC-1α in the cerebellum of 30 week-old fxSCA7 92Q mice, and observed increased acetylation in fxSCA7 92Q cerebellum compared to wild-type littermate controls (Figure 4.1C). This suggests that reduced PGC-1α activity may underlie reduced transcription of PPRE-containing target genes, and that increasing PGC-1α activity may improve transcriptional alterations in fxSCA7 92Q cerebellum. In order to address this hypothesis, we crossed fxSCA7 92Q mice with a mouse line in which Sirtuin-1 is overexpressed in all tissues. The resulting bigenic mice, referred to as Sirt1 uOE-fxSCA7 92Q, stably overexpress Sirt1 up to 36 weeks of age (Figure 4.1D). In order to determine whether constitutive overexpression of Sirt1 improves transcriptional alterations in fxSCA7 92Q mice, we performed a Nanostring

analysis of 100 mRNA transcripts which show the highest level of downregulation in fxSCA7 92Q cerebellum. When compared to fxSCA7 92Q mice, Sirt1 uOE-fxSCA7 92Q mice show a significant increase in mRNA transcript expression of *Itpr1* and *Trpc3*, two genes important for calcium homeostasis, while two other calcium-related genes, *Cacna1g* and *Calb1*, also showed a trend of increased transcript expression (Figure 4.1E). Overall, these data indicate that reduced expression of PPRE-containing genes in fxSCA7 92Q mice can be targeted by Sirt1 overexpression, and that Sirt1 uOE-fxSCA7 92Q mice show improvements in the cerebellar expression of genes related to calcium homeostasis.

4.4.3 Sirtuin-1 overexpression improves Purkinje neuron physiology and reduces neurodegeneration in fxSCA7 92Q mice

Changes in Purkinje neuron spiking accompany transcriptional alterations in fxSCA7 92Q mice (Chapter 3). We have illustrated that overexpression of Sirt1 improves transcript levels of several downregulated target genes in fxSCA7 92Q cerebellum, leading to the possibility of functional improvements in neuronal activity. In order to determine whether Sirt1 overexpression is able to influence Purkinje neuron spiking, we performed patch clamp recordings in Sirt1-uOE x fxSCA7 92Q mice, along with wild-type littermate controls, fxSCA7 92Q littermates, and Sirt1-uOE littermates. No changes in firing frequency were noted across genotypes (Figure 4.4B). However, the coefficient of variation (CV), which is significantly increased in fxSCA7 92Q Purkinje neurons, is rescued to wild-type levels upon Sirt1 overexpression (Figure 4.4C). This is also reflected in the distribution of CV values, which is right-shifted in fxSCA7 92Q Purkinje neurons and is partially improved in Sirt1-uOE x fxSCA7 92Q neurons,

especially at high CV values (Figure 4.4D). Since transcripts related to calcium homeostasis show increased expression in Sirt1-uOE x fxSCA7 92Q cerebellum, we wished to determine whether these improvements in the regularity of spiking are linked to normalized decay of the AHP. As shown previously (Chapter 3), fxSCA7 92Q Purkinje neurons demonstrate a significantly depolarized AHP throughout the interspike interval, indicating increased AHP decay. The decay of the AHP is rescued to wild-type levels upon Sirt1 overexpression (Figure 4.4E-F). Importantly, Sirt1 overexpression alone does not alter Purkinje neuron physiology, as all physiological parameters measured do not differ between Sirt1-uOE mice and wild-type littermate controls (Figure 4.5A-E). This suggests that improved expression of calcium homeostasis gene transcripts corresponds to functional improvements in the Purkinje neuron AHP, thereby improving the regularity of spiking in fxSCA7 92Q Purkinje neurons.

Improvements in transcript expression are not limited to ion-channels, or genes related to neuronal excitability, in Sirt1-uOE x fxSCA7 92Q cerebellum. Therefore, it is possible that other neuronal pathways which are influenced in SCA7 may also be improved upon Sirt1 overexpression. As shown in Chapter 3, neurodegeneration is present in fxSCA7 92Q Purkinje neurons in the posterior cerebellar lobules at 25 weeks of age, as shown by a decrease in neuronal capacitance. This reduction in capacitance was partially improved in Sirt1-uOE x fxSCA7 92Q Purkinje neurons, although not to wild-type levels (Figure 4.4G). Overall, this indicates that targeting the Sirt1 pathway may offer potential functional and neuroprotective benefit in SCA7.

4.5 Discussion

As illustrated in Chapter 3, fxSCA7 92Q mice exhibit a disrupted cerebellar transcriptome which is associated with reduced expression of genes important for calcium homeostasis, dendritic degeneration, and alterations in Purkinje neuron spiking. Purkinje neuron spiking can be improved by activating K_{Ca} channels, but strategies to improve neuronal physiology are unlikely to improve underlying transcriptional abnormalities. In this chapter, we explore the potential efficacy of Sirt1 overexpression on improving underlying transcriptional alterations in SCA7, and determine whether this strategy can similarly improve Purkinje neuron physiology. We found that genetic overexpression of Sirt1 can partially rescue transcriptional alterations in several genes related to calcium homeostasis, and that these slight increases in expression across multiple genes is sufficient to improve Purkinje neuron spiking in Sirt1 uOE-fxSCA7 92Q mice. Finally, we illustrate that transcriptional improvements through Sirt1 overexpression can partially rescue dendritic degeneration in fxSCA7 92Q mice, which indicates that targeting Sirt1 activity may be a potential strategy to improve patient outcomes in SCA7.

Although the studies in this chapter demonstrate the potential efficacy of improving Purkinje neuron physiology in SCA7 by increasing Sirt1 activity, these experiments have several caveats which should be taken into consideration. First, although Sirt1 overexpression does improve transcriptional alterations in fxSCA7 92Q mice, this rescue is modest. For instance, *Itrp1* expression increases only about 10% upon Sirt1 overexpression, and *Trpc3* and *Cacna1g* show similar improvements, although expression is still only at 70% of wild-type levels (Figure 4.1E). However, this

suggests an interesting possibility about how transcript levels of calcium homeostasis genes influence excitability in fxSCA7 92Q Purkinje neurons. It is possible that at baseline, calcium sources are redundant and provide calcium at saturating concentrations for K_{Ca} channels. Therefore, a reduction in expression of any one calcium source by close to 30% may not greatly alter Purkinje neuron spiking as calcium availability may still remain saturating under those conditions. In fact, this possibility is explored in Chapter 3, where partial blockade of a single calcium source is not sufficient to cause irregularity in Purkinje neuron spiking (Figure 3.7). The results of Sirt1 overexpression suggest that K_{Ca} channels may be sensitive to modest changes in calcium availability, and that a reduction in expression of about 25% may be tolerated while 30-40% reduction results in irregular spiking. Unfortunately, mRNA transcript expression of *Kcnma1* was not assessed in this study, so dosing information about the interaction between calcium sources and BK channels cannot be further explored with the present data. Future studies will determine the ability of Sirt1 overexpression to influence BK channel expression in fxSCA7 92Q mice.

A second caveat to these studies is that additional Sirt1 targets or interactors are not explored in the present studies. As illustrated in Figure 4.1, Sirt1 also deacetylates HIF-1α. It is unclear through our studies whether Sirt1 activation can directly regulate HIF-1α target genes in addition to putative PGC-1α-associated target genes. Additionally, these studies do not directly illustrate PGC-1α acetylation status in Sirt1 uOE-fxSCA7 92Q mice so it is possible that Sirt1 overexpression has benefits outside of transcriptional improvement. Sirt1 is dependent on NAD^+ as a substrate for activation, for which it competes with poly(ADP-ribose) polymerase-1 (PARP-1) [208]. If PARP-1

expression or activity is increased at baseline in fxSCA7 92Q mice, thereby outcompeting Sirt1 for NAD^+, it is possible that a larger pool of Sirt1 has access to NAD^+ in Sirt1 uOE-fxSCA7 92Q mice. This would be expected to have negative downstream effects on both PCG-1α and HIF-1α deacetylation, thereby decreasing transcription of target genes. In fact, hyperactivation of PARP-1 is observed in mutations that cause cerebellar ataxia in humans. Mutations in *XRCC1*, whose protein product is responsible for the assembly of complexes involved in DNA single-strand break repair, result in high levels of protein ADP-ribosylation (PARylation) indicating increased PARP-1 activity [209]. This is similar to an observance in *PKNP* mutations, which cause increased PARP-1 activity and result in cerebellar ataxia [210, 211]. Future studies will further explore the status of Sirt1, along with target proteins under the control of Sirt1 activation, and PARP-1, along with downstream proteins involved in DNA single-strand break repair.

Sirtuin activation has gained interest as a potential strategy to treat neurodegenerative disease. Sirt1 activators, such as resveratrol, have received attention due to its effects on lifespan extension across species [190-192], which is in addition to the known positive role of sirtuin activation in several rodent models of neurodegenerative disease [195-201]. Sirt1 activation is also achieved through caloric restriction, suggesting that managing energy balance could have positive effects on a multitude of neurodegenerative disorders [212]. NAD^+ supplementation has also been illustrated to have protective effects in various rodent models of disease (ref). These data suggest that overall, Sirt1 activation may be a reasonable drug target for many age-related disorders including SCA. Although Sirt1 overexpression improves transcriptional alterations and Purkinje neuron spiking in fxSCA7 92Q mice,

improvements in gene expression were modest. Future studies may identify more potent sirtuin activators which may have increased benefit on transcriptional alterations and disease outcomes in SCA. However, this strategy should be met with caution, as sirtuin target genes are abundant and therefore increase the risk of off-target effects.

4.6 Acknowledgements

I would like to thank Colleen Stoyas, Pawel Switonski, Terry Gaasterland, and Albert La Spada for their assistance with analyzing transcriptome data and PGC-1α acetylation in fxSCA7 92Q mice, and for providing Sirt1 uOE-fxSCA7 92Q mice for all studies. I would like to thank Annie Zalon, Brandon Lee, and Allison Sylvia for technical support, and Ravi Chopra and Vikram Shakkottai for providing thoughtful comments.

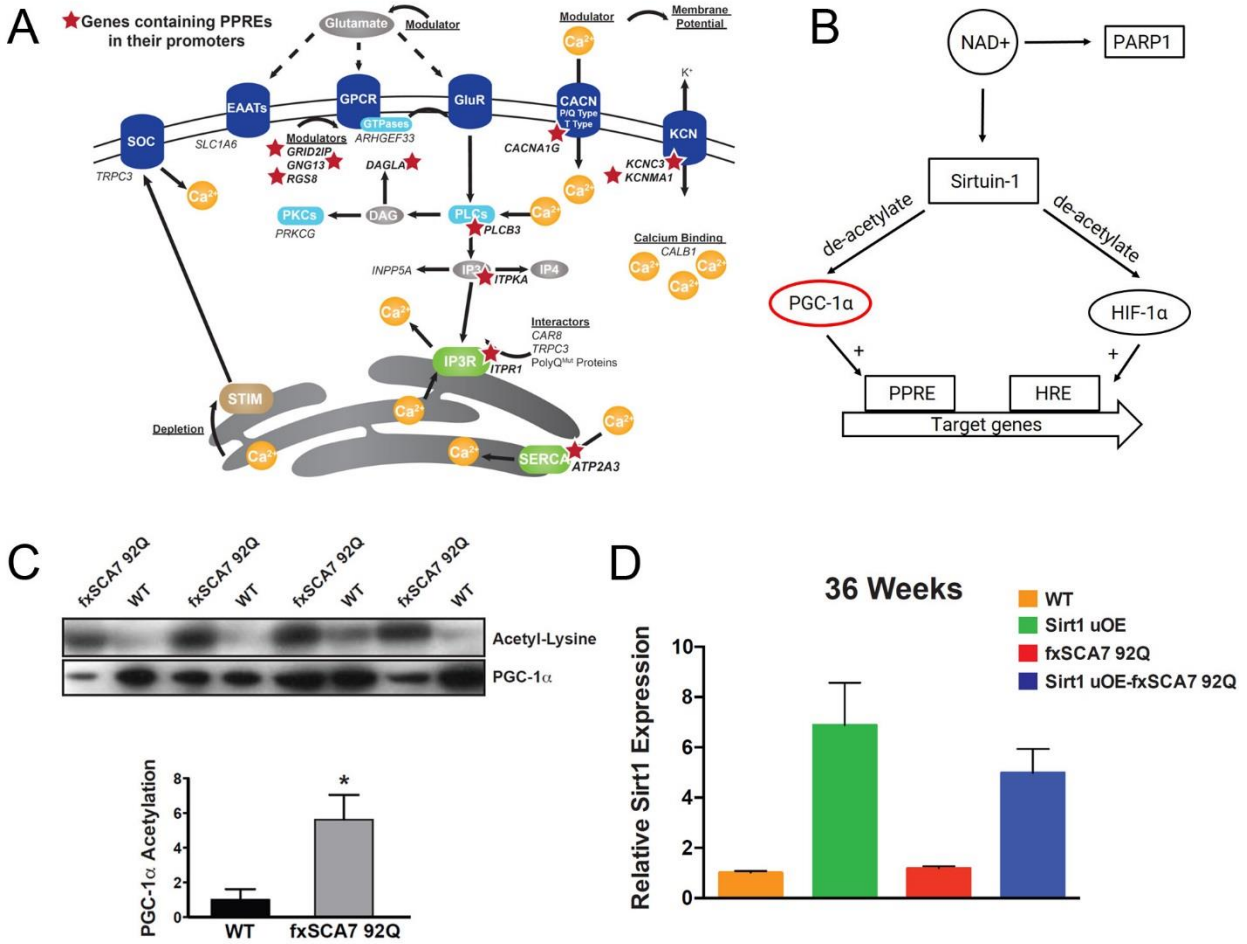

E

	Relative expression				
Transcript	Wild-type	Sirt1-uOE	fxSCA7 92Q	Sirt1 uOE-fxSCA7 92Q	p value
Cacna1g	1	0.967	0.651	0.679	0.0753
Calb1	1	0.892	0.676	0.759	0.0548
Itpr1	1	0.949	0.673	0.775	0.0311
Trpc3	1	0.943	0.633	0.733	0.0300

Figure 4.1 Sirtuin-1 overexpression improves the transcription of PPRE-containing target genes in fxSCA7 92Q mice. (A) Representative diagram of dysregulated calcium homeostasis genes in fxSCA7 92Q cerebellum. oPOSSUM analysis of putative transcription factor binding sites (TFBS) determined that hypoxia response elements (HRE) and peroxisome proliferator response elements (PPRE) are enriched in fxSCA7 92Q cerebellum. Genes which contain PPREs in their regulatory domains are indicated with a red star. **(B)** Sirtuin-1 deacetylates PGC-1α and HIF-1α in order to induce expression of target genes. Sirtuin-1 is dependent on NAD^+ for activation, for which it competes with PARP1. In order to investigate Sirtuin-1 activity in fxSCA7 92Q cerebellum, we measured (in red) PGC-1α acetylation status. **(C)** PGC-1α

acetylation is significantly increased in fxSCA7 92Q cerebellum, suggesting reduced sirtuin-1 activity. **(D)** Quantitative PCR analysis illustrates that sirtuin-1 is stably overexpressed in Sirt1 uOE-fxSCA7 92Q cerebellum at 36 weeks of age. **(E)** Transcriptome analysis of excitability-related genes within the calcium homeostasis pathway. Expression of *Itpr1* and *Trpc3* show significantly increased expression in Sirt1 uOE-fxSCA7 92Q cerebellum compared to fxSCA7 92Q cerebellum, while *Cacna1g* and *Calb1* appear to have improved expression as well (did not reach statistical significance). *$p<0.05$, Student's t-test (C), one-way ANOVA with Holm-Sidak test for multiple comparisons (D). *Note: Experiments in 4.1 (A and C-E) performed by Colleen Stoyas and Albert La Spada, University of California, San Diego.*

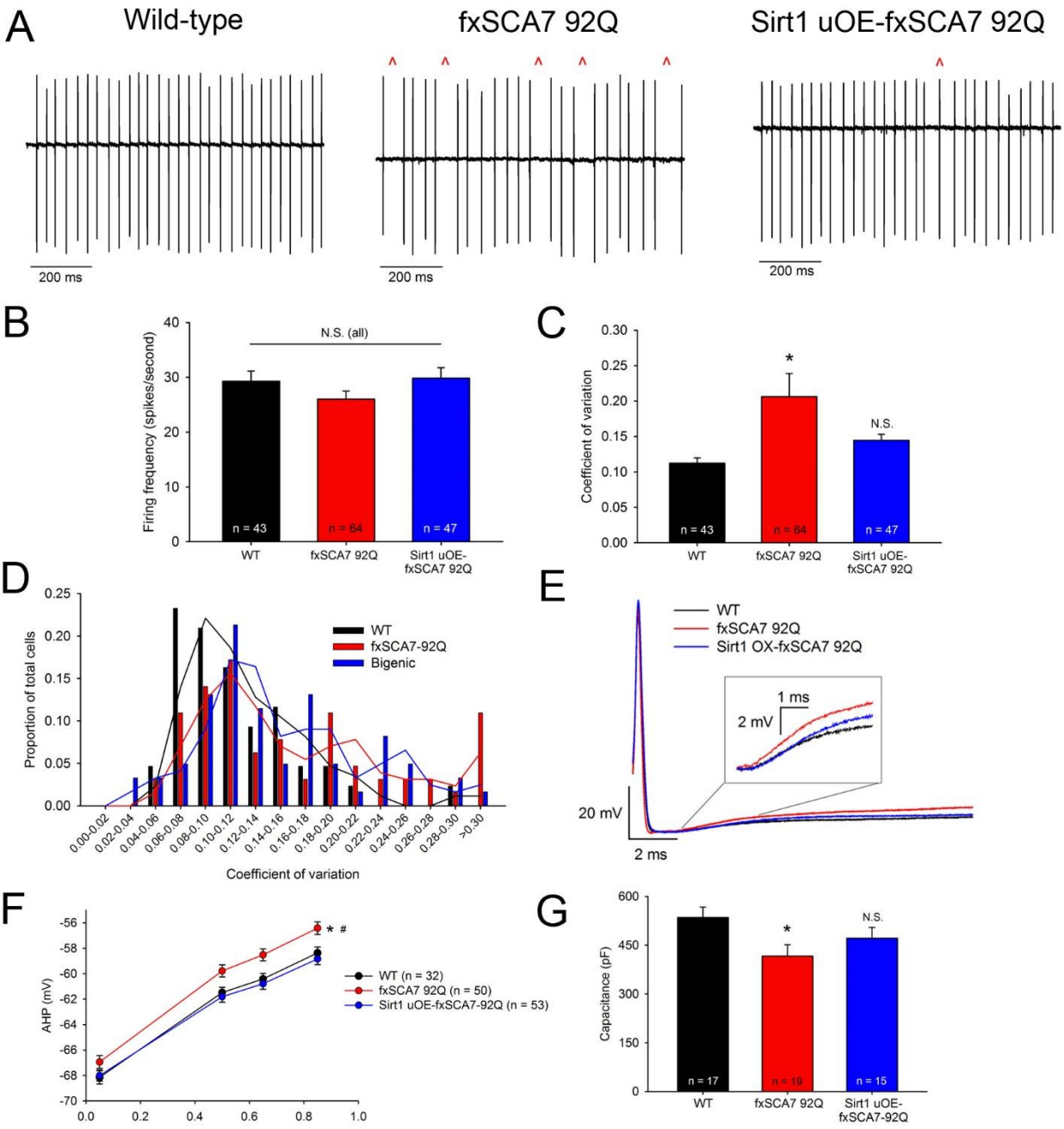

Figure 4.2 Sirtuin-1 overexpression improves alterations in Purkinje neuron physiology and dendritic degeneration in fxSCA7 92Q mice. (A) Representative traces of cell-attached firing from wild-type, fxSCA7 92Q, and Sirt1 uOE-fxSCA7 92Q Purkinje neurons. **(B)** Firing frequency is unchanged between genotypes. **(C)** The coefficient of variation (CV) of the interspike interval is significantly increased in fxSCA7 92Q Purkinje neurons and is partially rescued upon Sirt1 overexpression. **(D)** CV distributions indicate a slight leftward shift for Sirt1 uOE-fxSCA7 92Q compared to fxSCA7 92Q Purkinje neurons. **(E)** Representative action potentials from all genotypes, with the AHP decay highlighted in the inset. **(F)** AHP decay is significantly increased in fxSC7 92Q Purkinje neurons and is rescued upon Sirt1 overexpression. **(G)** Purkinje

neuron capacitance is decreased in fxSCA7 92Q Purkinje neurons, and is partially rescued upon Sirt1 overexpression. *p<0.05, one-way ANOVA with Holm-Sidak test for multiple comparisons (B, C, G) or two-way ANOVA with Holm-Sidak test for multiple comparisons (F). * denotes significantly different from wild-type, # denotes significantly different from all other groups.

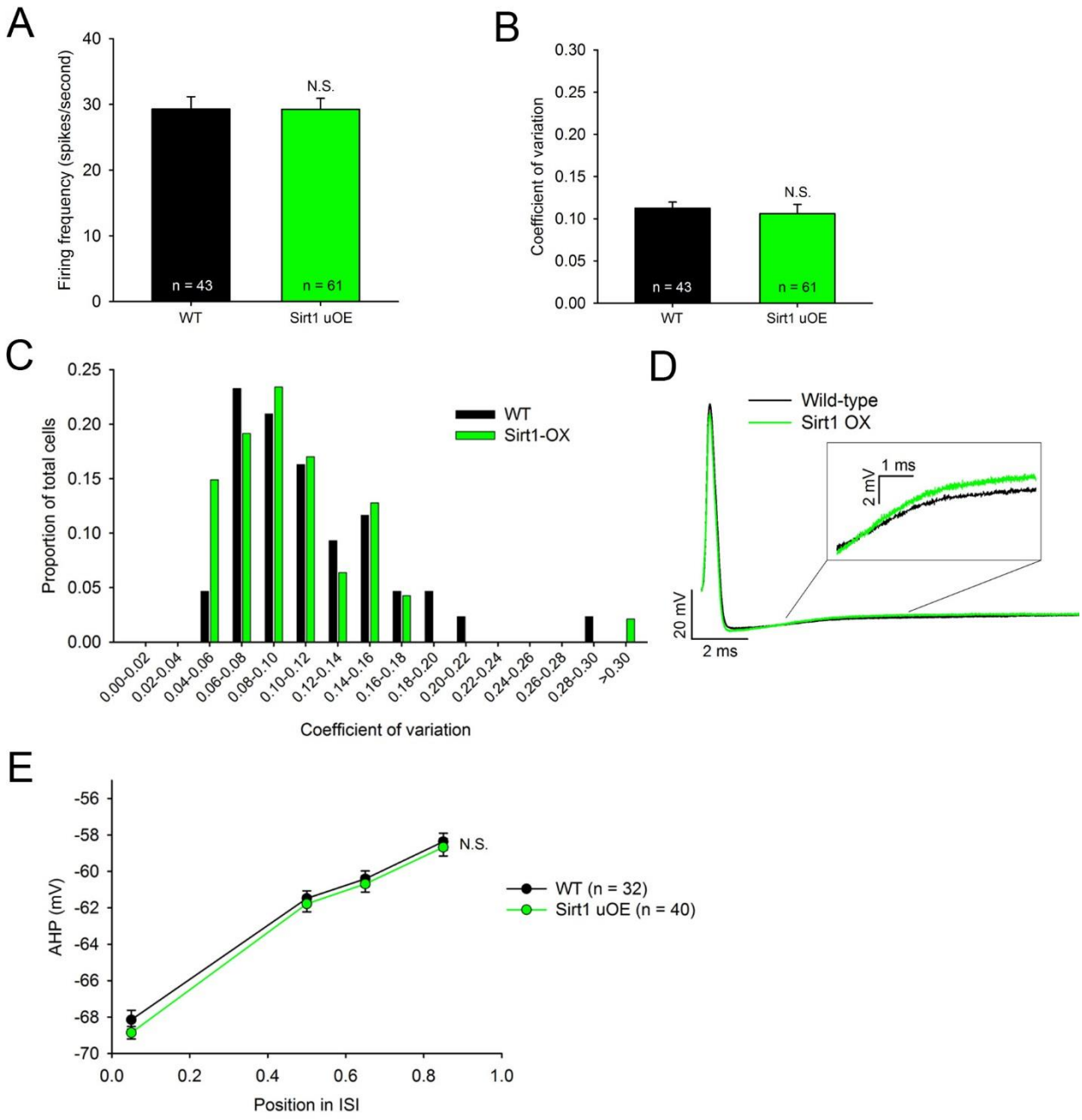

Figure 4.3 Sirtuin-1 overexpression does not affect Purkinje neuron physiology. **(A)** Firing frequency and **(B)** coefficient of variation (CV) of the interspike interval in Sirt1 uOE and wild-type littermate control Purkinje neurons. **(C)** Distribution of CV values illustrates no significant difference between Sirt1 uOE and wild-type littermate control Purkinje neurons. **(D)** Representative action potential waveforms from Sirt1 uOE and wild-type littermate control Purkinje neurons, illustrating no significant difference in decay of the AHP. **(E)** AHP decay is unchanged between Sirt1 uOE and wild-type littermate controls Purkinje neurons. N.S., not significant, Student's t-test (A-B) or two-way ANOVA with Holm-Sidak test for multiple comparisons.

Chapter 5

Conclusions and Future Directions

The results of this dissertation lead to the following main conclusions. First, K_{Ca} channel dysfunction underlies altered Purkinje neuron spiking in mouse models of both SCA1 and SCA7. Second, these alterations in K_{Ca} channel function, along with other dendritic potassium channels in SCA1, can be targeted by pharmacologic ion-channel modulators to improve Purkinje neuron spiking and motor phenotypes in both SCA1 and SCA7 mouse models. Third, these studies have established a role for a functional "calcium homeostasis" module as important for alterations in Purkinje neuron physiology in a mouse model of SCA7, and suggest that the dysfunction of both calcium sources and effector K_{Ca} channels may be important across multiple models of polyglutamine SCA. Fourth, studies in a mouse model of SCA7 indicate that Sirtuin-1 may be an upstream target of transcriptional alterations which directly affect Purkinje neuron physiology, and that activating the Sirtuin-1 pathway may be a potential strategy to normalize changes in gene expression which contribute to symptoms in SCA7. Finally, potassium channel activators are tolerated by human SCA patients and may improve symptoms, as indicated by pilot trials with the compounds baclofen and chlorzoxazone. Together, this dissertation argues that dysfunction of K_{Ca} channels and their calcium sources is a common feature of mouse models of SCA, and that potassium channel activators have outstanding therapeutic potential, as indicated by their effects on

improving Purkinje neuron spiking in mouse models and their tolerability and potential efficacy in human SCA patients. However, many aspects of the relationship between ion-channel dysfunction and motor impairment in ataxia remain poorly understood. This chapter will outline the implications of the studies in this dissertation, and will highlight potential opportunities to expand this research further.

5.1 Understanding the relationship between Purkinje neuron excitability, motor impairment, and neurodegeneration in spinocerebellar ataxia

The studies in this dissertation have outlined a clear relationship between alterations in Purkinje neuron membrane excitability and motor impairment. Previous studies have provided evidence that this relationship exists, in mouse models of episodic ataxia [82], SCA resulting from primary channelopathies [2-6, 28, 33-35, 51], polyQ SCA [71-73, 77, 78, 104], and direct mutations in ion-channels [18, 42] (reviewed in [213]). In many instances, the onset of motor impairment corresponds to initial changes in Purkinje neuron membrane excitability, or throughout development in the case of ion-channel-mutant mice. Strong evidence for the relationship between ion-channel dysfunction and motor impairment comes from *in vivo* studies involving ion-channel modulators, which can improve motor impairment in conjunction with restored Purkinje neuron membrane excitability [73, 76, 78, 82, 83]. Together, these studies indicate that altered Purkinje neuron membrane excitability is sufficient to result in motor impairment.

A good illustration of the relationship between ion-channel dysfunction and motor impairment comes from studies in $K_v3.3$-knockout mice. $K_v3.3$-knockout mice serve as a mouse model of SCA13, since point mutations in the *KCNC3* gene result in the

production of K_v3.3 with either no functional current or altered kinetics [30-32]. In these mice, the lack of K_v3.3 current reduces the slope of action potential repolarization in cerebellar Purkinje neurons [33, 214]. Since full and efficient repolarization, which is mediated by K_v channels and calcium-activated potassium channels, allows for complete de-activation of voltage-gated sodium channels in preparation of the next action potential, the available resurgent sodium current through Na_v1.6 is reduced in these neurons. Purkinje neurons from K_v3.3-knockout mice therefore display reduced firing frequency due to the altered interaction between K_v3.3 and other ion-channels that are active during the interspike interval [33]. Purkinje neuron-specific re-expression of K_v3.3 completely rescues spiking and motor function in K_v3.3-knockout mice, indicating that Purkinje neuron electrophysiologic dysfunction is a primary source of behavioral impairment in these mice [34, 35]. This study clearly identifies Purkinje neuron dysfunction as the source of ataxia in these mice, although other studies have illustrated that dysfunction in other neuronal populations within the cerebellar motor circuit can also influence behavioral changes.

The genes which cause polyQ SCA are either widely or ubiquitously expressed throughout the central nervous system [7], which suggests that Purkinje neurons may not be the only source of electrophysiologic dysfunction that contributes to motor impairment in polyQ SCA. For example, mutations in FGF14 cause SCA27 in humans [117], and similar mutations greatly affect cerebellar granule cell excitability in mice [215]. This suggests that other neuronal populations may contribute to altered function of cerebellar processing through changes in membrane excitability. The argument for additional sources of dysfunction within the cerebellar motor circuit is strengthened by

human autopsy studies in SCA patients, which indicate that neuronal populations both presynaptic and postsynaptic to Purkinje neurons can undergo significant degeneration [7]. For these reasons, it is important to consider whether neurodegeneration in these other neuronal populations is also associated with electrophysiologic dysfunction, and whether these potential alterations are primary sources of motor impairment in ataxia. While the studies in this dissertation demonstrate a clear link between changes in intrinsic Purkinje neuron excitability and motor impairment in SCA, they fail to investigate to contribution of synaptic alterations to ataxia in these mouse models, or consequences on the function of postsynaptic neuronal populations in the deep cerebellar nuclei and vestibular nuclei. Therefore, we are left with an incomplete picture of both additional sources of dysfunction and whether ion-channel modulators have additional targets outside of Purkinje neurons, which is likely since the expression of relevant ion-channel targets is not restricted to Purkinje neurons.

In order to identify these potential contributing factors in SCA, it is first necessary to identify the components of the cerebellar motor circuit which may potentially modulate cerebellar output. Individual Purkinje neurons receive excitatory input from single climbing fiber (CF) projections which initiate at the inferior olive, along with hundreds of parallel fiber (PF) projections from granule cells via the mossy fiber pathway [9]. Precise timing of CF and PF input to Purkinje neurons has been proposed as a mechanism for cerebellar learning [9, 11], with PF input alone resulting in Purkinje neuron long-term potentiation (LTP) and simultaneous PF-CF input resulting in Purkinje neuron long-term depression (LTD), both at the PF-Purkinje neuron synapse [216]. Recent work has shown that cerebellar microarchitecture is divided into unique cerebellar

“modules”, which are composed of several neighboring Purkinje neurons innervated by climbing fiber axons from a single inferior olive neuron, and also project output to a single neuron in the cerebellar nucleus [9, 217]. This modular architecture is thought to allow for precise control of specific muscle groups during movement, and suggests that regional dysfunction in the cerebellum may be responsible for specific symptoms such as abnormal limb or eye movements. Inhibitory projections onto Purkinje neurons come from basket cells and molecular layer interneurons, whose activation may modulate cerebellar learning and Purkinje neuron LTD in particular [217, 218]. Purkinje neurons send inhibitory projections to neurons in the deep cerebellar nuclei and vestibular nuclei, which are motor output centers. Although Purkinje neurons are GABAergic and send inhibitory projections to these nuclei, Purkinje neuron input does not inhibit neuronal firing in cerebellar nuclei as would be expected; rather, cerebellar nuclei spiking becomes time-locked to the firing rate of Purkinje neurons in the input module, thereby causing increased inhibitory cerebellar nuclei firing with increased cerebellar input, and vice versa [219]. This spiking relationship indicates that observed dysfunction in Purkinje neuron simple spiking may be a reliable measure of dysfunction in the cerebellar and vestibular nuclei. Therefore, dysfunction at any of these sites could potentially influence movement and result in cerebellar ataxia, although the relevance of these nuclei to the pathogenesis of SCA is not yet fully explored in many cases. I propose a series of future experiments in order to further dissect the individual contributions of distinct neuronal populations to motor impairment in ataxia mice.

First, I would perform *in vivo* recordings in awake, head-fixed SCA mice and wild-type littermate controls. This recording technique has been used reliably in many

studies and can achieve low-noise single-unit recordings of Purkinje neuron activity [220]. During these recordings, mice will be placed on a treadmill which will allow free running and movements will be recorded on video. This time-locked video data can be used to correlate specific movements with alterations in Purkinje neuron spiking. Criteria such as simple spike frequency and regularity, complex spike frequency and regularity, complex spike pause, and number of spikelets during the complex spike can then be recorded and analyzed. Alternatively, Purkinje neuron activity could be recorded during a postural or learning task which varies between SCA and wild-type mice, thereby providing maximal information from single-unit activity.

In tandem with this recording strategy, transcriptome analyses will be essential for formulating hypotheses about sources of neuronal dysfunction within the cerebellum. RNA sequencing could provide information about changes in ion-channel or receptor expression in whole-cerebellar lysates. The functional connectivity of the cerebellum is well-defined, and ion-channel distribution is known at least in part for many neuronal populations within the cerebellum. For instance, specific potassium channel subtypes are known to be expressed mostly in Purkinje neurons, while other classes may be specific for other neuronal populations. Narrowing potential ion-channel targets will limit the time and resources necessary to perform the following experiments.

Next, correlates of the altered spiking noted during *in vivo* recordings can be further analyzed during *in vitro* patch clamp recordings from acute cerebellar slices. Recordings of spontaneous simple spike firing, evoked spiking through PF or CF stimulation, and spontaneous inhibitory synaptic drive can be recorded from Purkinje neurons. *In vivo* electrophysiology and transcriptomic studies will provide initial

evidence of whether presynaptic, synaptic, or intrinsic spiking is most likely to be altered in Purkinje neurons during slice recordings. Once alterations are identified, treatments can be identified which improve these correlates of altered spiking during patch clamp recordings. These may include genetic or pharmacologic strategies, ideally specifically targeting specific ion-channel or receptor subtypes.

Finally, any identified treatments would be tested during *in vivo* recordings to determine whether physiological alterations and behavioral changes are improved. Previous studies have correlated alterations in spiking with motor impairment, and have demonstrated that compounds which improve Purkinje neuron physiology during patch-clamp recordings are also effective at improving motor function during behavioral assays [73, 76, 78, 82, 83, 104]. However, recordings of Purkinje neuron activity during these behavioral tasks is seldom performed, making it difficult to know whether target engagement *in vivo* is equivalent to what is presumed by patch-clamp recordings. This strategy will allow us to determine the actual mechanisms of potassium channel modulators *in vivo*, since we cannot know the actual targets which correspond to improved motor function based on slice physiology alone.

While this series of experiments is a large undertaking, this is the only way to fully determine which aspects of cerebellar dysfunction truly contribute to behavioral deficits in SCA mice. In addition, these studies will more fully connect the mode-of-action of pharmacologic modulators to their appropriate targets *in vivo*, and will allow a more direct connection between specific ion-channel dysfunction and motor impairment in ataxia. Finally, these experiments will more fully dissect the cerebellar motor circuit at baseline and in SCA and will help determine whether Purkinje neuron spiking is the

most relevant output which must be targeted by pharmacological modulators, or whether other aspects of cerebellar physiology should be more heavily considered when designing therapies to treat neuronal dysfunction.

5.2 Determining the relevance and regulation of a dysfunctional "calcium homeostasis" module in spinocerebellar ataxia

With Purkinje neuron excitability becoming increasingly recognized as an important contributing factor to the phenotypic motor changes observed in SCA, it is important to understand the mechanisms which contribute to these alterations in excitability. To this end, the studies in this dissertation have outlined a potentially important mechanism of neuronal dysfunction in SCA7 which may have widespread implications for other SCAs as well. In Chapter 3, a functional "calcium homeostasis" module was determined to have altered function in fxSCA7 92Q Purkinje neurons, and improving the function of this module through either pharmacologic or genetic strategies could also improve Purkinje neuron spiking. These alterations in function are tied to disruptions in the cerebellar transcriptome, and importantly converge on calcium homeostasis and IP3 receptor signaling pathways. Based on transcriptome analysis from mouse models of SCA of various etiologies, the essential components of this calcium homeostasis module (i.e. *Kcnma1, Cacna1g, Itpr1, Trpc3*) appear to be downregulated across models of SCA (Chapter 3). This suggests that changes in Purkinje neuron excitability may be tied to altered function of this module in several ataxias, and that the members of this module may therefore be a convergent mechanism of disease and an outstanding target for therapeutic intervention.

This begs an important question: why are transcriptional profiles similarly altered across several mouse models of SCA, even though the underlying mutations are contained in unique proteins with independent known functions? One piece of evidence comes from the established roles of these proteins. Many of the disease-causing proteins for polyQ SCA are involved with transcriptional regulation, RNA homeostasis, or ubiquitination. For example, ATXN1 (the disease-causing protein in SCA1) has known roles involving both transcriptional regulation and RNA splicing [56-58], ATXN2 (SCA2) contributes to RNA metabolism [59-61], ATXN3 (SCA3) functions as a de-ubiquitinating enzyme [62, 63], ATXN7 (SCA7) is a core component of the SAGA transcriptional complex [64], and *TBP* (SCA17) is an essential component of tata box-based transcriptional initiation [65] (reviewed in [66]). This suggests potential overlap involving the regulation of transcriptional control and indicates that common co-factors may regulate essential genes for Purkinje neuron excitability.

The native roles of these disease-causing proteins in polyQ SCA, combined with the evidence of widespread transcriptional disruption presented in chapter 3, suggests that transcriptional dysfunction is a common disease mechanism in SCA. Moreover, the downregulated transcriptional targets appear to converge at least partially on neuronal excitability pathways important for Purkinje neuron function, which were predicted to be important risk factor genes in human ataxia [67]. It is possible that there is functional overlap between the disease-causing proteins in polyQ SCA and these enriched transcriptional targets. For instance, there is a potential role for transcriptional overlap if the disease-causing proteins act as sensor molecules in some way, causing them to respond to different cellular signals. As an example, a growth factor response may

result in direct activation of a protein such as ATXN1, or a co-factor which interacts with ATXN1, resulting in transcription of a set of target genes. Meanwhile, an increase in excitatory synaptic activity could trigger activation of ATXN2, leading to a change in the expression level of the same proteins which influence excitability. Similar situations could exist for other ATXN proteins, or *TBP* (in SCA17), where responses to intrinsic signaling, cellular stressors, or other mechanisms may influence transcriptional activation or inhibition. In these cases, why would Purkinje neuron excitability pathways be enriched as targets for such diverse stimuli? Purkinje neurons are extremely unique in the central nervous system because of their large size, high tonic firing rate, and subsequently immense metabolic load. Since Purkinje neurons are the sole output of the cerebellar cortex, and their main role is to modulate activity in motor output centers such as the deep cerebellar nuclei and vestibular nuclei, the ability to alter intrinsic excitability in response to stimuli appears to be a likely mechanism for cerebellar learning and motor output. Ultimately, these pathways must be tied to neuronal excitability in some way in order to influence true changes in motor learning or behavior. While these interactions are hypothetical, they describe a situation in which neuronal excitability pathways could be common functional targets of ATXN proteins and may therefore be commonly disrupted across SCAs with different underlying genetic causes.

In order to explore whether this type of convergent transcriptional regulation is possible in SCAs, a series of experiments would be necessary. The most obvious link between excitability genes and ATXN proteins is either by direct binding to regulatory domains or by association with a transcriptional co-activator/co-repressor which influences target gene transcription. Co-immunoprecipitation (Co-IP) experiments would

help identify protein-protein interactions with transcriptional co-factors, chromatin immunoprecipitation (ChIP) would assess direct binding to promoter regions of genetic targets, and assessments of epigenetic modification may be informative in some situations. In chapter 4, we illustrate PPRE and HRE target genes show altered expression in fxSCA7 92Q mice (Figure 4.1). ATXN7 is a known member of the STAGA transcriptional complex which has both histone acetyltransferase (HAT) and protein deubiquitinase (DUB) activity [221]. ATXN7 is positioned within the DUB module of STAGA and has been proposed to anchor this module to the native complex. Under polyQ expansion, it is possible that STAGA function shifts away from a normal ratio of HAT:DUB activity, either causing loss of DUB activity or a dissociated, constitutively active DUB module [221]. In this case, histone occupancy and ubiquitination could be assessed in the promoter regions of excitability target genes, such as *Kcnma1*, in order to illustrate the direct mechanism of decreased expression in fxSCA7 92Q mice. An alternative mechanism would be direct binding of ATXN7 to the regulatory domains of target genes, independent of STAGA function. Such a role for ATXN7 is not currently known and appears less likely than a potential alteration of the native function of STAGA, but should be explored for a more complete picture of molecular alterations in SCA7.

In the case of SCA1, several studies have presented evidence that ATXN1 protein directly interacts with the transcriptional repressor Capicua, and this interaction appears to be altered upon polyQ expansion. In SCA1 mice, polyQ expansion of ATXN1 increases the interaction between ATXN1 and Capicua, which ultimately accelerates motor impairment and neurodegeneration [57, 222]. Interestingly, knockout of Capicua

prevents neurodegeneration and motor impairment in the ATXN1^{154Q} mouse model of SCA1, as does the introduction of genetic mutations which prevent ATXN1 from binding to Capicua [223]. In this sense, the toxicity of polyQ-expanded ATXN1 appears to be dependent on Capicua binding. The authors of this study also illustrate that transcriptome changes seen in ATXN1^{154Q} mice are almost the complete opposite of those seen in Capicua knockout mice, suggesting that a large number of the transcriptional changes observed in SCA1 are likely under direct transcriptional regulation by Capicua [223]. In order to determine whether calcium homeostasis genes, especially BK, are under transcriptional regulation by Capicua, chromatin immunoprecipitation will be performed to determine occupancy by Capicua in both wild-type and ATXN1[82Q] mice. Since Capicua is a transcriptional repressor and polyQ expansion increases the association of ATXN1 and Capicua, BK channel expression would be expected to decrease in ATXN1[82Q] mice since this repression should become stronger. In fact, BK channel downregulation is observed in ATXN1[82Q] mice, although the reason is not yet known [71]. If confirmed, other members of the calcium homeostasis module could also be investigated for their regulation by Capicua in order to determine whether this is a master regulator of trafnscriptional control of calcium homeostasis genes related to Purkinje neuron excitability.

It is possible that transcriptional regulators other than Capicua may be involved in the regulation of excitability genes in SCA1 and other SCAs. One potential control element is the protein 14-3-3, which stabilizes the Ser-776 phosphorylation site of ATXN1 which controls its transport to the nucleus [224].14-3-3 binds more strongly to polyQ-expanded ATXN1 [225] and might therefore result in overrepresentation of ATXN1

in the nucleus upon polyQ expansion. Interestingly, a D776 phosphomimetic mutation induces motor impairment and minor dendritic structural alterations in mice which express a sub-pathogenic polyQ repeat sequence in ATXN1 [226], suggesting that increasing the strength of the interaction between 14-3-3 and ATXN1 may be sufficient to influence toxicity in SCA1. This is an alternative mechanism to Capicua but may also contribute to the increased presence of ATXN1 in the nucleus upon polyQ expansion. As in the case of SCA1 and SCA7, similar studies of transcriptional regulation by specific co-factors should be performed in mouse models of SCA2 and SCA3, although Purkinje neuron pathology is not the most prominent feature of SCA3 [7]. This would generate a broader understanding of transcriptional control in SCA and why specific genetic targets may be overrepresented in SCA.

In human SCA patients, Purkinje neuron involvement is variable and not the exclusive degenerative feature of disease. In many polyQ SCAs, neurons in the midbrain, pons, thalamus, and medulla oblongata demonstrate significant degeneration [7]. It is likely that neuronal dysfunction is not restricted to Purkinje neurons and may be significant in several of these additional nuclei. In particular, the olivary nuclei are heavily affected across SCAs [7] and play an important functional role in the cerebellar motor circuit. The inferior olive sends climbing fiber projections to cerebellar Purkinje neurons in order to elicit complex spikes. Complex spikes are an important feature of cerebellar learning [217] and alterations of the complex spike, such as frequency, pause length, and number of spikelets, may influence Purkinje neuron dysfunction in SCA. As mentioned in Section 5.1, future studies must focus on the function of the entire cerebellar motor circuit in order to fully study contributions to altered cerebellar output

and motor impairment. Alterations in olivary function can be assessed directly via patch-clamp recordings, or indirectly via the observance of complex spikes during *in vivo* recordings of Purkinje neuron activity. In order to uncover the underlying mechanisms to potential sources of dysfunction within brainstem nuclei, similar studies to the aforementioned could be performed in the inferior olive and other nuclei across SCAs to determine whether these neurons are similarly affected to Purkinje neurons. In the inferior olive, neurons in the dorsal cap of Kooy are spontaneously active [227], although they rely on a different cohort of ion-channels in order to support repetitive spiking than Purkinje neurons. It is possible that transcriptional control of these channels is also altered in SCA, although separate transcriptional co-factors may be important in the brainstem outside of Capicua. Since olivary neurons are also reliant on K_{Ca} channels for repetitive spiking [228-232], a calcium homeostasis module may also be relevant in these neurons and could be investigated. I would hypothesize that an altered transcriptome would be observed in the brainstem of knockin models of ataxia, or where a transgene is driven throughout the CNS, similar to the pattern of pathology observed in human SCA patients. I would also hypothesize that neuronal excitability pathways which converge on K_{Ca} channels would contribute to altered membrane excitability in olivary neurons, although BK channels and the exact calcium sources highlighted in this dissertation may be different in this nucleus. Studies investigating this possibility will strengthen our understanding of neuronal dysfunction in polyQ SCA, including how neuronal dysfunction may be common not only across SCAs of different etiologies but also across multiple neuronal populations within the same genetic cause of disease. This finding would have profound implications for the design of new therapies, in

particular if similar ion-channel targets are disrupted in multiple neuronal populations, as a single pharmacologic agent may demonstrate efficacy by targeting dysfunction across these brain regions.

5.3 Towards the design of novel potassium channel modulators to improve cerebellar function in spinocerebellar ataxia

The studies in Chapter 2 of this dissertation have identified a combination of FDA-approved potassium channel-activating compounds, baclofen and chlorzoxazone, which are tolerated in human SCA patients. While these studies are promising, several caveats remain. First, this combination of agents was chosen based off of studies in the ATXN1[82Q] mouse model of SCA1. While baclofen and chlorzoxazone were shown to improve Purkinje neuron spiking and reduce dendritic hyperexcitability in this model, the targets of baclofen and chlorzoxazone are not fully known, leading to the possibility of off-target effects. Second, it is unclear whether the effects of baclofen and chlorzoxazone in SCA patients are due to a preservation of Purkinje neuron function, or due to their effects as muscle relaxants [132]. Third, the trial involving SCA patients was intended to be a tolerability study and was not blinded or placebo-controlled. Therefore, effects of these compounds *in vivo* are difficult to interpret. Finally, since clinical trials with other reagents, such as riluzole, also demonstrate potential efficacy [110, 111], it remains unclear which molecular targets are most important for the improvement of patient symptoms or whether alternative molecular targets are more appropriate. Therefore, it is crucial to fully understand the proper molecular targets in SCA1 and other ataxias, and then design new therapeutic agents with increased specificity and

potency, in order to maximize the potential benefit of a pharmacologic treatment strategy for SCA.

Baclofen has several known targets in Purkinje neurons, but the studies in this dissertation suggest that other targets may remain undiscovered. The effect of baclofen on potentiating $GABA_B$ signaling is well-characterized. Baclofen is known to activate $GABA_B$ receptors in Purkinje neurons to produce an outward current. Upon activation of the $G_{i/o}$ complex, the $G_{\beta\gamma}$ subunit dissociates and interacts with G-protein coupled inwardly-rectifying potassium (GIRK) channels, resulting in activation and potentiation of this current [233]. In Purkinje neuron somata, GIRK1 channels have been shown to become activated upon baclofen administration [136]. This role of baclofen is consistent with the observation of Figure 2.3A in this dissertation, which illustrates that baclofen administration results in hyperpolarization of the somatic membrane potential in ATXN1[82Q] mice. However, another established role for baclofen is known in Purkinje neurons. In mouse models of SCA1 and SCA2, prolonged metabotropic glutamate receptor type 1 (mGluR1) currents have been observed [147, 152, 153]. In these cases, baclofen alone would therefore be expected to worsen motor performance by acting through increased mGluR1 activation [152]. This suggests that baclofen treatment *in vivo* may influence postsynaptic signaling in Purkinje neurons, a possibility which was not investigated with the studies of this dissertation. However, baclofen does not seem to reduce dendritic hyperexcitability in ATXN1[82Q] mice by activating either mGluR, since a phospholipase-C inhibitor does not change the effect of baclofen on the threshold to elicit dendritic calcium spikes, nor GIRK1, since barium does not occlude the effect of baclofen on the threshold to elicit calcium spikes. This limits the potential target of

baclofen to a relatively barium-insensitive inwardly-rectifying potassium channel, although the exact target remains unknown. Therefore, an ideal potassium channel-activating compound would need to activating a dendritic potassium channel current to reduce dendritic hyperexcitability, while also remaining neutral to mGluR signaling or even acting as a negative allosteric modulator of mGluR current in order to prevent negative effects on motor function through synaptic mechanisms.

Chlorzoxazone is considered a K_{Ca} channel activator, since it has been shown to activate BK, IK, and SK channel currents [134, 135]. In mouse models of cerebellar ataxia, chlorzoxazone has been demonstrated to simultaneously improve aberrant Purkinje neuron spiking and activate K_{Ca} currents in the AHP [73, 82, 83]. In Chapter 2 of this dissertation, I demonstrate that chlorzoxazone also reduces dendritic hyperexcitability in ATXN1[82Q] mice by activating a subthreshold-activated potassium channel current and not a K_{Ca} current (Figure 2.5). Chlorzoxazone appears to activate $K_{ir}6.2$ in Purkinje neuron dendrites, since tolbutamide partially occluded the effect of chlorzoxazone on increasing the threshold to elicit dendritic calcium spikes. However, it is likely that other targets of chlorzoxazone remain in Purkinje neuron dendrites, since the effect of tolbutamide was only partial. Future studies will be required to determine whether activating $K_{ir}6.2$ current is sufficient to reduce dendritic hyperexcitability or whether additional targets should be considered.

While K_{Ca} activation appears to be a desired quality for an agent designed to treat SCA, currently-approved K_{Ca} activators do possess some undesirable off-target effects. Riluzole is known to activate K_{Ca} channels at close to 20 μM, but inhibits sodium channels at 1-50 μM [112, 114]. Chlorzoxazone may also possess similar off-target effects

including sodium channel inhibition, although other potential molecular targets are not clearly documented. Despite these potential negative effects, both riluzole and chlorzoxazone have shown some therapeutic potential in human patients [110, 111, 149]. However, improved specificity would be a desired feature of any newly-designed therapeutic agent designed to target K_{Ca} activity. In addition, both riluzole and chlorzoxazone lack potency, thereby requiring high doses for treatment. While these compounds can achieve high plasma concentrations, prolonged administration risks liver toxicity and makes these compounds non-ideal for long-term treatment.

Taking these factors into account, the ideal agent for the treatment of SCA may possess the following qualities: (1) activate K_{Ca} channels in order to improve somatic spiking, (2) activate $K_{ir}6.2$ channels, and potentially other subthreshold-activated potassium channels, in order to reduce dendritic hyperexcitability, (3) either not affect synaptic signaling, or potentially act as a negative allosteric modulator of mGluR signaling, (4) work on the appropriate ion-channel targets with intermediate potency, so as to make a range of dosing possible without requiring millimolar concentrations of drug for efficacy, and (5) stable pharmacodynamics, possibly in a pro-drug formulation, in order to facilitate easy dosing for patients. In order to design such a compound, a series of experiments must take place.

Since K_{Ca}-activating properties seem to be important for improving Purkinje neuron spiking, both in the studies throughout this dissertation and in previous literature [73, 76-78, 82, 83, 105], using a known K_{Ca} activator as a scaffold for new reagents. Many K_{Ca} activators are substituted benzothiazoles or benzoxazoles, with substitutions influencing target specificity and potency [137]. Therefore, I would propose starting with

chlorzoxazone, a benzozoxazole, as it is known to target both K_{Ca} channels to improve Purkinje neuron spiking and $K_{ir}6.2$ in the dendrites in order to reduce dendritic hyperexcitability. Next, with the assistance of medicinal chemists, a library of substituted compounds can be generated, and their ability to activate $K_{ir}6.2$ currents can be assessed in a heterologous expression system with automated patch clamp recordings. Any compounds that activate $K_{ir}6.2$ will then be tested in acute cerebellar slices from ATXN1[82Q] mice in order to determine their effects on Purkinje neuron spiking and dendritic excitability. If a single compound is identified to successfully target both somatic spiking and dendritic excitability, it will be tested *in vivo* to confirm improvement of motor function in ATXN1[82Q] mice. If these attempts are unsuccessful, alternative molecular targets could be considered, or another known K_{Ca} activator could be used as a scaffold for the design of novel compounds. The ultimate goal of this drug development pipeline would be to design a compound specifically for the treatment of cerebellar ataxia, through improving target specificity and reducing the need for multiple agents in order to properly activate all molecular targets.

5.4 Current status of therapeutic options in spinocerebellar ataxia, and a potential role for pharmacologic modulators in treating disease

Currently, no proven symptomatic or disease-modifying therapies exist for the treatment of SCA. Through decades of research, several viable treatment strategies have been proposed and are still being explored to varying degrees of success. These include RNA interference-based technologies, gene editing approaches, and pharmacological targeting of altered neuronal physiology. Each of these approaches

show promise for treating specific underlying causes of ataxia, but they also demonstrate potential risks and concerns which must be considered.

In several of the polyQ SCAs, toxic gain-of-function mutations are thought to be the cause of disease [66]. In those cases, polyQ-expanded protein accumulates into insoluble aggregates, also disrupting cellular processes. Although it is unclear whether soluble oligomeric species are more or less toxic than these large aggregates, it is clear that reducing overall levels of the polyQ-expanded species or, in some cases, both polyQ-expanded and wild-type alleles would be beneficial for slowing or halting disease progression. Much of this recent work comes from studies involving RNA interference-based therapies including antisense oligonucleotides (ASO) therapy. ASO therapy is based on synthetic oligonucleotides which are targeted to bind to specific mRNA strands via Watson-Crick hybridization. Once bound, ASOs trigger an RNAse-H response in which the target mRNA is degraded but the ASO remains intact within the cell. This allows the ASO to consistently degrade mRNA for an extended period before re-dosing is required [108, 234]. Nusinersen, an ASO-based therapy, is now approved for the treatment of spinal muscular atrophy (SMA) [235-238], while clinical trials have advanced for the treatment of Huntington's disease and amyotrophic lateral sclerosis [239, 240] and proof-of-concept studies have been demonstrated in models of SCA1, SCA2, SCA3, and prion protein infection [108, 109, 241]. Although ASO treatment appears very promising for neurological disease, and clinical trials may begin within several years for SCA, there are still risks associated with this strategy. ASOs do not cross the blood-brain barrier and must therefore be delivered directly to the CNS via intrathecal injection [242]. In addition, although ASO-based therapies have the potential to be highly effective

for the treatment of ataxias caused by gain-of-function mutations, individual ASO treatments must be designed for each underlying cause of SCA, many of which are presumed loss-of-function mutations. Therefore, strategies to broadly treat symptoms across SCA of multiple etiologies will not be possible with the use of ASO technology. The safety of protein knockdown must also be considered for each individual genetic cause of SCA. ASO-based approaches appear appropriate for SCA3, as complete genetic knockdown or non-allele specific silencing of ATXN3 shows no adverse effects, suggesting that ATXN3 is a non-essential protein which could be safely targeted with full RNA knockdown approaches such as ASO-based therapies [108, 243, 244]. However, this is likely not the case for SCA1, as other studies have determined that reduction of more than 20% of ATXN1 may be toxic in mice and humans [223, 245]. This indicates that precise ASO dosing for each individual genetic variant is essential, making basic research and preclinical animal dosing studies fundamentally important. Another important consideration must be made for the cost of these treatments, as ASO-based therapies are tremendously expensive and must be delivered throughout the lifetime of the patient. Currently, Nusinersen costs $125,000 per treatment, which equates to $750,000 in the first year and $375,000 in each subsequent year [246]. Future research and development efforts must focus on reducing cost in order to provide maximum benefit to patients. Finally, as with any new and untested treatment strategy, adverse effects of ASO therapy can be predicted through animal studies but cannot be fully known until human trials are performed.

In cases where point mutations may result in either loss-of-function or gain-of-function mutations which cause ataxia, gene editing approaches may be considered. As

opposed to ASO therapies, or other RNA interference-based approaches, gene editing would directly target underlying genetic mutations within patient DNA. AAV2 and AAV9 have both been illustrated to efficiently deliver transgenes to adult neurons [247-249], and similar approaches could be considered for SCA. This also applies to CRISPR/Cas9, zinc finger nuclease (ZFN), and transcription activator-like effector (TALEN) technology, of which CRISPR/Cas9 appears to be easiest and most cost-effective approach [250, 251]. The most obvious benefit to gene editing approaches is that they attempt to genetically correct underlying genetic mutations, thereby requiring only one or few treatments in order to provide full benefit, provided that delivery is efficient and global throughout the CNS. Many of the concerns with AAV or CRISPR/Cas9 treatments are centered on efficient delivery and safety. For example, data from mouse models of SCA3 has indicated that RNAi, via AAV delivery methods, is ineffective at improving disease symptoms when solely targeted to the cerebellum [243, 252]. This is likely because many other brain regions are affected in SCA, including brainstem and thalamic nuclei [7]. Therefore, efforts must be made to improve global delivery methods for AAV-based therapies, while similar attempts to maximize delivery and efficacy will be required from CRISPR/Cas9 approaches. Other factors, such as cost and secondary effects of treatment, are not yet known as these approaches are still in their infancy for the treatment of SCA.

A final therapeutic strategy is outlined by the studies in this dissertation. As mentioned previously, alterations in Purkinje neuron electrophysiology are a major phenotypic component of mouse models of polyQ SCA. Alterations in spiking correlate with impaired motor function, and improving spiking also improves motor performance

[71, 73, 82, 83]. While is it assumed that mouse models are reflective of the human condition in disease, it cannot be known with current methods whether alterations in Purkinje neuron spiking contribute to motor symptoms in SCA patients. However, there is some evidence that ion-channel activators appropriately target and treat neuronal dysfunction in ataxia and other movement disorders. Chlorzoxazone, a K_{Ca} channel activator, improves symptoms of downbeat nystagmus in human SCA patients [149]. Another K_{Ca} channel activator, riluzole, has shown some potential efficacy for the treatment of SCA of multiple genetic causes in a series of clinical trials based in Italy [110, 111]. Finally, the studies outlined in Chapter 2 of this dissertation contain data from human SCA patients of multiple genetic causes and indicate that a combined treatment of chlorzoxazone and baclofen is tolerated by patients and may improve motor symptoms [73]. A major benefit of pharmacologic treatment with agents such as baclofen and chlorzoxazone is that they are already FDA approved for other uses, are easily accessible, and are cost-effective. Additionally, mouse models indicate that many SCAs are diseases of Purkinje neuron hyperexcitability, meaning that potassium channel activation could be a broad approach for improving symptoms in many different causes of SCA. Many cerebellar ataxia patients remain undiagnosed, even after genetic testing, and pharmacologic modulators are likely the only hope of symptomatic treatment in these cases. There are inherent concerns with prescribing treatments in cases with no confirmed diagnosis. However, these drugs can be discontinued if patients experience adverse objective or subjective effects, and these adverse effects would likely be transient. One obvious downfall of pharmacologic treatment for SCA is that it does not treat the underlying genetic cause of these disorders, but rather manages and potentially improves motor

symptoms. It is unclear whether pharmacologic approaches could also be neuroprotective, but this seems unlikely based on the studies from Chapter 2 of this dissertation. Therefore, potassium channel modulators appear to be limited in their therapeutic benefit when compared to genetic approaches but remain a good candidate for symptomatic treatment of ataxias of both known and unknown genetic causes.

5.5 Concluding remarks

In this dissertation, I have presented evidence that K_{Ca} channel dysfunction contributes to Purkinje neuron dysfunction in multiple models of SCA, and that targeting these alterations in Purkinje neuron spiking is a reasonable approach for the treatment of motor impairment in ataxia. The studies which have contributed to this conclusion were performed in mouse models of SCA1 and SCA7, and in human SCA patients. I have demonstrated that while changes in ion-channel function are important for Purkinje neuron dysfunction in SCA, functional alterations are not restricted to K_{Ca} channels but comprise a functional module of calcium sources and effector K_{Ca} channels. These changes are important for somatic spiking in Purkinje neurons, but independent dendritic pathology appears to exist across multiple models of SCA and should be considered when investigating the efficacy of potential therapeutics. Finally, these studies have outlined several potential treatment strategies for SCA, including potassium channel modulation and Sirt1 activation.

The studies in this dissertation add to current understating of how ion-channel dysfunction contributes to motor impairment in ataxia and can thereby act a therapeutic target for the treatment of ataxia. The work of this thesis, and future research that may

be inspired by these studies, may help generate novel therapies to improve patient outcomes in spinocerebellar ataxia.

References

1. Durr A. Autosomal dominant cerebellar ataxias: polyglutamine expansions and beyond. Lancet Neurol. 2010 Sep;9(9):885-94.

2. Coutelier M, Blesneac I, Monteil A, et al. A Recurrent Mutation in CACNA1G Alters Cav3.1 T-Type Calcium-Channel Conduction and Causes Autosomal-Dominant Cerebellar Ataxia. Am J Hum Genet. 2015 Nov 05;97(5):726-37.

3. Fogel BL, Hanson SM, Becker EB. Do mutations in the murine ataxia gene TRPC3 cause cerebellar ataxia in humans? Mov Disord. 2015 Feb;30(2):284-6.

4. Morino H, Matsuda Y, Muguruma K, et al. A mutation in the low voltage-gated calcium channel CACNA1G alters the physiological properties of the channel, causing spinocerebellar ataxia. Mol Brain. 2015 Dec 29;8:89.

5. Staisch J, Du X, Carvalho-de-Souza J, Kubota T, Bezanilla F, Gomez C. A mutation causing reduced BK channel activity leads to cognitive impairment and progressive cerebellar ataxia. Neurology. 2016 April 5, 2016;86(16):P5.394.

6. Staisch J, Du X, Kubota T, de Souza J, Bezanilla F, Gomez C. A novel KNCMA1 mutation associated with progressive cerebellar ataxia. Neurology. 2015 April 6, 2015;84(14):P2.118.

7. Seidel K, Siswanto S, Brunt ER, den Dunnen W, Korf HW, Rub U. Brain pathology of spinocerebellar ataxias. Acta Neuropathol. 2012 Jul;124(1):1-21.

8. Thach WT. Discharge of Purkinje and cerebellar nuclear neurons during rapidly alternating arm movements in the monkey. J Neurophysiol. 1968 Sep;31(5):785-97.

9. Heck DH, De Zeeuw CI, Jaeger D, Khodakhah K, Person AL. The neuronal code(s) of the cerebellum. J Neurosci. 2013 Nov 06;33(45):17603-9.

10. De Zeeuw CI, Hoebeek FE, Bosman LW, Schonewille M, Witter L, Koekkoek SK. Spatiotemporal firing patterns in the cerebellum. Nat Rev Neurosci. 2011 Jun;12(6):327-44.

11. Hong S, Negrello M, Junker M, Smilgin A, Thier P, De Schutter E. Multiplexed coding by cerebellar Purkinje neurons. Elife. 2016 Jul 26;5.

12. Raman IM, Bean BP. Resurgent sodium current and action potential formation in dissociated cerebellar Purkinje neurons. J Neurosci. 1997 Jun 15;17(12):4517-26.

13. Martina M, Metz AE, Bean BP. Voltage-dependent potassium currents during fast spikes of rat cerebellar Purkinje neurons: inhibition by BDS-I toxin. J Neurophysiol. 2007 Jan;97(1):563-71.

14. Raman IM, Bean BP. Ionic currents underlying spontaneous action potentials in isolated cerebellar Purkinje neurons. J Neurosci. 1999 Mar 01;19(5):1663-74.

15. Swensen AM, Bean BP. Ionic mechanisms of burst firing in dissociated Purkinje neurons. J Neurosci. 2003 Oct 22;23(29):9650-63.

16. Womack MD, Chevez C, Khodakhah K. Calcium-activated potassium channels are selectively coupled to P/Q-type calcium channels in cerebellar Purkinje neurons. J Neurosci. 2004 Oct 06;24(40):8818-22.

17. Edgerton JR, Reinhart PH. Distinct contributions of small and large conductance Ca2+-activated K+ channels to rat Purkinje neuron function. J Physiol. 2003 Apr 01;548(Pt 1):53-69.

18. Sausbier M, Hu H, Arntz C, et al. Cerebellar ataxia and Purkinje cell dysfunction caused by Ca2+-activated K+ channel deficiency. Proc Natl Acad Sci U S A. 2004 Jun 22;101(25):9474-8.

19. Cingolani LA, Gymnopoulos M, Boccaccio A, Stocker M, Pedarzani P. Developmental regulation of small-conductance Ca2+-activated K+ channel expression and function in rat Purkinje neurons. J Neurosci. 2002 Jun 01;22(11):4456-67.

20. Kindler CH, Pietruck C, Yost CS, Sampson ER, Gray AT. Localization of the tandem pore domain K+ channel TASK-1 in the rat central nervous system. Brain Res Mol Brain Res. 2000 Aug 14;80(1):99-108.

21. Kanjhan R, Anselme AM, Noakes PG, Bellingham MC. Postnatal changes in TASK-1 and TREK-1 expression in rat brain stem and cerebellum. Neuroreport. 2004 Jun 07;15(8):1321-4.

22. Bushell T, Clarke C, Mathie A, Robertson B. Pharmacological characterization of a non-inactivating outward current observed in mouse cerebellar Purkinje neurones. Br J Pharmacol. 2002 Feb;135(3):705-12.

23. Fernandez-Alacid L, Aguado C, Ciruela F, et al. Subcellular compartment-specific molecular diversity of pre- and post-synaptic GABA-activated GIRK channels in Purkinje cells. J Neurochem. 2009 Aug;110(4):1363-76.

24. Pruss H, Derst C, Lommel R, Veh RW. Differential distribution of individual subunits of strongly inwardly rectifying potassium channels (Kir2 family) in rat brain. Brain Res Mol Brain Res. 2005 Sep 13;139(1):63-79.

25. Aguado C, Colon J, Ciruela F, et al. Cell type-specific subunit composition of G protein-gated potassium channels in the cerebellum. J Neurochem. 2008 Apr;105(2):497-511.

26. Hartmann J, Dragicevic E, Adelsberger H, et al. TRPC3 channels are required for synaptic transmission and motor coordination. Neuron. 2008 Aug 14;59(3):392-8.

27. Kim SJ. TRPC3 channel underlies cerebellar long-term depression. Cerebellum. 2013 Jun;12(3):334-7.

28. Tada M, Nishizawa M, Onodera O. Roles of inositol 1,4,5-trisphosphate receptors in spinocerebellar ataxias. Neurochem Int. 2016 Mar;94:1-8.

29. Berridge MJ. Inositol trisphosphate and calcium signalling. Nature. 1993 Jan 28;361(6410):315-25.

30. Figueroa KP, Minassian NA, Stevanin G, et al. KCNC3: phenotype, mutations, channel biophysics-a study of 260 familial ataxia patients. Hum Mutat. 2010 Feb;31(2):191-6.

31. Waters MF, Minassian NA, Stevanin G, et al. Mutations in voltage-gated potassium channel KCNC3 cause degenerative and developmental central nervous system phenotypes. Nat Genet. 2006 Apr;38(4):447-51.

32. Zhang Y, Kaczmarek LK. Kv3.3 potassium channels and spinocerebellar ataxia. J Physiol. 2016 Aug 15;594(16):4677-84.

33. Akemann W, Knopfel T. Interaction of Kv3 potassium channels and resurgent sodium current influences the rate of spontaneous firing of Purkinje neurons. J Neurosci. 2006 Apr 26;26(17):4602-12.

34. Hurlock EC, Bose M, Pierce G, Joho RH. Rescue of motor coordination by Purkinje cell-targeted restoration of Kv3.3 channels in Kcnc3-null mice requires Kcnc1. J Neurosci. 2009 Dec 16;29(50):15735-44.

35. Hurlock EC, McMahon A, Joho RH. Purkinje-cell-restricted restoration of Kv3.3 function restores complex spikes and rescues motor coordination in Kcnc3 mutants. J Neurosci. 2008 Apr 30;28(18):4640-8.

36. Duarri A, Jezierska J, Fokkens M, et al. Mutations in potassium channel kcnd3 cause spinocerebellar ataxia type 19. Ann Neurol. 2012 Dec;72(6):870-80.

37. Lee YC, Durr A, Majczenko K, et al. Mutations in KCND3 cause spinocerebellar ataxia type 22. Ann Neurol. 2012 Dec;72(6):859-69.

38. Hsu YH, Huang HY, Tsaur ML. Contrasting expression of Kv4.3, an A-type K+ channel, in migrating Purkinje cells and other post-migratory cerebellar neurons. Eur J Neurosci. 2003 Aug;18(3):601-12.

39. Serodio P, Rudy B. Differential expression of Kv4 K+ channel subunits mediating subthreshold transient K+ (A-type) currents in rat brain. J Neurophysiol. 1998 Feb;79(2):1081-91.

40. Duarri A, Lin MC, Fokkens MR, et al. Spinocerebellar ataxia type 19/22 mutations alter heterocomplex Kv4.3 channel function and gating in a dominant manner. Cell Mol Life Sci. 2015 Sep;72(17):3387-99.

41. Smets K, Duarri A, Deconinck T, et al. First de novo KCND3 mutation causes severe Kv4.3 channel dysfunction leading to early onset cerebellar ataxia, intellectual disability, oral apraxia and epilepsy. BMC Med Genet. 2015 Jul 21;16:51.

42. Chen X, Kovalchuk Y, Adelsberger H, et al. Disruption of the olivo-cerebellar circuit by Purkinje neuron-specific ablation of BK channels. Proc Natl Acad Sci U S A. 2010 Jul 06;107(27):12323-8.

43. Iwaki A, Kawano Y, Miura S, et al. Heterozygous deletion of ITPR1, but not SUMF1, in spinocerebellar ataxia type 16. J Med Genet. 2008 Jan;45(1):32-5.

44. Knight MA, Kennerson ML, Anney RJ, et al. Spinocerebellar ataxia type 15 (sca15) maps to 3p24.2-3pter: exclusion of the ITPR1 gene, the human orthologue of an ataxic mouse mutant. Neurobiol Dis. 2003 Jul;13(2):147-57.

45. van de Leemput J, Chandran J, Knight MA, et al. Deletion at ITPR1 underlies ataxia in mice and spinocerebellar ataxia 15 in humans. PLoS Genet. 2007 Jun;3(6):e108.

46. Zambonin JL, Bellomo A, Ben-Pazi H, et al. Spinocerebellar ataxia type 29 due to mutations in ITPR1: a case series and review of this emerging congenital ataxia. Orphanet J Rare Dis. 2017 Jun 28;12(1):121.

47. Huang L, Chardon JW, Carter MT, et al. Missense mutations in ITPR1 cause autosomal dominant congenital nonprogressive spinocerebellar ataxia. Orphanet J Rare Dis. 2012 Sep 17;7:67.

48. Barresi S, Niceta M, Alfieri P, et al. Mutations in the IRBIT domain of ITPR1 are a frequent cause of autosomal dominant nonprogressive congenital ataxia. Clin Genet. 2017 Jan;91(1):86-91.

49. Ogura H, Matsumoto M, Mikoshiba K. Motor discoordination in mutant mice heterozygous for the type 1 inositol 1,4,5-trisphosphate receptor. Behav Brain Res. 2001 Aug 01;122(2):215-9.

50. Aiba A, Kano M, Chen C, et al. Deficient cerebellar long-term depression and impaired motor learning in mGluR1 mutant mice. Cell. 1994 Oct 21;79(2):377-88.

51. Becker EB, Oliver PL, Glitsch MD, et al. A point mutation in TRPC3 causes abnormal Purkinje cell development and cerebellar ataxia in moonwalker mice. Proc Natl Acad Sci U S A. 2009 Apr 21;106(16):6706-11.

52. Sekerkova G, Kim JA, Nigro MJ, et al. Early onset of ataxia in moonwalker mice is accompanied by complete ablation of type II unipolar brush cells and Purkinje cell dysfunction. J Neurosci. 2013 Dec 11;33(50):19689-94.

53. Ly R, Bouvier G, Schonewille M, et al. T-type channel blockade impairs long-term potentiation at the parallel fiber-Purkinje cell synapse and cerebellar learning. Proc Natl Acad Sci U S A. 2013 Dec 10;110(50):20302-7.

54. Petrenko AB, Tsujita M, Kohno T, Sakimura K, Baba H. Mutation of alpha1G T-type calcium channels in mice does not change anesthetic requirements for loss of the righting reflex and minimum alveolar concentration but delays the onset of anesthetic induction. Anesthesiology. 2007 Jun;106(6):1177-85.

55. Zhuchenko O, Bailey J, Bonnen P, et al. Autosomal dominant cerebellar ataxia (SCA6) associated with small polyglutamine expansions in the alpha 1A-voltage-dependent calcium channel. Nat Genet. 1997 Jan;15(1):62-9.

56. Irwin S, Vandelft M, Pinchev D, et al. RNA association and nucleocytoplasmic shuttling by ataxin-1. J Cell Sci. 2005 Jan 01;118(Pt 1):233-42.

57. Lam YC, Bowman AB, Jafar-Nejad P, et al. ATAXIN-1 interacts with the repressor Capicua in its native complex to cause SCA1 neuropathology. Cell. 2006 Dec 29;127(7):1335-47.

58. Yue MM, Lv K, Meredith SC, Martindale JL, Gorospe M, Schuger L. Novel RNA-binding protein P311 binds eukaryotic translation initiation factor 3 subunit b (eIF3b) to promote translation of transforming growth factor beta1-3 (TGF-beta1-3). J Biol Chem. 2014 Dec 05;289(49):33971-83.

59. McCann C, Holohan EE, Das S, et al. The Ataxin-2 protein is required for microRNA function and synapse-specific long-term olfactory habituation. Proc Natl Acad Sci U S A. 2011 Sep 06;108(36):E655-62.

60. Neuwald AF, Koonin EV. Ataxin-2, global regulators of bacterial gene expression, and spliceosomal snRNP proteins share a conserved domain. J Mol Med (Berl). 1998 Jan;76(1):3-5.

61. Shibata H, Huynh DP, Pulst SM. A novel protein with RNA-binding motifs interacts with ataxin-2. Hum Mol Genet. 2000 May 22;9(9):1303-13.

62. Li X, Liu H, Fischhaber PL, Tang TS. Toward therapeutic targets for SCA3: Insight into the role of Machado-Joseph disease protein ataxin-3 in misfolded proteins clearance. Prog Neurobiol. 2015 Sep;132:34-58.

63. Costa Mdo C, Paulson HL. Toward understanding Machado-Joseph disease. Prog Neurobiol. 2012 May;97(2):239-57.

64. Helmlinger D, Hardy S, Sasorith S, et al. Ataxin-7 is a subunit of GCN5 histone acetyltransferase-containing complexes. Hum Mol Genet. 2004 Jun 15;13(12):1257-65.

65. Yang S, Li XJ, Li S. Molecular mechanisms underlying Spinocerebellar Ataxia 17 (SCA17) pathogenesis. Rare Dis. 2016;4(1):e1223580.

66. Paulson HL, Shakkottai VG, Clark HB, Orr HT. Polyglutamine spinocerebellar ataxias - from genes to potential treatments. Nat Rev Neurosci. 2017 Oct;18(10):613-26.

67. Bettencourt C, Ryten M, Forabosco P, et al. Insights from cerebellar transcriptomic analysis into the pathogenesis of ataxia. JAMA Neurol. 2014 Jul 01;71(7):831-9.

68. Ingram M, Wozniak EAL, Duvick L, et al. Cerebellar Transcriptome Profiles of ATXN1 Transgenic Mice Reveal SCA1 Disease Progression and Protection Pathways. Neuron. 2016 Mar 16;89(6):1194-207.

69. Pflieger LT, Dansithong W, Paul S, et al. Gene co-expression network analysis for identifying modules and functionally enriched pathways in SCA2. Hum Mol Genet. 2017;26(16):3069-80.

70. Dell'Orco JM, Pulst SM, Shakkottai VG. Potassium channel dysfunction underlies Purkinje neuron spiking abnormalities in spinocerebellar ataxia type 2. Human Molecular Genetics. 2017.

71. Dell'Orco JM, Wasserman AH, Chopra R, et al. Neuronal Atrophy Early in Degenerative Ataxia Is a Compensatory Mechanism to Regulate Membrane Excitability. J Neurosci. 2015 Aug 12;35(32):11292-307.

72. Hansen ST, Meera P, Otis TS, Pulst SM. Changes in Purkinje cell firing and gene expression precede behavioral pathology in a mouse model of SCA2. Hum Mol Genet. 2013 Jan 15;22(2):271-83.

73. Bushart DD, Chopra R, Singh V, Murphy GG, Wulff H, Shakkottai VG. Targeting potassium channels to treat cerebellar ataxia. Ann Clin Transl Neurol. 2018 Mar;5(3):297-314.

74. Chopra R, Wasserman AH, Pulst SM, De Zeeuw CI, Shakkottai VG. Protein kinase C activity is a protective modifier of Purkinje neuron degeneration in cerebellar ataxia. Hum Mol Genet. 2018 Apr 15;27(8):1396-410.

75. Egorova PA, Zakharova OA, Vlasova OL, Bezprozvanny IB. In vivo analysis of cerebellar Purkinje cell activity in SCA2 transgenic mouse model. J Neurophysiol. 2016 Jun 01;115(6):2840-51.

76. Kasumu AW, Hougaard C, Rode F, et al. Selective positive modulator of calcium-activated potassium channels exerts beneficial effects in a mouse model of spinocerebellar ataxia type 2. Chem Biol. 2012 Oct 26;19(10):1340-53.

77. Shakkottai VG, do Carmo Costa M, Dell'Orco JM, Sankaranarayanan A, Wulff H, Paulson HL. Early changes in cerebellar physiology accompany motor dysfunction in the polyglutamine disease spinocerebellar ataxia type 3. J Neurosci. 2011 Sep 07;31(36):13002-14.

78. Jayabal S, Chang HH, Cullen KE, Watt AJ. 4-aminopyridine reverses ataxia and cerebellar firing deficiency in a mouse model of spinocerebellar ataxia type 6. Sci Rep. 2016 Jul 06;6:29489.

79. Bushart DD, Chopra R, Singh V, Murphy GG, Wulff H, Shakkottai VG. Targeting potassium channels to treat cerebellar ataxia. Ann Clin Transl Neurol. 2018.

80. Schiffmann SN, Cheron G, Lohof A, et al. Impaired motor coordination and Purkinje cell excitability in mice lacking calretinin. Proc Natl Acad Sci U S A. 1999 Apr 27;96(9):5257-62.

81. Ryu C, Jang DC, Jung D, et al. STIM1 Regulates Somatic Ca(2+) Signals and Intrinsic Firing Properties of Cerebellar Purkinje Neurons. J Neurosci. 2017 Sep 13;37(37):8876-94.

82. Walter JT, Alvina K, Womack MD, Chevez C, Khodakhah K. Decreases in the precision of Purkinje cell pacemaking cause cerebellar dysfunction and ataxia. Nat Neurosci. 2006 Mar;9(3):389-97.

83. Gao Z, Todorov B, Barrett CF, et al. Cerebellar ataxia by enhanced Ca(V)2.1 currents is alleviated by Ca2+-dependent K+-channel activators in Cacna1a(S218L) mutant mice. J Neurosci. 2012 Oct 31;32(44):15533-46.

84. Kaufmann WA, Ferraguti F, Fukazawa Y, et al. Large-conductance calcium-activated potassium channels in purkinje cell plasma membranes are clustered at sites of hypolemmal microdomains. J Comp Neurol. 2009 Jul 10;515(2):215-30.

85. Hirono M, Ogawa Y, Misono K, et al. BK Channels Localize to the Paranodal Junction and Regulate Action Potentials in Myelinated Axons of Cerebellar Purkinje Cells. J Neurosci. 2015 May 6;35(18):7082-94.

86. Indriati DW, Kamasawa N, Matsui K, Meredith AL, Watanabe M, Shigemoto R. Quantitative localization of Cav2.1 (P/Q-type) voltage-dependent calcium channels in Purkinje cells: somatodendritic gradient and distinct somatic coclustering with calcium-activated potassium channels. J Neurosci. 2013 Feb 20;33(8):3668-78.

87. Hosy E, Piochon C, Teuling E, Rinaldo L, Hansel C. SK2 channel expression and function in cerebellar Purkinje cells. J Physiol. 2011 Jul 15;589(Pt 14):3433-40.

88. Engbers JD, Anderson D, Asmara H, et al. Intermediate conductance calcium-activated potassium channels modulate summation of parallel fiber input in cerebellar Purkinje cells. Proc Natl Acad Sci U S A. 2012 Feb 14;109(7):2601-6.

89. Lev-Ram V, Miyakawa H, Lasser-Ross N, Ross WN. Calcium transients in cerebellar Purkinje neurons evoked by intracellular stimulation. J Neurophysiol. 1992 Oct;68(4):1167-77.

90. Kitamura K, Hausser M. Dendritic calcium signaling triggered by spontaneous and sensory-evoked climbing fiber input to cerebellar Purkinje cells in vivo. J Neurosci. 2011 Jul 27;31(30):10847-58.

91. Zagha E, Manita S, Ross WN, Rudy B. Dendritic Kv3.3 potassium channels in cerebellar purkinje cells regulate generation and spatial dynamics of dendritic Ca2+ spikes. J Neurophysiol. 2010 Jun;103(6):3516-25.

92. Womack MD, Khodakhah K. Somatic and dendritic small-conductance calcium-activated potassium channels regulate the output of cerebellar Purkinje neurons. J Neurosci. 2003 Apr 01;23(7):2600-7.

93. Ohtsuki G, Piochon C, Adelman JP, Hansel C. SK2 channel modulation contributes to compartment-specific dendritic plasticity in cerebellar Purkinje cells. Neuron. 2012 Jul 12;75(1):108-20.

94. Rancz EA, Hausser M. Dendritic spikes mediate negative synaptic gain control in cerebellar Purkinje cells. Proc Natl Acad Sci U S A. 2010 Dec 21;107(51):22284-9.

95. Rancz EA, Hausser M. Dendritic calcium spikes are tunable triggers of cannabinoid release and short-term synaptic plasticity in cerebellar Purkinje neurons. J Neurosci. 2006 May 17;26(20):5428-37.

96. Miyakawa H, Lev-Ram V, Lasser-Ross N, Ross WN. Calcium transients evoked by climbing fiber and parallel fiber synaptic inputs in guinea pig cerebellar Purkinje neurons. J Neurophysiol. 1992 Oct;68(4):1178-89.

97. Takechi H, Eilers J, Konnerth A. A new class of synaptic response involving calcium release in dendritic spines. Nature. 1998 Dec 24-31;396(6713):757-60.

98. Otsu Y, Marcaggi P, Feltz A, et al. Activity-dependent gating of calcium spikes by A-type K+ channels controls climbing fiber signaling in Purkinje cell dendrites. Neuron. 2014 Oct 1;84(1):137-51.

99. Dove LS, Abbott LC, Griffith WH. Whole-cell and single-channel analysis of P-type calcium currents in cerebellar Purkinje cells of leaner mutant mice. J Neurosci. 1998 Oct 01;18(19):7687-99.

100. Lorenzon NM, Lutz CM, Frankel WN, Beam KG. Altered calcium channel currents in Purkinje cells of the neurological mutant mouse leaner. J Neurosci. 1998 Jun 15;18(12):4482-9.

101. Wakamori M, Yamazaki K, Matsunodaira H, et al. Single tottering mutations responsible for the neuropathic phenotype of the P-type calcium channel. J Biol Chem. 1998 Dec 25;273(52):34857-67.

102. Hoebeek FE, Stahl JS, van Alphen AM, et al. Increased noise level of purkinje cell activities minimizes impact of their modulation during sensorimotor control. Neuron. 2005 Mar 24;45(6):953-65.

103. Shakkottai VG, Chou CH, Oddo S, et al. Enhanced neuronal excitability in the absence of neurodegeneration induces cerebellar ataxia. J Clin Invest. 2004 Feb;113(4):582-90.

104. Hourez R, Servais L, Orduz D, et al. Aminopyridines correct early dysfunction and delay neurodegeneration in a mouse model of spinocerebellar ataxia type 1. J Neurosci. 2011 Aug 17;31(33):11795-807.

105. Alvina K, Khodakhah K. The therapeutic mode of action of 4-aminopyridine in cerebellar ataxia. J Neurosci. 2010 May 26;30(21):7258-68.

106. Liu J, Tang TS, Tu H, et al. Deranged calcium signaling and neurodegeneration in spinocerebellar ataxia type 2. J Neurosci. 2009 Jul 22;29(29):9148-62.

107. Chen X, Tang TS, Tu H, et al. Deranged calcium signaling and neurodegeneration in spinocerebellar ataxia type 3. J Neurosci. 2008 Nov 26;28(48):12713-24.

108. Moore LR, Rajpal G, Dillingham IT, et al. Evaluation of Antisense Oligonucleotides Targeting ATXN3 in SCA3 Mouse Models. Mol Ther Nucleic Acids. 2017 Jun 16;7:200-10.

109. Scoles DR, Meera P, Schneider MD, et al. Antisense oligonucleotide therapy for spinocerebellar ataxia type 2. Nature. 2017 Apr 20;544(7650):362-6.

110. Ristori G, Romano S, Visconti A, et al. Riluzole in cerebellar ataxia: a randomized, double-blind, placebo-controlled pilot trial. Neurology. 2010 Mar 09;74(10):839-45.

111. Romano S, Coarelli G, Marcotulli C, et al. Riluzole in patients with hereditary cerebellar ataxia: a randomised, double-blind, placebo-controlled trial. Lancet Neurol. 2015 Oct;14(10):985-91.

112. Doble A. The pharmacology and mechanism of action of riluzole. Neurology. 1996 Dec;47(6 Suppl 4):S233-41.

113. Cao YJ, Dreixler JC, Couey JJ, Houamed KM. Modulation of recombinant and native neuronal SK channels by the neuroprotective drug riluzole. Eur J Pharmacol. 2002 Aug 02;449(1-2):47-54.

114. Lam J, Coleman N, Garing AL, Wulff H. The therapeutic potential of small-conductance KCa2 channels in neurodegenerative and psychiatric diseases. Expert Opin Ther Targets. 2013 Oct;17(10):1203-20.

115. Jodice C, Mantuano E, Veneziano L, et al. Episodic ataxia type 2 (EA2) and spinocerebellar ataxia type 6 (SCA6) due to CAG repeat expansion in the CACNA1A gene on chromosome 19p. Hum Mol Genet. 1997 Oct;6(11):1973-8.

116. Claes L, Del-Favero J, Ceulemans B, Lagae L, Van Broeckhoven C, De Jonghe P. De novo mutations in the sodium-channel gene SCN1A cause severe myoclonic epilepsy of infancy. Am J Hum Genet. 2001 Jun;68(6):1327-32.

117. van Swieten JC, Brusse E, de Graaf BM, et al. A mutation in the fibroblast growth factor 14 gene is associated with autosomal dominant cerebellar ataxia [corrected]. Am J Hum Genet. 2003 Jan;72(1):191-9.

118. Ferrer I, Genis D, Davalos A, Bernado L, Sant F, Serrano T. The Purkinje cell in olivopontocerebellar atrophy. A Golgi and immunocytochemical study. Neuropathol Appl Neurobiol. 1994 Feb;20(1):38-46.

119. Bean BP. The action potential in mammalian central neurons. Nat Rev Neurosci. 2007 Jun;8(6):451-65.

120. Raman IM, Bean BP. Properties of sodium currents and action potential firing in isolated cerebellar Purkinje neurons. Ann N Y Acad Sci. 1999 Apr 30;868:93-6.

121. Chopra R, Wasserman AH, Bushart DD, Dell'Orco JM, Shakkottai VG. Increased dendritic excitability and calcium-dependent PKC activation: a novel mechanism underlying Purkinje neuron dendritic degeneration in cerebellar ataxias. Ann Neurol. 2016;80(s20):S33-S4.

122. Burright EN, Clark HB, Servadio A, et al. SCA1 transgenic mice: a model for neurodegeneration caused by an expanded CAG trinucleotide repeat. Cell. 1995 Sep 22;82(6):937-48.

123. Khaliq ZM, Gouwens NW, Raman IM. The contribution of resurgent sodium current to high-frequency firing in Purkinje neurons: an experimental and modeling study. J Neurosci. 2003 Jun 15;23(12):4899-912.

124. Womack MD, Khodakhah K. Characterization of large conductance Ca2+-activated K+ channels in cerebellar Purkinje neurons. Eur J Neurosci. 2002 Oct;16(7):1214-22.

125. Benton MD, Lewis AH, Bant JS, Raman IM. Iberiotoxin-sensitive and -insensitive BK currents in Purkinje neuron somata. J Neurophysiol. 2013 May;109(10):2528-41.

126. Benton MD, Raman IM. Stabilization of Ca current in Purkinje neurons during high-frequency firing by a balance of Ca-dependent facilitation and inactivation. Channels (Austin). 2009 Nov;3(6):393-401.

127. Fierro L, Llano I. High endogenous calcium buffering in Purkinje cells from rat cerebellar slices. J Physiol. 1996 Nov 1;496 (Pt 3):617-25.

128. Shakkottai VG, Xiao M, Xu L, et al. FGF14 regulates the intrinsic excitability of cerebellar Purkinje neurons. Neurobiology of disease. 2009 Jan;33(1):81-8.

129. Mercer AA, Palarz KJ, Tabatadze N, Woolley CS, Raman IM. Sex differences in cerebellar synaptic transmission and sex-specific responses to autism-linked Gabrb3 mutations in mice. Elife. 2016 Apr 14;5.

130. Ankri L, Yarom Y, Uusisaari MY. Slice it hot: acute adult brain slicing in physiological temperature. J Vis Exp. 2014 Oct 30(92):e52068.

131. Alvina K, Khodakhah K. KCa channels as therapeutic targets in episodic ataxia type-2. J Neurosci. 2010 May 26;30(21):7249-57.

132. Lexicomp. Clinical Drug Information. Wolters Kluwer. 2017.

133. The American Geriatrics Society. American Geriatrics Society Updated Beers Criteria for Potentially Inappropriate Medication Use in Older Adults. Journal of the American Geriatrics Society. 2012;60:616-31.

134. Liu YC, Lo YK, Wu SN. Stimulatory effects of chlorzoxazone, a centrally acting muscle relaxant, on large conductance calcium-activated potassium channels in pituitary GH3 cells. Brain Res. 2003 Jan 03;959(1):86-97.

135. Cao Y, Dreixler JC, Roizen JD, Roberts MT, Houamed KM. Modulation of recombinant small-conductance Ca(2+)-activated K(+) channels by the muscle relaxant chlorzoxazone and structurally related compounds. J Pharmacol Exp Ther. 2001 Mar;296(3):683-9.

136. Tabata T, Haruki S, Nakayama H, Kano M. GABAergic activation of an inwardly rectifying K+ current in mouse cerebellar Purkinje cells. J Physiol. 2005 Mar 01;563(Pt 2):443-57.

137. Sankaranarayanan A, Raman G, Busch C, et al. Naphtho[1,2-d]thiazol-2-ylamine (SKA-31), a new activator of KCa2 and KCa3.1 potassium channels, potentiates the endothelium-derived hyperpolarizing factor response and lowers blood pressure. Mol Pharmacol. 2009 Feb;75(2):281-95.

138. Pedarzani P, Mosbacher J, Rivard A, et al. Control of electrical activity in central neurons by modulating the gating of small conductance Ca2+-activated K+ channels. J Biol Chem. 2001 Mar 30;276(13):9762-9.

139. Imlach WL, Finch SC, Dunlop J, Meredith AL, Aldrich RW, Dalziel JE. The molecular mechanism of "ryegrass staggers," a neurological disorder of K+ channels. J Pharmacol Exp Ther. 2008 Dec;327(3):657-64.

140. Clark HB, Burright EN, Yunis WS, et al. Purkinje cell expression of a mutant allele of SCA1 in transgenic mice leads to disparate effects on motor behaviors, followed by a progressive cerebellar dysfunction and histological alterations. J Neurosci. 1997 Oct 01;17(19):7385-95.

141. Coetzee WA, Amarillo Y, Chiu J, et al. Molecular diversity of K+ channels. Ann N Y Acad Sci. 1999 Apr 30;868:233-85.

142. Quayle JM, McCarron JG, Brayden JE, Nelson MT. Inward rectifier K+ currents in smooth muscle cells from rat resistance-sized cerebral arteries. Am J Physiol. 1993 Nov;265(5 Pt 1):C1363-70.

143. Sepulveda FV, Pablo Cid L, Teulon J, Niemeyer MI. Molecular aspects of structure, gating, and physiology of pH-sensitive background K2P and Kir K+-transport channels. Physiol Rev. 2015 Jan;95(1):179-217.

144. Hibino H, Inanobe A, Furutani K, Murakami S, Findlay I, Kurachi Y. Inwardly rectifying potassium channels: their structure, function, and physiological roles. Physiol Rev. 2010 Jan;90(1):291-366.

145. Alagem N, Dvir M, Reuveny E. Mechanism of Ba(2+) block of a mouse inwardly rectifying K+ channel: differential contribution by two discrete residues. J Physiol. 2001 Jul 15;534(Pt. 2):381-93.

146. Zhou M, Tanaka O, Suzuki M, et al. Localization of pore-forming subunit of the ATP-sensitive K(+)-channel, Kir6.2, in rat brain neurons and glial cells. Brain Res Mol Brain Res. 2002 May 30;101(1-2):23-32.

147. Shuvaev AN, Hosoi N, Sato Y, Yanagihara D, Hirai H. Progressive impairment of cerebellar mGluR signalling and its therapeutic potential for cerebellar ataxia in spinocerebellar ataxia type 1 model mice. J Physiol. 2017 Jan 01;595(1):141-64.

148. Hirono M, Yoshioka T, Konishi S. GABA(B) receptor activation enhances mGluR-mediated responses at cerebellar excitatory synapses. Nat Neurosci. 2001 Dec;4(12):1207-16.

149. Feil K, Claassen J, Bardins S, et al. Effect of chlorzoxazone in patients with downbeat nystagmus: a pilot trial. Neurology. 2013 Sep 24;81(13):1152-8.

150. Schmitz-Hubsch T, du Montcel ST, Baliko L, et al. Scale for the assessment and rating of ataxia: development of a new clinical scale. Neurology. 2006 Jun 13;66(11):1717-20.

151. Inoue T, Lin X, Kohlmeier KA, Orr HT, Zoghbi HY, Ross WN. Calcium dynamics and electrophysiological properties of cerebellar Purkinje cells in SCA1 transgenic mice. J Neurophysiol. 2001 Apr;85(4):1750-60.

152. Power EM, Morales A, Empson RM. Prolonged Type 1 Metabotropic Glutamate Receptor Dependent Synaptic Signaling Contributes to Spino-Cerebellar Ataxia Type 1. J Neurosci. 2016 May 04;36(18):4910-6.

153. Meera P, Pulst S, Otis T. A positive feedback loop linking enhanced mGluR function and basal calcium in spinocerebellar ataxia type 2. Elife. 2017 May 18;6.

154. Jacobi H, Bauer P, Giunti P, et al. The natural history of spinocerebellar ataxia type 1, 2, 3, and 6: a 2-year follow-up study. Neurology. 2011 Sep 13;77(11):1035-41.

155. Ashizawa T, Figueroa KP, Perlman SL, et al. Clinical characteristics of patients with spinocerebellar ataxias 1, 2, 3 and 6 in the US; a prospective observational study. Orphanet J Rare Dis. 2013 Nov 13;8:177.

156. David G, Giunti P, Abbas N, et al. The gene for autosomal dominant cerebellar ataxia type II is located in a 5-cM region in 3p12-p13: genetic and physical mapping of the SCA7 locus. Am J Hum Genet. 1996 Dec;59(6):1328-36.

157. David G, Abbas N, Stevanin G, et al. Cloning of the SCA7 gene reveals a highly unstable CAG repeat expansion. Nat Genet. 1997 Sep;17(1):65-70.

158. Helmlinger D, Hardy S, Eberlin A, Devys D, Tora L. Both normal and polyglutamine- expanded ataxin-7 are components of TFTC-type GCN5 histone acetyltransferase- containing complexes. Biochem Soc Symp. 2006(73):155-63.

159. Furrer SA, Mohanachandran MS, Waldherr SM, et al. Spinocerebellar ataxia type 7 cerebellar disease requires the coordinated action of mutant ataxin-7 in neurons and glia, and displays non-cell-autonomous bergmann glia degeneration. J Neurosci. 2011 Nov 9;31(45):16269-78.

160. Bootman MD, Collins TJ, Mackenzie L, Roderick HL, Berridge MJ, Peppiatt CM. 2-aminoethoxydiphenyl borate (2-APB) is a reliable blocker of store-operated Ca2+ entry but an inconsistent inhibitor of InsP3-induced Ca2+ release. FASEB J. 2002 Aug;16(10):1145-50.

161. van Rossum DB, Patterson RL, Ma HT, Gill DL. Ca2+ entry mediated by store depletion, S-nitrosylation, and TRP3 channels. Comparison of coupling and function. J Biol Chem. 2000 Sep 15;275(37):28562-8.

162. Martin RL, Lee JH, Cribbs LL, Perez-Reyes E, Hanck DA. Mibefradil block of cloned T-type calcium channels. J Pharmacol Exp Ther. 2000 Oct;295(1):302-8.

163. Llano I, Marty A, Armstrong CM, Konnerth A. Synaptic- and agonist-induced excitatory currents of Purkinje cells in rat cerebellar slices. J Physiol. 1991 Mar;434:183-213.

164. Zagha E, Lang EJ, Rudy B. Kv3.3 channels at the Purkinje cell soma are necessary for generation of the classical complex spike waveform. J Neurosci. 2008 Feb 06;28(6):1291-300.

165. Trapnell C, Pachter L, Salzberg SL. TopHat: discovering splice junctions with RNA-Seq. Bioinformatics. 2009 May 1;25(9):1105-11.

166. Trapnell C, Williams BA, Pertea G, et al. Transcript assembly and quantification by RNA-Seq reveals unannotated transcripts and isoform switching during cell differentiation. Nat Biotechnol. 2010 May;28(5):511-5.

167. Sturn A, Quackenbush J, Trajanoski Z. Genesis: cluster analysis of microarray data. Bioinformatics. 2002 Jan;18(1):207-8.

168. Klimpel KE, Lee MY, King WM, Raphael Y, Schacht J, Neitzel RL. Vestibular dysfunction in the adult CBA/CaJ mouse after lead and cadmium treatment. Environ Toxicol. 2017 Mar;32(3):869-76.

169. Lee MY, Takada T, Takada Y, et al. Mice with conditional deletion of Cx26 exhibit no vestibular phenotype despite secondary loss of Cx30 in the vestibular end organs. Hear Res. 2015 Oct;328:102-12.

170. Gatchel JR, Watase K, Thaller C, et al. The insulin-like growth factor pathway is altered in spinocerebellar ataxia type 1 and type 7. Proc Natl Acad Sci U S A. 2008 Jan 29;105(4):1291-6.

171. Dansithong W, Paul S, Figueroa KP, et al. Ataxin-2 regulates RGS8 translation in a new BAC-SCA2 transgenic mouse model. PLoS Genet. 2015 Apr;11(4):e1005182.
172. Voogd J, Glickstein M. The anatomy of the cerebellum. Trends Cogn Sci. 1998 Sep 1;2(9):307-13.

173. Bademkiran F, Uludag B, Guler A, Celebisoy N. The effects of the cerebral, cerebellar and vestibular systems on the head stabilization reflex. Neurol Sci. 2016 May;37(5):737-42.

174. Shaikh AG, Zee DS, Crawford JD, Jinnah HA. Cervical dystonia: a neural integrator disorder. Brain. 2016 Oct;139(Pt 10):2590-9.

175. Sugihara I, Shinoda Y. Molecular, topographic, and functional organization of the cerebellar nuclei: analysis by three-dimensional mapping of the olivonuclear projection and aldolase C labeling. J Neurosci. 2007 Sep 5;27(36):9696-710.

176. Zhou H, Lin Z, Voges K, et al. Cerebellar modules operate at different frequencies. Elife. 2014 May 07;3:e02536.

177. Wadiche JI, Jahr CE. Patterned expression of Purkinje cell glutamate transporters controls synaptic plasticity. Nat Neurosci. 2005 Oct;8(10):1329-34.

178. Mateos JM, Osorio A, Azkue JJ, et al. Parasagittal compartmentalization of the metabotropic glutamate receptor mGluR1b in the cerebellar cortex. European Journal of Anatomy. 2001;5:15-21.

179. Dehnes Y, Chaudhry FA, Ullensvang K, Lehre KP, Storm-Mathisen J, Danbolt NC. The glutamate transporter EAAT4 in rat cerebellar Purkinje cells: a glutamate-gated chloride channel concentrated near the synapse in parts of the dendritic membrane facing astroglia. J Neurosci. 1998 May 15;18(10):3606-19.

180. Furutama D, Morita N, Takano R, et al. Expression of the IP3R1 promoter-driven nls-lacZ transgene in Purkinje cell parasagittal arrays of developing mouse cerebellum. J Neurosci Res. 2010 Oct;88(13):2810-25.

181. Hoche F, Seidel K, Brunt ER, et al. Involvement of the auditory brainstem system in spinocerebellar ataxia type 2 (SCA2), type 3 (SCA3) and type 7 (SCA7). Neuropathol Appl Neurobiol. 2008 Oct;34(5):479-91.

182. Zhu CW, Sano M. Economic considerations in the management of Alzheimer's disease. Clin Interv Aging. 2006;1(2):143-54.

183. Roselli F, Caroni P. From intrinsic firing properties to selective neuronal vulnerability in neurodegenerative diseases. Neuron. 2015 Mar 4;85(5):901-10.

184. Saxena S, Caroni P. Selective neuronal vulnerability in neurodegenerative diseases: from stressor thresholds to degeneration. Neuron. 2011 Jul 14;71(1):35-48.

185. Lin MT, Beal MF. Mitochondrial dysfunction and oxidative stress in neurodegenerative diseases. Nature. 2006 Oct 19;443(7113):787-95.

186. Williams AJ, Paulson HL. Polyglutamine neurodegeneration: protein misfolding revisited. Trends Neurosci. 2008 Oct;31(10):521-8.

187. Mather M, Jacobsen LA, Pollard KM. Aging in the United States. Population Bulletin. 2015;70(2).

188. Kaeberlein M, McVey M, Guarente L. The SIR2/3/4 complex and SIR2 alone promote longevity in Saccharomyces cerevisiae by two different mechanisms. Genes Dev. 1999 Oct 1;13(19):2570-80.

189. Houtkooper RH, Pirinen E, Auwerx J. Sirtuins as regulators of metabolism and healthspan. Nat Rev Mol Cell Biol. 2012 Mar 7;13(4):225-38.

190. Howitz KT, Bitterman KJ, Cohen HY, et al. Small molecule activators of sirtuins extend Saccharomyces cerevisiae lifespan. Nature. 2003 Sep 11;425(6954):191-6.

191. Wood JG, Rogina B, Lavu S, et al. Sirtuin activators mimic caloric restriction and delay ageing in metazoans. Nature. 2004 Aug 5;430(7000):686-9.

192. Baur JA, Pearson KJ, Price NL, et al. Resveratrol improves health and survival of mice on a high-calorie diet. Nature. 2006 Nov 16;444(7117):337-42.

193. Pearson KJ, Baur JA, Lewis KN, et al. Resveratrol delays age-related deterioration and mimics transcriptional aspects of dietary restriction without extending life span. Cell Metab. 2008 Aug;8(2):157-68.

194. Finkel T, Deng CX, Mostoslavsky R. Recent progress in the biology and physiology of sirtuins. Nature. 2009 Jul 30;460(7255):587-91.

195. Duan W, Guo Z, Jiang H, Ware M, Li XJ, Mattson MP. Dietary restriction normalizes glucose metabolism and BDNF levels, slows disease progression, and increases survival in huntingtin mutant mice. Proc Natl Acad Sci U S A. 2003 Mar 4;100(5):2911-6.

196. Halagappa VK, Guo Z, Pearson M, et al. Intermittent fasting and caloric restriction ameliorate age-related behavioral deficits in the triple-transgenic mouse model of Alzheimer's disease. Neurobiol Dis. 2007 Apr;26(1):212-20.

197. Patel NV, Gordon MN, Connor KE, et al. Caloric restriction attenuates Abeta-deposition in Alzheimer transgenic models. Neurobiol Aging. 2005 Jul;26(7):995-1000.

198. Wang J, Ho L, Qin W, et al. Caloric restriction attenuates beta-amyloid neuropathology in a mouse model of Alzheimer's disease. FASEB J. 2005 Apr;19(6):659-61.

199. Jeong H, Cohen DE, Cui L, et al. Sirt1 mediates neuroprotection from mutant huntingtin by activation of the TORC1 and CREB transcriptional pathway. Nat Med. 2011 Dec 18;18(1):159-65.

200. Jiang M, Wang J, Fu J, et al. Neuroprotective role of Sirt1 in mammalian models of Huntington's disease through activation of multiple Sirt1 targets. Nat Med. 2011 Dec 18;18(1):153-8.

201. Wang J, Fivecoat H, Ho L, Pan Y, Ling E, Pasinetti GM. The role of Sirt1: at the crossroad between promotion of longevity and protection against Alzheimer's disease neuropathology. Biochim Biophys Acta. 2010 Aug;1804(8):1690-4.

202. Donmez G, Outeiro TF. SIRT1 and SIRT2: emerging targets in neurodegeneration. EMBO Mol Med. 2013 Mar;5(3):344-52.

203. Jesko H, Strosznajder RP. Sirtuins and their interactions with transcription factors and poly(ADP-ribose) polymerases. Folia Neuropathologica. 2016;54(3):212-33.

204. Firestein R, Blander G, Michan S, et al. The SIRT1 deacetylase suppresses intestinal tumorigenesis and colon cancer growth. PLoS One. 2008 Apr 16;3(4):e2020.

205. Schmittgen TD, Livak KJ. Analyzing real-time PCR data by the comparative C(T) method. Nat Protoc. 2008;3(6):1101-8.

206. Joo HY, Yun M, Jeong J, et al. SIRT1 deacetylates and stabilizes hypoxia-inducible factor-1alpha (HIF-1alpha) via direct interactions during hypoxia. Biochem Biophys Res Commun. 2015 Jul 10;462(4):294-300.

207. Rodgers JT, Lerin C, Haas W, Gygi SP, Spiegelman BM, Puigserver P. Nutrient control of glucose homeostasis through a complex of PGC-1alpha and SIRT1. Nature. 2005 Mar 3;434(7029):113-8.

208. Kolthur-Seetharam U, Dantzer F, McBurney MW, de Murcia G, Sassone-Corsi P. Control of AIF-mediated cell death by the functional interplay of SIRT1 and PARP-1 in response to DNA damage. Cell Cycle. 2006 Apr;5(8):873-7.

209. Hoch NC, Hanzlikova H, Rulten SL, et al. XRCC1 mutation is associated with PARP1 hyperactivation and cerebellar ataxia. Nature. 2017 Jan 5;541(7635):87-91.

210. Bras J, Alonso I, Barbot C, et al. Mutations in PNKP cause recessive ataxia with oculomotor apraxia type 4. Am J Hum Genet. 2015 Mar 5;96(3):474-9.

211. Poulton C, Oegema R, Heijsman D, et al. Progressive cerebellar atrophy and polyneuropathy: expanding the spectrum of PNKP mutations. Neurogenetics. 2013 Feb;14(1):43-51.

212. Cohen HY, Miller C, Bitterman KJ, et al. Calorie restriction promotes mammalian cell survival by inducing the SIRT1 deacetylase. Science. 2004 Jul 16;305(5682):390-2.

213. Bushart DD, Shakkottai VG. Ion channel dysfunction in cerebellar ataxia. Neurosci Lett. 2018 Feb 5.

214. McMahon A, Fowler SC, Perney TM, Akemann W, Knopfel T, Joho RH. Allele-dependent changes of olivocerebellar circuit properties in the absence of the voltage-gated potassium channels Kv3.1 and Kv3.3. Eur J Neurosci. 2004 Jun;19(12):3317-27.

215. Laezza F, Gerber BR, Lou JY, et al. The FGF14(F145S) mutation disrupts the interaction of FGF14 with voltage-gated Na+ channels and impairs neuronal excitability. J Neurosci. 2007 Oct 31;27(44):12033-44.

216. Vogt KE, Canepari M. On the induction of postsynaptic granule cell-Purkinje neuron LTP and LTD. Cerebellum. 2010 Sep;9(3):284-90.

217. De Zeeuw CI, Ten Brinke MM. Motor Learning and the Cerebellum. Cold Spring Harb Perspect Biol. 2015 Sep 1;7(9):a021683.

218. Jorntell H, Bengtsson F, Schonewille M, De Zeeuw CI. Cerebellar molecular layer interneurons - computational properties and roles in learning. Trends Neurosci. 2010 Nov;33(11):524-32.

219. Person AL, Raman IM. Purkinje neuron synchrony elicits time-locked spiking in the cerebellar nuclei. Nature. 2011 Dec 25;481(7382):502-5.

220. Arancillo M, White JJ, Lin T, Stay TL, Sillitoe RV. In vivo analysis of Purkinje cell firing properties during postnatal mouse development. J Neurophysiol. 2015 Jan 15;113(2):578-91.

221. Mohan RD, Abmayr SM, Workman JL. Pulling complexes out of complex diseases: Spinocerebellar Ataxia 7. Rare Dis. 2014;2:e28859.

222. Kim E, Lu HC, Zoghbi HY, Song JJ. Structural basis of protein complex formation and reconfiguration by polyglutamine disease protein Ataxin-1 and Capicua. Genes Dev. 2013 Mar 15;27(6):590-5.

223. Rousseaux MWC, Tschumperlin T, Lu HC, et al. ATXN1-CIC Complex Is the Primary Driver of Cerebellar Pathology in Spinocerebellar Ataxia Type 1 through a Gain-of-Function Mechanism. Neuron. 2018 Mar 21;97(6):1235-43 e5.

224. Lai S, O'Callaghan B, Zoghbi HY, Orr HT. 14-3-3 Binding to ataxin-1(ATXN1) regulates its dephosphorylation at Ser-776 and transport to the nucleus. J Biol Chem. 2011 Oct 7;286(40):34606-16.

225. Chen HK, Fernandez-Funez P, Acevedo SF, et al. Interaction of Akt-phosphorylated ataxin-1 with 14-3-3 mediates neurodegeneration in spinocerebellar ataxia type 1. Cell. 2003 May 16;113(4):457-68.

226. Duvick L, Barnes J, Ebner B, et al. SCA1-like disease in mice expressing wild-type ataxin-1 with a serine to aspartic acid replacement at residue 776. Neuron. 2010 Sep 23;67(6):929-35.

227. Urbano FJ, Simpson JI, Llinas RR. Somatomotor and oculomotor inferior olivary neurons have distinct electrophysiological phenotypes. Proc Natl Acad Sci U S A. 2006 Oct 31;103(44):16550-5.

228. Llinas R, Yarom Y. Properties and distribution of ionic conductances generating electroresponsiveness of mammalian inferior olivary neurones in vitro. J Physiol. 1981 Jun;315:569-84.

229. Llinas R, Yarom Y. Electrophysiology of mammalian inferior olivary neurones in vitro. Different types of voltage-dependent ionic conductances. J Physiol. 1981 Jun;315:549-67.

230. Lang EJ, Sugihara I, Llinas R. Differential roles of apamin- and charybdotoxin-sensitive K+ conductances in the generation of inferior olive rhythmicity in vivo. J Neurosci. 1997 Apr 15;17(8):2825-38.

231. Choi S, Yu E, Kim D, et al. Subthreshold membrane potential oscillations in inferior olive neurons are dynamically regulated by P/Q- and T-type calcium channels: a study in mutant mice. J Physiol. 2010 Aug 15;588(Pt 16):3031-43.

232. Zhang Y, Zhang Z, Xiao S, et al. Inferior Olivary TMEM16B Mediates Cerebellar Motor Learning. Neuron. 2017 Aug 30;95(5):1103-11 e4.

233. Bichet D, Haass FA, Jan LY. Merging functional studies with structures of inward-rectifier K(+) channels. Nat Rev Neurosci. 2003 Dec;4(12):957-67.

234. Cerritelli SM, Crouch RJ. Ribonuclease H: the enzymes in eukaryotes. FEBS J. 2009 Mar;276(6):1494-505.

235. Finkel RS, Chiriboga CA, Vajsar J, et al. Treatment of infantile-onset spinal muscular atrophy with nusinersen: a phase 2, open-label, dose-escalation study. Lancet. 2016 Dec 17;388(10063):3017-26.

236. Finkel RS, Mercuri E, Darras BT, et al. Nusinersen versus Sham Control in Infantile-Onset Spinal Muscular Atrophy. N Engl J Med. 2017 Nov 2;377(18):1723-32.

237. Mercuri E, Darras BT, Chiriboga CA, et al. Nusinersen versus Sham Control in Later-Onset Spinal Muscular Atrophy. N Engl J Med. 2018 Feb 15;378(7):625-35.

238. Corey DR. Nusinersen, an antisense oligonucleotide drug for spinal muscular atrophy. Nat Neurosci. 2017 Apr;20(4):497-9.

239. Kordasiewicz HB, Stanek LM, Wancewicz EV, et al. Sustained therapeutic reversal of Huntington's disease by transient repression of huntingtin synthesis. Neuron. 2012 Jun 21;74(6):1031-44.

240. Miller TM, Pestronk A, David W, et al. An antisense oligonucleotide against SOD1 delivered intrathecally for patients with SOD1 familial amyotrophic lateral sclerosis: a phase 1, randomised, first-in-man study. Lancet Neurol. 2013 May;12(5):435-42.

241. Nazor Friberg K, Hung G, Wancewicz E, et al. Intracerebral Infusion of Antisense Oligonucleotides Into Prion-infected Mice. Mol Ther Nucleic Acids. 2012 Feb 7;1:e9.

242. Chiriboga CA, Swoboda KJ, Darras BT, et al. Results from a phase 1 study of nusinersen (ISIS-SMN(Rx)) in children with spinal muscular atrophy. Neurology. 2016 Mar 8;86(10):890-7.

243. Costa Mdo C, Luna-Cancalon K, Fischer S, et al. Toward RNAi therapy for the polyglutamine disease Machado-Joseph disease. Mol Ther. 2013 Oct;21(10):1898-908.

244. Schmitt I, Linden M, Khazneh H, et al. Inactivation of the mouse Atxn3 (ataxin-3) gene increases protein ubiquitination. Biochem Biophys Res Commun. 2007 Oct 26;362(3):734-9.

245. Lu HC, Tan Q, Rousseaux MW, et al. Disruption of the ATXN1-CIC complex causes a spectrum of neurobehavioral phenotypes in mice and humans. Nat Genet. 2017 Apr;49(4):527-36.

246. Burgart AM, Magnus D, Tabor HK, et al. Ethical Challenges Confronted When Providing Nusinersen Treatment for Spinal Muscular Atrophy. JAMA Pediatr. 2018 Feb 1;172(2):188-92.

247. Duque S, Joussemet B, Riviere C, et al. Intravenous administration of self-complementary AAV9 enables transgene delivery to adult motor neurons. Mol Ther. 2009 Jul;17(7):1187-96.

248. Marks WJ, Jr., Bartus RT, Siffert J, et al. Gene delivery of AAV2-neurturin for Parkinson's disease: a double-blind, randomised, controlled trial. Lancet Neurol. 2010 Dec;9(12):1164-72.

249. Federici T, Taub JS, Baum GR, et al. Robust spinal motor neuron transduction following intrathecal delivery of AAV9 in pigs. Gene Ther. 2012 Aug;19(8):852-9.

250. Gaj T, Gersbach CA, Barbas CF, 3rd. ZFN, TALEN, and CRISPR/Cas-based methods for genome engineering. Trends Biotechnol. 2013 Jul;31(7):397-405.

251. Im W, Moon J, Kim M. Applications of CRISPR/Cas9 for Gene Editing in Hereditary Movement Disorders. J Mov Disord. 2016 Sep;9(3):136-43.

252. Rodriguez-Lebron E, Costa Mdo C, Luna-Cancalon K, et al. Silencing mutant ATXN3 expression resolves molecular phenotypes in SCA3 transgenic mice. Mol Ther. 2013 Oct;21(10):1909-18.